Dehydrofluorination Induced High Piezoelectric Poly(Vinylidene Fluoride) and Applications

By

Jiajun Lin

A dissertation submitted in partial fulfillment
of the requirements for the degree of
Doctor of Philosophy
(Macromolecular Science and Engineering)
in The University of Michigan
2019

Doctoral Committee:

Professor Henry A. Sodano, Chair
Professor Jay Guo
Assistant Professor John T. Heron
Associate Professor Timothy F. Scott

Jiajun Lin

jjlin@umich.edu

ORCID id: 0000-0001-7086-7150

ACKNOWLEDGEMENTS

I would like to thank my advisor Dr. Henry Sodano for his exceptional guidance and assistance throughout my PhD program. The opportunities and suggestions he provided were very precious and important to me for completing this dissertation. I feel lucky to have the chance to explore various fields of material science under his mentoring and the I believe that my learning experiences from him will benefit my entire life. I am also grateful to my dissertation committee members: Dr. Jay Guo, Dr. John Heron, and Dr. Timothy Scott, for their kindly help and advices.

I also would like to express my sincere gratitude to Dr. Haixiong Tang and Dr. Zhi Zhou, who gave me a lot of valuable suggestions and helped me quickly step into the right track of my PhD life. I want to thank Dr. Mohammad Malakooti for his precious advices and excellent teamwork in the last four years. I want to than all the present and graduated members of Dr. Sodano's research group for their company and support. We shared a lot of happy moments together, which make my research work more memorable.

Last but not the least, I would like to specially thank my parents, whose love and support are always with me in whatever I pursue. It was their tremendous encouragement that kept up my spirits and let me step steadily toward the right direction.

TABLE OF CONTENTS

LIST OF FIGURES

LIST OF TABLES

ABSTRACT

The piezoelectric effect in poly (vinylidene fluoride) (PVDF) and its copolymers allows the exchange of mechanical and electrical energy. Combined with their unique properties as soft materials, piezoelectric polymers have attracted great interest in actuating, sensing and energy harvesting applications. The electromechanical coupling capacity of the piezoelectric polymers is governed by their crystalline phase composition. The β-phase of PVDF, which has an all-trans chain conformation, is desired because it has the highest aligned dipole density and piezoelectricity. However, the production and application of β-phase PVDF has been restricted by complex processing methods (i.e. *in situ* mechanical stretching) and limited thermal stability. Developing a method to prepare a thermally stable high β-phase PVDF homopolymer that does not require mechanical stretching is of great importance for high-performance PVDF devices and has been a long-lasting challenge in the PVDF industry.

This dissertation details investigations into the structure-property relationships in piezoelectric fluoropolymers and the development of a novel and versatile method to synthesize high β-phase PVDF with improved piezoelectricity and thermal stability. Initially, the effects of molecular structural defects on the crystallization behavior of PVDF are studied through molecular simulations. It is demonstrated that defects consisting of carbon-carbon double bonds on the PVDF backbone can effectively reduce the relative conformational energy of β-phase thus leading to preferential β-phase crystallization. Secondly, a novel dehydrofluorination method is developed and optimized in this work to induce the discussed molecular defects into PVDF in order to promote β-phase formation without mechanical drawing. It is demonstrated that after chemical modification by the developed method, PVDF with β-phase fraction of over 80% can be directly produced through solution casting. Further research is then performed to thoroughly investigate both the direct and inverse piezoelectric effects of this dehydrofluorinated PVDF. Record-breaking piezoelectric strain coefficients are observed from dehydrofluorinated PVDF which achieves as much as a 107% increase in the piezoelectric strain coefficient d_{33} and a 40% increase in d_{31}, compared with conventional drawn PVDF. Furthermore, the dehydrofluorination method

removes the restrictions encountered during high-temperature processing of conventional drawn PVDF. The improved thermal stability of dehydrofluorinated PVDF allows it to recrystallize in the β-phase from any temperature below 210 ˚C which allows a variety of polymer processing methods to be used for PVDF device fabrication. Lastly, this work evaluates the performance of dehydrofluorinated PVDF in piezoelectric applications. Two novel additive manufacturing methods are developed to fully utilize the unique properties of dehydrofluorinated PVDF: a direct-writing method and an electrospin-assisted 3D printing method. Based on these methods, energy harvesters and actuators are fabricated using dehydrofluorinated PVDF and their performance is evaluated. The power density of a dehydrofluorinated PVDF-based stretching mode energy harvester is shown to reach 34.80 mW/cc, which exceeds previously reported PVDF-based energy harvesters and is almost five times higher than the power density of similar devices based on conventional drawn PVDF. By integrating dehydrofluorinated PVDF using novel additive manufacturing methods, the advances described in this dissertation provide new approaches to the development of future piezoelectric devices. This dissertation will serve to disseminate a novel and versatile method of preparing high β-phase PVDF with excellent piezoelectricity and improved thermal stability for the future development of high-performance piezoelectric devices.

CHAPTER 1

Introduction

1.1 Motivation

The motivation for this study lies in the development of electroactive polymers and the increasing demand for soft and flexible materials in sensor and actuator applications.(1-5) Over the past few decades, electroactive polymers that can realize efficient energy conversion between the mechanical and electrical domains have attracted significant attention for the development of frontier research fields such as wearable medical devices, artificial muscles, smart skins, and soft robotics.(5-12) In particular, piezoelectric polymers like poly (vinylidene fluoride) (PVDF) and its copolymers have been studied due to their usefulness in electromechanical device applications. As a piezoelectric material, PVDF can respond to external electric fields with high precision and speed and generate relatively high stresses. Conversely, PVDF can also generate precise charges and voltage signals in response to mechanical stimuli.(13-16) Compared with traditional piezoelectric ceramics such as barium titanate (BTO) and lead zirconate titanate (PZT), PVDF has a large advantage because of its light weight and flexibility. Additionally, PVDF is able to generate piezoelectric strain much larger than that generated by piezoelectric ceramics and has access to a broader variety of fabrication techniques.(17) The piezoelectricity of PVDF is determined by its phase composition, and more specifically, its fraction of the phase in all-trans conformations, which is called the β-phase.(18, 19) Unfortunately, the natural crystallization of PVDF usually leads to the formation of the non-piezoelectric α-phase due to its lower conformational energy.(20, 21) Thus, extra processing is always needed to achieve high fraction of β-phase in the PVDF homopolymer. The most widely used method to prepare high β-phase PVDF is uniaxial drawing.(21-25) By mechanically drawing PVDF to a large elongation, the polymer chains are forced into the all-trans conformation and become parallelly aligned. This method places large limitations on the use of PVDF as piezoelectric devices and necessitates the production of only fibers and films of β-phase PVDF. Furthermore, the drawing-induced β-phase will revert to the α-phase through relaxation which is accelerated by heat treatment. This heat accelerated reversion

blocks access to most polymer processing techniques and limits the use of drawn PVDF in applications requiring high temperatures.(24, 26) Therefore, decades of effort have been made in developing a non-mechanical method to prepare high β-phase PVDF films due to its great importance for the fabrication of high performance PVDF devices.

The defect-engineering strategy is among the techniques investigated to increase the piezoelectric phase content of PVDF without mechanical treatments. In this strategy, stable piezoelectric polymers are formed by effectively modifying the crystallization behavior of fluoropolymers.(17, 27) Several PVDF-based copolymers that show preferential crystallization in the β-phase have been successfully synthesized by adding bulky comonomers during the polymerization of PVDF.(28) However, the copolymerization process has significant issues. For example, it is usually complicated and expensive, and adding large fraction of less polar comonomers affects the piezoelectric property as well as other bulk properties of PVDF.(29-31)

In this dissertation, a new defect-engineering method that intrinsically promotes the β-phase formation through a chemical modification process called dehydrofluorination is presented. Investigations into the relationship between the structure and crystallization behavior of dehydrofluorination-modified PVDF is also presented. Based on these findings, a novel dehydrofluorination method that can be used to prepare high-quality β-phase PVDF without mechanical treatment has been established. The novel dehydrofluorinated PVDF possesses enormous piezoelectricity and improved thermal stability which will both be demonstrated using well-designed characterization techniques. Furthermore, additive manufacturing techniques based on the dehydrofluorinated PVDF have been developed, thus providing new approaches for the future development of high-performance piezoelectric devices.

1.2 Fundamentals of Piezoelectric Materials

Piezoelectricity is a word used to describe the electromechanical coupling ability of a material. Piezoelectric materials can realize two-way energy conversion between the mechanical and electrical domains. Since their discovery in 1880 by Jacques and Pierre Curie, piezoelectric materials have found great value in industry, scientific research, and everyday use.(32, 33) In

recent research, piezoelectric materials have become popular candidates for applications such as actuators, sensors and energy harvesters.

1.2.1 Mechanism of Piezoelectricity

The piezoelectric effect originates from the electric dipoles that exist in solid materials. The electric dipoles are formed by the non-centrosymmetric arrangements of charge-carrying ions or polar molecular groups.(34) Summation of the dipole moments per volume of the piezoelectric material provides a value of polarization (or dipole density). To exhibit the piezoelectric effect, the material needs to possess a non-zero total polarization. Thus, only materials with non-centrosymmetric crystalline structure possess piezoelectric coupling. Among 32 crystal classes, 21 of them are non-centrosymmetric and 20 of these crystal classes exhibit piezoelectricity.(35, 36) There are ten polar crystal classes which contain a permanent electric dipole moment in their unit cell, while there are ten nonpolar but piezoelectric crystal classes which show a non-zero polarization under mechanical stress.(34) When mechanical stress is applied to a piezoelectric material, the polarization changes due to the structural changes around the molecular dipoles. These changes appear as a variation of the surface charge density which can be observed as a voltage signal. In this way, the mechanical energy input in forms of compression, stretching, and vibration is transferred to output electrical energy. Conversely, the structure around the molecular dipoles can be affected by external electric fields, leading to mechanical deformation of the material.(37, 38) This leads to a generated strain, or surface stress if the solid material is blocked, so that the input electrical energy is transferred to mechanical energy. Thus, piezoelectricity can be exhibited through two effects: the direct piezoelectric effect, where an applied mechanical stress causes the accumulation of electric charge on the surface of the material, and the inverse piezoelectric effect, where mechanical strain is generated from the material by an external electric field, as shown in Figure 1.1.(39, 40)

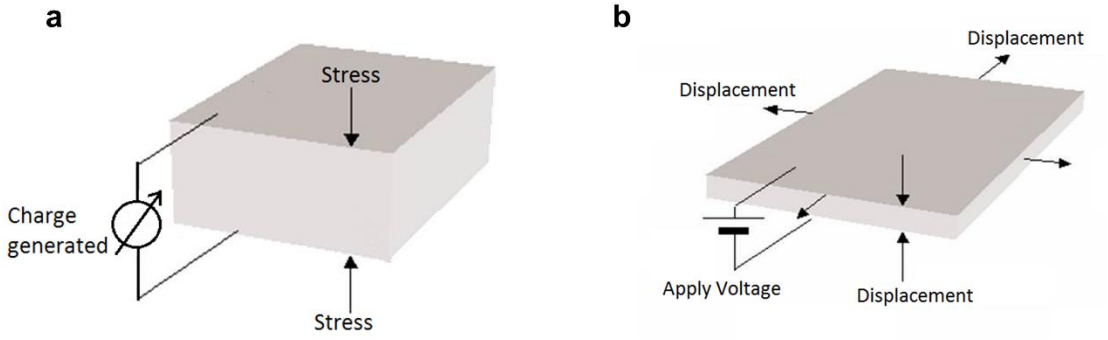

Figure 1.1. Piezoelectric responses: (a) Direct piezoelectric effect and (b) Inverse piezoelectric effect.

Piezoelectric coefficients are used to describe the piezoelectric effects mathematically. The piezoelectric strain coefficient, or the *d* coefficient, relates the charge generated on the surface of the material to the applied mechanical stress and is thus expressed in terms of generated charge density per unit stress. In the direct effect, the piezoelectric response can be represented by the following matrix equation: (37, 40)

$$\{D\} = [d]\{T\} + [\varepsilon^T]\{E\} \qquad \text{Equation 1.1}$$

For materials of the 4mm and 6mm crystal classes such as the well-known piezoelectric ceramic barium titanate, the equation can be also rewritten according to their symmetry as can be seen in Equation 1.2:

$$\begin{bmatrix} D_1 \\ D_2 \\ D_3 \end{bmatrix} = \begin{bmatrix} 0 & 0 & 0 & 0 & d_{15} & 0 \\ 0 & 0 & 0 & d_{24} & 0 & 0 \\ d_{31} & d_{32} & d_{33} & 0 & 0 & 0 \end{bmatrix} \begin{bmatrix} T_1 \\ T_2 \\ T_3 \\ T_4 \\ T_5 \\ T_6 \end{bmatrix} + \begin{bmatrix} \varepsilon_{11} & 0 & 0 \\ 0 & \varepsilon_{22} & 0 \\ 0 & 0 & \varepsilon_{33} \end{bmatrix} \begin{bmatrix} E_1 \\ E_2 \\ E_3 \end{bmatrix} \qquad \text{Equation 1.2}$$

where *{D}* is the matrix of electric charge density displacement, *{T}* is the external stress field, *{E}* is the external electric field, *[d]* is the matrix of piezoelectric strain coefficients for the direct effect, and *[ε]* is the electric permittivity matrix. Conversely, piezoelectric *d* coefficients may be viewed as relating the generated mechanical strain to an applied electric field to model the inverse

piezoelectric effect. In this case, the piezoelectric response can be represented by the following equation:

$$\{S\} = [s^E]\{T\} + [d^T]\{E\} \qquad \text{Equation 1.3}$$

Again, for materials of the 4mm and 6mm crystal classes, the equation can be also rewritten according to their symmetry as in the following equation:

$$\begin{bmatrix} S_1 \\ S_2 \\ S_3 \\ S_4 \\ S_5 \\ S_6 \end{bmatrix} = \begin{bmatrix} s_{11}^E & s_{12}^E & s_{13}^E & 0 & 0 & 0 \\ s_{21}^E & s_{22}^E & s_{23}^E & 0 & 0 & 0 \\ s_{31}^E & s_{32}^E & s_{33}^E & 0 & 0 & 0 \\ 0 & 0 & 0 & s_{44}^E & 0 & 0 \\ 0 & 0 & 0 & 0 & s_{55}^E & 0 \\ 0 & 0 & 0 & 0 & 0 & 2(s_{11}^E - s_{22}^E) \end{bmatrix} \begin{bmatrix} T_1 \\ T_2 \\ T_3 \\ T_4 \\ T_5 \\ T_6 \end{bmatrix} + \begin{bmatrix} 0 & 0 & d_{31} \\ 0 & 0 & d_{32} \\ 0 & 0 & d_{33} \\ 0 & d_{24} & 0 \\ d_{15} & 0 & 0 \\ 0 & 0 & 0 \end{bmatrix} \begin{bmatrix} E_1 \\ E_2 \\ E_3 \end{bmatrix} \qquad \text{Equation 1.4}$$

where *{S}* is the strain matrix, *{T}* is the external stress field, *{E}* is the external electric field, $[s^E]$ is the elastic compliance matrix, $[d^T]$ is the matrix of piezoelectric strain coefficients for the inverse effect which ideally is the transposition of the *[d]* for the direct piezoelectric effect. Note that if the component of piezoelectric strain coefficients is zero, the equations above become merely Gauss's Law and Hooke's Law. This indicates that the piezoelectric performance of a material is dependent upon its bulk properties, and the piezoelectric strain coefficients act as a medium for the energy conversion mechanism to work. (41) The discussed *d* coefficients have units of either pC/N, indicating generated charge per applied force, or pm/V, indicating generated deformation per applied voltage, for the direct or inverse piezoelectric effects respectively.

Besides the piezoelectric *d* coefficient, the piezoelectric voltage coefficient, or so-called *g* coefficient, is also commonly used for evaluating the piezoelectricity of a material. The piezoelectric voltage coefficient indicates the electric field generated per unit of applied mechanical stress and is therefore directly related to the conversion efficiency from stress to voltage of the piezoelectric materials, or the capacity of a material to act as a strain sensor. The *g* coefficient is defined by the following equation and can be calculated by ratio of the *d* coefficient and the dielectric permittivity, resulting in a unit of Vm/N:

$$g_{ij} = -\left(\frac{\partial E_i}{\partial T_i}\right)^D = \left(\frac{\partial S_i}{\partial D_i}\right)^T = -\frac{d_{ij}}{\varepsilon_{ij}} \qquad \text{Equation 1.5}$$

where E is the external electrical field, T is the stress, S is the strain, D is the charge displacement, d is the piezoelectric strain coefficient, and ε is the dielectric permittivity of the piezoelectric material. Because the g coefficients directly relate the strength of the electric field generated by a piezoelectric material in response to an applied mechanical stress, they are important in the assessment of a material in sensing applications.

1.2.2 Piezoelectric Materials

Piezoelectricity was first found in natural crystalline materials such as quartz, topaz, Rochelle salt and cane sugar.(32, 33) Some natural organic materials such as collagen, tendon, wood, and silk also exhibit piezoelectricity due to the uniaxial polar orientation of dipoles in their molecular structures or textures.(42, 43) Piezoelectric materials were first utilized in practical applications when quartz was widely used to make sonar devices during World War I. As a result of this initial successful application, more attention has been given to the development of piezoelectric materials over the past century, and the demands for high performance piezoelectric materials have expanded rapidly. Synthetic piezoelectric ceramics were created and soon became the most investigated and most widely used piezoelectric materials because of their much higher coupling coefficients when compared to natural piezoelectric crystals. The most well-known synthetic piezoelectric ceramics are the barium titanate (BTO) family and the lead zirconate titanate (PZT) family.(34, 40, 44) Their piezoelectricity originates from their non-centrosymmetric perovskite crystal structures.(45) For example, in BTO crystals, the off-centered Ti^{4+} ion forms a permanent dipole within every unit cell (Figure 1.3). Perovskite ceramics can generate a measurable piezoelectric charge when less than 0.1% strain is induced by mechanical stress. They can also produce up to 0.1% strain when an external electric field is applied.

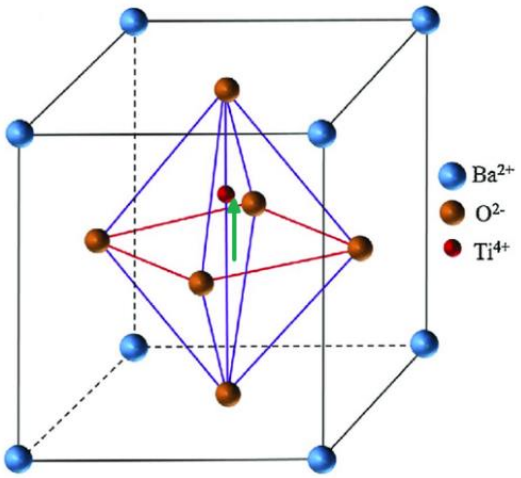

Figure 1.2 Structure scheme barium titanate perovskite unit cell(44). The permanent Dipole is labeled with arrow.

Recently, most research and development of piezoelectric ceramics have put effort in two directions, the first of which is the development of doping and synthesis methods for perovskite ceramics with various metallic elements. In this way, to achieve desired properties such as piezoelectric coupling coefficient, dielectric constant, Curie temperature, stiffness, etc. can be achieved.(46-48) For example, single crystalline $Pb(Mg_{1/3}Nb_{2/3})O_3$-$PbTiO_3$ (PMN-PT) have been reported and have attracted a lot of attention due to its extraordinary high piezoelectric coefficients (d_{33}=2500 pC/N) and low stiffness when compared to traditional PZT ceramics.(49, 50) Along this same direction, multiple efforts have also been made in developing new lead-free piezoelectric ceramics such as bismuth/alkaline titanate and alkaline niobite based perovskites, thus avoiding the toxicity of lead.(48, 51-53) In addition to doping and synthesis, effort has also been focused in the direction of the development of growth methods for piezoelectric ceramics with textured or oriented grain structures. As mentioned above, the piezoelectricity of these ceramics originates from the molecular dipole in their crystallographic unit cells, and the electromechanical coupling ability depends on the total polarization of the material. Thus, an oriented grain structure with highly aligned dipoles will lead to significantly improved piezoelectric performance. Synthesis of perovskite single crystal nanowires have been widely investigated to create one-dimensional structured piezoelectric materials so that their properties can be maximized. A variety of growth techniques have been reported for both BTO family and PZT family perovskites, including

chemical epitaxial growth, chemical vapor deposition, template growth, hydrothermal growth, etc.(54-61) Such piezoelectric nanostructures are widely reported in high-performance sensing and energy harvesting applications. Besides perovskite nanowires, zinc oxide (ZnO) nanowires are also widely used although they exhibit relatively weak piezoelectricity. ZnO ceramics possess a non-centrosymmetric wurtzite structure and only exhibit piezoelectricity when the grain structure is textured.(40) However, the versatile synthesis methods of growing ZnO nanowires arrays on different surfaces make them an excellent candidate for the structural and sensing component of a multifunctional material.(62-64)

There are also some synthetic polymers that exhibit piezoelectricity because of their polar molecular structures. These polymers contain molecular dipoles formed by polar covalent bonds along their backbones, and the total polarization is dependent on the alignment of these polymer chains. Piezoelectricity has been observed from common synthetic polymers such as Nylon and polylactic acid.(65-68) However, the most well-known and investigated piezoelectric polymers are poly (vinylidene fluoride) (PVDF) and its copolymers because of their strong piezoelectricity as well as high ferroelectric and pyroelectric properties.(39, 69) These piezoelectric polymers were first reported in the 1970s and have attracted great interest as soft piezoelectrics.(70-73) In the PVDF molecule, each $-CH_2-CF_2-$ (or VDF) repeating unit serves as a permanent dipole. (Figure 1.3) The piezoelectricity of PVDF is determined by the crystalline phases that make up the bulk material; different chain conformations in these phases align the dipoles in different ways.(18, 19) Once crystallized in the most favorable phase, the molecular dipoles within PVDF will be parallelly aligned to sum up to a large total polarization, leading to strong piezoelectric and ferroelectric effects.

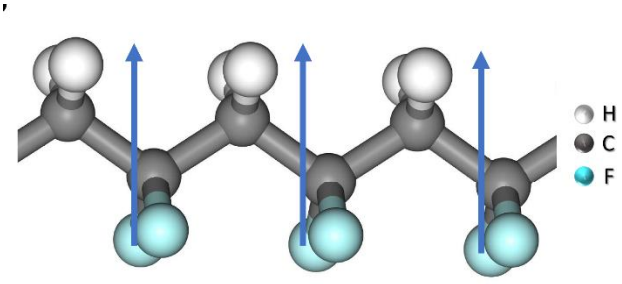

Figure 1.3 Structure scheme of PVDF polymer chain. Dipoles are labeled with arrows.

The piezoelectric d_{33} coefficient and g_{33} coefficient of several common piezoelectric materials are shown in Figure 1.4.(68, 74-76) Piezoelectric materials with lower permittivity, such as PVDF and its copolymers, provide greater energy conversation capacity due to a lower capacitance, which traps a lower portion of the generated charge, compared to the piezoelectric ceramics with higher permittivity. This leads to high *g* coefficients and indicates the potential of PVDF and its copolymer in sensing applications although their *d* coefficients are much lower than piezoelectric ceramics. In addition to high *g* coefficients, PVDF also carries the added benefit of its classification as a thermoplastic polymer. Unlike hard and brittle ceramics, PVDF is a soft and flexible material with low density, which is preferable in many applications such as wearable devices and soft robotics.(6, 8, 10, 11) The softness of PVDF allows the generation of large piezoelectric strains as well as the ability to withstand large deformation in sensing applications using the direct piezoelectric effect. Previously reported PVDF-based materials can easily generate deformation of a few percent of their static structures, while most piezoelectric ceramics can only generate ~0.1% strain.(14, 16, 77) Additionally, the metal-free composition and chemical inertness of PVDF and its copolymers makes them more suitable in biomedical applications. Furthermore, unlike the high-temperature sintering and complicated nanowire growing techniques used in the processing of piezoelectric ceramics, piezoelectric polymers can be processed using a variety of plastic processing techniques, such as solution casting and extrusion, which are cheaper and more efficient. PVDF and its copolymers can be cast into flexible thin films, which broaden their potential applications to include microelectromechanical systems (MEMS) and wearable devices.(12, 78) The described advantages over traditional piezoelectric ceramics indicate the great potential of PVDF for a variety of piezoelectric applications. However, to fully utilize the piezoelectricity of PVDF, there are still problems to be solved, and one of the most important and long-standing problems lies in the crystallization behavior of PVDF.

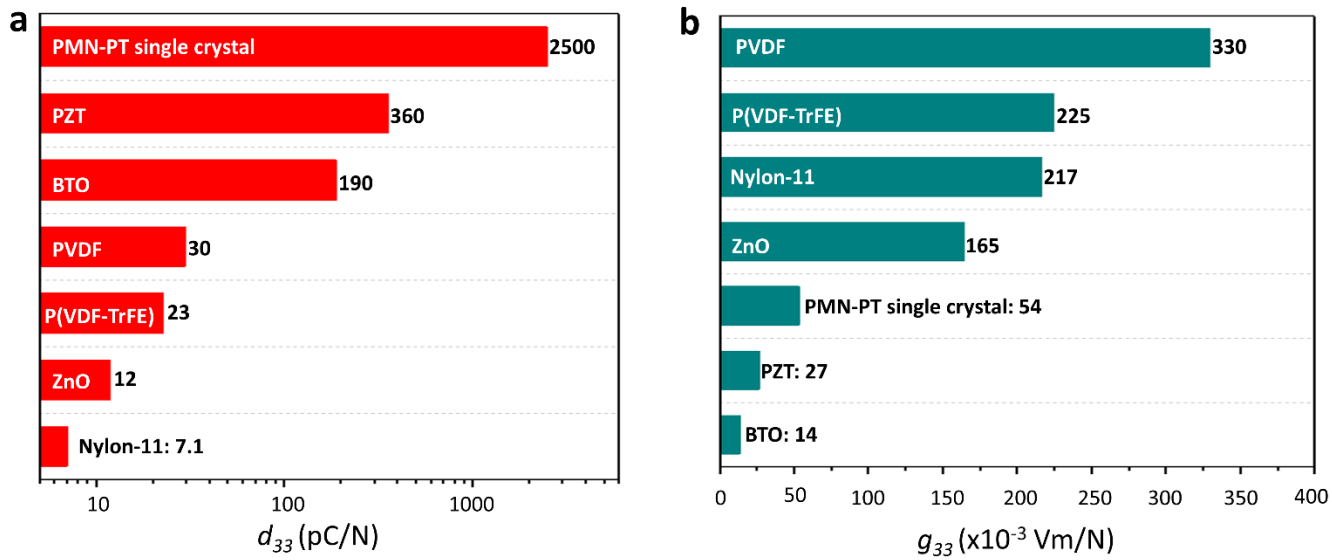

Figure 1.4 Piezoelectric coefficients of common piezoelectric materials: (a) piezoelectric strain coefficients d_{33}, (b) piezoelectric voltage coefficient g_{33}. (68, 74-76)

1.3 Development of Piezoelectric PVDF

Unlike ceramics, PVDF is semi-crystalline with multiple phases. Maximizing the piezoelectric properties of PVDF thus requires additional processing due to the instability of the piezoelectric phase in the polymer. This places limitations on the available manufacturing processes and prevents the use of this unique responsive material in many practical applications.(21, 25) Therefore, extensive research has been conducted to understand the crystallization behavior of PVDF in order to improve the piezoelectric properties.

1.3.1 Crystalline Phases of PVDF and Drawing-Induced Phase Transition

As a semi-crystalline polymer, PVDF can form five crystalline phases depending on different processing methods.(79-82) Among these phases, there are three phases that are most commonly observed and investigated (Figure 1.5): a non-polar α-phase, a polar β-phase, and a less polar γ-phase.(20, 69) In the α-phase, PVDF polymer chains are crystallized in trans-gauche-trans-gauche minus (TGTG') conformation and align in an antiparallel orientation in the crystallographic unit cell. This chain conformation and alignment leads to zero polarization of the unit cell, thus α-phase PVDF does not possess piezoelectricity. The β-phase is the most polar of

the phases in PVDF and possesses the highest piezoelectricity. In the β-phase, PVDF polymer chains are crystallized in an all-trans conformation and align in a parallel orientation. This planar conformation and parallel alignment orients all of the molecular dipoles in the same direction, causing them to sum up to a large total polarization.(18, 83, 84) The γ-phase is a less common phase that usually appears as an intermediate state between α-phase and β-phase PVDF. In the γ-phase, PVDF polymer chains are crystallized in a trans x3 -gauche-trans x3-gauche minus (T_3GT_3G') conformation and are aligned in a parallel orientation in the unit cell. The partially planar conformation leads to a polarization that is smaller than the polarization seen in the β-phase, which results in a weaker piezoelectricity. Among these phases, the α-phase possesses the lowest conformational energy and is thus the most common phase of PVDF. As a result, it can be easily formed directly from polymer melts and during solvent casting of PVDF. However, as the β-phase and γ-phase are the most electrically active phases, a large amount of interest has been attracted to investigate the phase transformation behavior of PVDF to promote the formation of these polar phases.

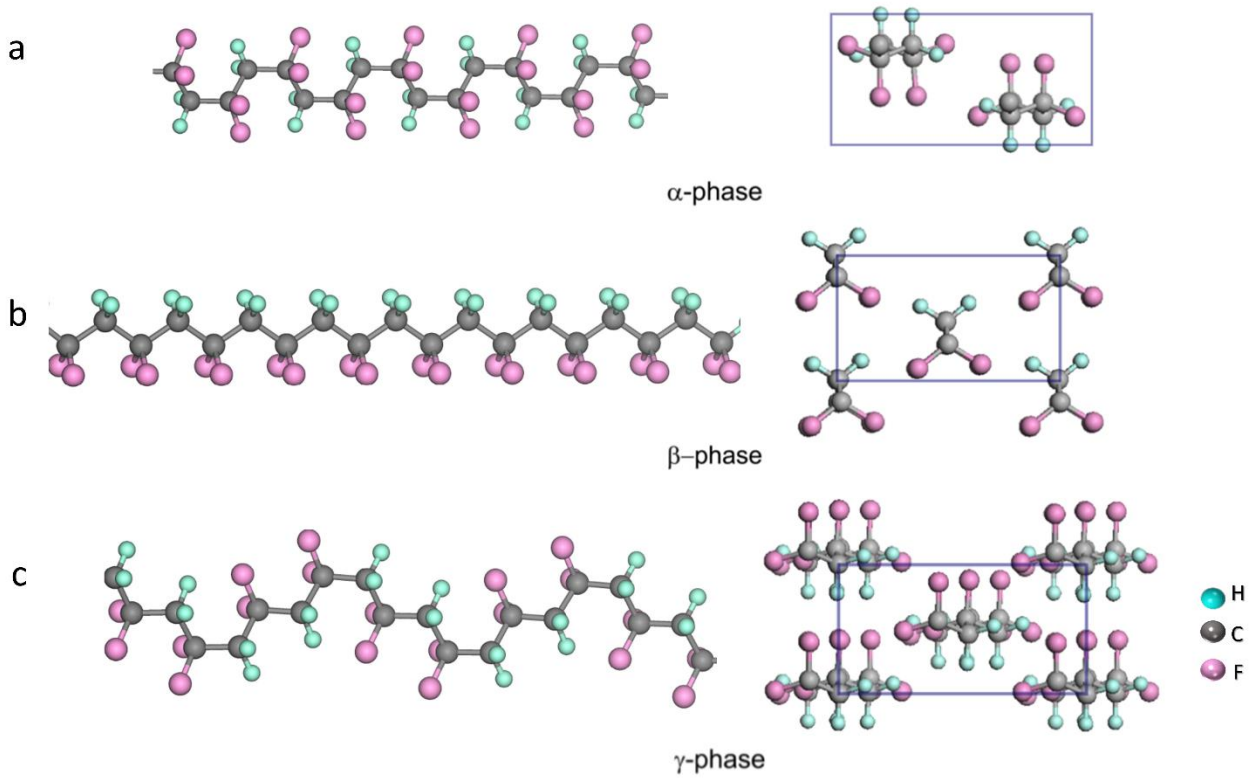

Figure 1.5 Crystalline phases of PVDF: (a) α-phase, (b) β-phase and (c) γ-phase.

As previously stated, among the phases of PVDF, the β-phase exhibits the highest piezoelectricity; thus, it is the most desired phase for piezoelectric applications. The ideal process to fully utilize the piezoelectricity of PVDF would prepare PVDF of high β-phase content and apply sufficient electric poling, preferably at an elevated temperature, to completely align the dipoles in the same direction. Multiple efforts have been made to develop a method that promotes the formation of β-phase in PVDF. Because β-phase PVDF has a zigzag conformation, which is the most extended conformation for a polymer chain, one of the common ideas is to utilize mechanical stress to promote phase transition from other phases to β-phase. It has been widely reported that the α-to-β phase transition of PVDF can be achieved through a mechanical drawing process.(21, 22, 24, 25, 85) This drawing method has been widely investigated at different drawing rates, temperatures, and elongations, and quickly became the most widely used manufacturing technique for high β-phase PVDF in industrial applications.(24) By drawing PVDF under elevated temperature to an elongation of 300% to 500%, the polymer chains are forced into all-trans conformation and are aligned along the drawing direction (Figure 1.6).(86) This drawing process thus greatly increases the degree of crystallinity of the resulting PVDF and produces a large fraction of β-phase.(87, 88) However, it should be noted that the β-phase prepared using this drawing method alone does not produce PVDF that exhibits piezoelectric effects due to the fact that the polymer chains are randomly oriented in the direction normal to the drawing force. To maximize the piezoelectric properties of the drawn PVDF, state-of-the-art processing methods perform mechanical drawing of PVDF under an external electrical field.(24, 89) The applied electric field can orient the molecular dipole along the field during the drawing process thus providing *in situ* electric poling. This manufacturing process allows large-scale, continuous production of highly-piezoelectric PVDF films.

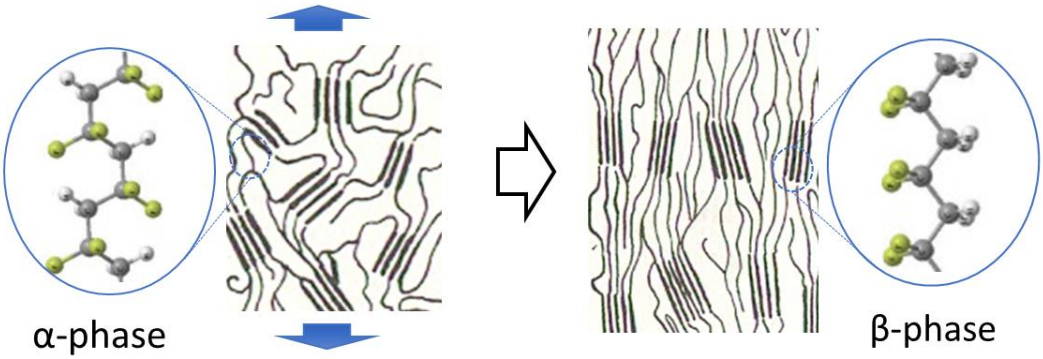

Figure 1.6 Phase transition of PVDF during mechanical drawing.

Unfortunately, the mechanical drawing process also leads to significant limitations in the potential applications of PVDF. One of the major disadvantages of mechanically drawn PVDF is that the β-phase produced by the drawing process is accompanied by significant residual internal stresses. Once the drawn PVDF is heated to a temperature high enough to allow free movement of chain segments, thermal relaxation will occur, and the stressed polymer chains will revert to the original α-phase.(90, 91) This thermal relaxation effect can be significantly accelerated when the drawn PVDF is subjected to high temperatures (>100 ˚C).(92, 93) This feature of drawn PVDF blocks access to high-temperature electric poling and limits its application at elevated temperatures. Additionally, the uniaxial drawing method can only produce β-phase PVDF in the form of films and fibers. Once it has been mechanically drawn, the product PVDF cannot be further processed using common polymer processing techniques because of low thermal stability. This lack of variety in product forms largely restricts the application of drawn PVDF. The development of a method to synthesize stable, highly-piezoelectric PVDF films without uniaxial drawing is thus of great importance for the fabrication of high-performance PVDF devices and has been the focus of decades of research.

1.3.2 Previous Efforts to Prepare Undrawn β-phase PVDF

Over the past few decades, a significant amount of research has been dedicated to developing alternative preparation methods for high β-phase PVDF. The previous reported non-

mechanical methods to prepare PVDF with high piezoelectric properties is divided into the following categories of approaches: thermal methods which involve modification to the solvent evaporation process and the melt crystallization process, electric poling methods which use electric fields instead of mechanical stress, additive methods using the addition of nucleating fillers, including nanoparticles, ionic chemicals, hydrated salts and polymer blends, nanofabrication methods including the electrospinning method and Langmuir-Blodgett method, and defect-engineering copolymerization methods. Each of these methods are further explained in the following section.

1.3.2.1 Thermal Methods

In early research of the crystallization behavior of PVDF, it was observed that the evaporation process during solvent casting affects the crystalline composition.(94-96) In particular, the parameters that affect the final phase composition include evaporation rate, evaporation temperature, and the choice of solvent. Gregorio Jr. *et al.* and Salimi *et al.* reported that PVDF crystallizes in a higher β-phase fraction at lower evaporation temperature during the solution crystallization process from dimethylacetamide (DMAc).(94, 96) It was shown that the cast PVDF film could achieve a β-phase fraction over 80% when the evaporation temperature is lower than 70℃, while PVDF films dried at temperature above 120℃ only contain a β-phase fraction less than 20%. In a later report, Gregorio Jr. *et al.* reported that PVDF films with increased fraction of β-phase can be formed during low temperature evaporation of PVDF from other solvents including dimethylformamide (DMF), N-methyl-2-pyrrolidone (NMP), and hexamethylphosphoramide (HMPA).(97) It was shown that the resulting crystalline phase formed during solution casting is determined by the evaporation rate of the solvent, which depends on the evaporation temperature and the boiling point of the solvent. Low evaporation rates favor the formation of β-phase, while high rates favor the formation of α-phase.

The solvent used in PVDF solution crystallization also affect the resulting phase composition. Gal'perin *et al.* first reported that polar PVDF was obtained by solution crystallization in DMF, DMAc, and dimethyl sulfoxide (DMSO).(98) Furthermore, Benz *et al.* performed research on a variety of solvents to investigate the solvent effects on the phase composition of PVDF.(99) It was reported that solvents with a high dipole moment promoted the formation of a polar phase in PVDF. However, it was also reported that the phase composition of the resultant polar PVDF is dominated by the γ-phase instead of the β-phase (Table 1.1).

Nonetheless, the effects of polar solvents on promoting the formation of planar chain conformation in PVDF was confirmed. The reason for increased planar conformation is given by the strong intermolecular interactions between polar solvents and PVDF. Such intermolecular interactions lead to the expansion of the coil dimensions of PVDF polymer chains so that more planar conformation is induced. This effect is more significant at lower temperatures where the proton exchange rate of the polar solvent is lower.(99) Thus, a combination of both polar solvents and low evaporation temperature are usually used for preparing piezoelectric PVDF films from solution casting. However, low evaporation temperature also leads to increased roughness and porousness in the resulting PVDF films, which then leads to decreased electrical and mechanical properties.

Table 1.1 Solvent effects on the phase composition of solution-casted PVDF films.(Films were solution casted and dried at 70℃) (99)

Solvent	**Dipole moment (D)**	**Phases Obtained**
Dimethyl Sulfoxide (DMSO)	3.96	γ-phase
Dimethylformamide (DMF)	3.82	γ-phase
Dimethylacetamide (DMAc)	3.81	γ-phase
Acetone	2.88	γ-phase
Tetrahydrofuran (THF)	1.75	Mixture of α- and γ-phase
Ethanol	1.69	α-phase
Toluene	0.37	α-phase

Heat treatments methods directly performed on the PVDF melts or PVDF films have also been reported for the preparation of piezoelectric PVDF in early studies. Many efforts have focused on finding the optimum crystallization condition for polar PVDF. Lovinger *et al.* reported an isothermal crystallization method to prepare polar phase PVDF.(100, 101) Formation of the γ-phase was observed when the PVDF melt was crystalized at elevated temperature. Osaki *et al.* found γ-phase dominated PVDF was obtained from melt by isothermal crystallization at 170℃.(102) However, β-phase PVDF cannot be obtained through such methods. Quenching and annealing processes are also reported to promote the phase transition to polar phase.(103, 104)

Yang *et al.* reported that a quenching process of PVDF melts from 210℃ to -50℃ leads to the formation of β-phase.(105) Additionally, Kang *et al.* reported that the ferroelectric behavior of spin-coated PVDF films largely increased as a result of an annealing process at 150℃ because of increased β-phase fraction.(106) In addition to these heat treatments, promoted β-phase formation was also observed in crystallization processes under high pressure and on special substrates.(107, 108) Early studies reported that epitaxial growth of β-phase PVDF is observed when the PVDF is crystallized from melt on a potassium bromide substrate leading to high fraction of oriented β-phase.(109) However, because of the high viscosity of PVDF melt and the degradation of PVDF at high temperature, the process using PVDF melt to produce β-phase PVDF can be very complicated and expensive. It should be noted that these studies of the melt crystallization of PVDF were mostly conducted in 1980s; many other more efficient and processable methods have been developed since then.

1.3.2.2 Electric Poling Methods

An electric poling process at elevated temperature is often reported as an alternative method to mechanical drawing to induce phase transitions in PVDF. In this method, an electric field is used as an external drawing force instead of the mechanical forces used in the conventional drawing method.(26, 93) Since the molecular dipoles can be stressed and reoriented using a strong electric field, the electric poling process is often used as a method to maximize the piezoelectric response of prepared PVDF films. In the high temperature electric poling process, PVDF films are subjected to a strong electric field at elevated temperature close to the melting point to increase the flexibility of chain segments. The VDF dipoles are then aligned along the field direction and frozen by cooling the film down to room temperature under the electric field. Satyanarayana *et al.* investigated the phase transition of PVDF under external electric fields through molecular dynamics simulation.(110) The simulation showed the molecular motion of PVDF phase transition under electric fields was similar to that of the phase transition under mechanical stress, and lower electric field is required for a complete α-to β- phase transition when a low uniaxial strain of 4.75% is applied to the PVDF film simultaneously. During the electric poling process, α-phase usually transits to δ-phase first, in which PVDF chains still have the same conformation but are aligned parallelly.(111, 112) Generally, the electric poling method is more effective at higher temperatures and electric fields, however, the risks of sample failure due to electric breakdown also increases under such conditions. Electric poling induced phase transition from γ-

and δ-phase to β-phase are also reported.(108, 112) Since these two phases are high-energy intermediate states between α- and β-phases, the transition is easier to realize at lower electric field and temperature.

It should be noted that although the use of electric field instead of mechanical forces allows high flexibility in product form, the β-phase PVDF prepared by electric methods is still drawn PVDF. The problem of thermal relaxation still exists in these PVDF products because of the presence of internal stress. Thus, although the electric poling method can slightly broaden the physical form of PVDF products because of the flexibility of applying electric fields, it cannot solve the problems caused by low thermal stability.

1.3.2.3 Additive Methods

Many additives such as hydrated salt, nanoscale fillers, and polymers are reported to have influence on the crystallization behavior of PVDF. These methods are focused on the properties of solution cast PVDF films since the additives are usually mixed in PVDF solutions. The most frequently reported additives for the preparation of the β-phase are hydrated metal salts such as magnesium chloride hexahydrate and nickel cerium nitrate hexahydrate.(113-116) The mechanism of metal salt induced β-phase formation lies in the strong interfacial interactions between PVDF and the added salt. Such interfacial interactions are formed by ion-dipole interactions and hydrogen bonds between PVDF and the water molecules of the salts (Figure 1.5).(117) A single molecular layer of PVDF chains with all-trans conformation are adsorbed on the salt surfaces because of the interactions between the water molecule and the fluoride atoms. Such molecular layers serve as the initial crystal nuclei, and polymer chains crystallize around these nuclei with same conformation to form the β-phase.(118) The addition of hydrated metal salts can thus effectively improve the ferroelectricity and piezoelectricity of cast PVDF films; however, the residual salts have no contributions to either the structural or electrical properties of the resultant PVDF.

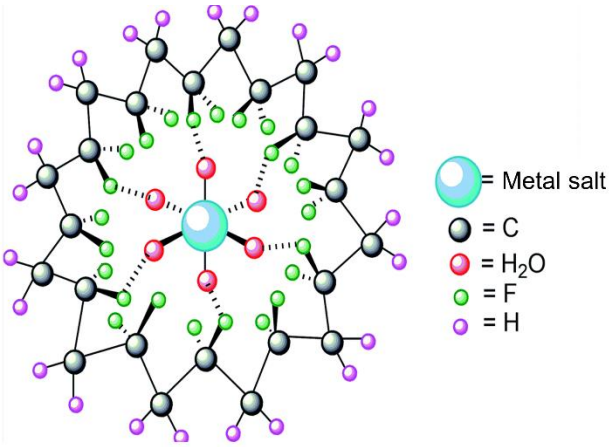

Figure 1.7 Promoted β-phase formation on the surface of hydrated salt.(117)

Nanoparticles of TiO_2, BTO, and ferrite can also serve as nucleating seeds for the formation of β-phase PVDF.(119-122) The mechanism of the nucleating of β-phase around these nanoparticles is explained by the negative electrostatic charges on these nanoparticles. Strong molecular interactions occur between these negatively charged surfaces and the positively charged CH_2 segments of PVDF chains, thus leading to initial crystal nuclei of β-phase at the interface (Figure 1.8).(120) The process of β-phase nucleation by these nanoparticles is very similar to the process promoted by hydrated salts. However, use of BTO and ferrite nanoparticles have great advantages compared to the use of hydrated salts because of the unique properties of the filler itself. Inclusion of piezoelectric ceramic nanoparticles like BTO can adjust the dielectric and piezoelectric properties of PVDF, resulting in piezoelectric nanocomposites that may exhibit better performances in sensing, energy storage, and energy harvesting.(123, 124) The addition of magnetostrictive ferrite particles such as $NiFe_2O_4$ and $NiFe_2O_4$ in piezoelectric PVDF results in a multiferroic nanocomposite that allows application in electromagnetic coupling sensing and actuating.(120, 125)

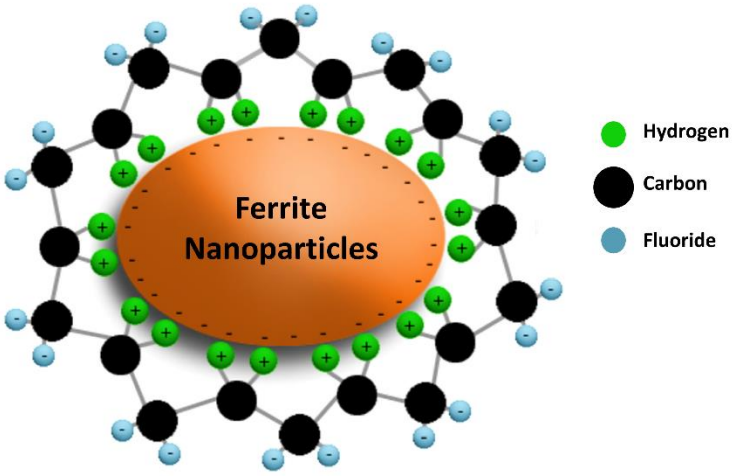

Figure 1.8 Promoted β-phase formation on the surface of negatively charged ferrite nanoparticles. (120)

In recent years, high strength nanofillers such as carbon nanotubes (CNTs), graphene oxides, and nanoclays have also been used as reinforcement materials for PVDF nanocomposites, and have been found to be influential for the crystallization of PVDF.(126-129) El Achaby *et al.* reported that the addition of graphene oxide in PVDF/DMF solution enhanced the β-phase formation in cast films.(127) The results showed a β-phase dominated PVDF film was directly obtained from solution-casting with 2 wt.% of the graphene oxide filler. Ramasundaram *et al.* reported an organically modified silicate filler that can induce preferential β-phase formation in PVDF base nanocomposites.(128) The surface of the silicate filler was modified to enhance the interaction with PVDF molecules. The formation of β-phase PVDF is then promoted by the interfacial interactions in which the all-trans conformation chains have a lower energy barrier to be absorbed on the surface of nanofiller.(130, 131) The efficiency of increasing β-phase through nanofillers, especially CNTs, are still controversial,(130) however, the addition of high strength nanofillers can improve the mechanical properties of PVDF and may open new routes to the fabrication of multi-functional nanocomposites.

Another category of additives that can be used to induce β-phase formation is poly (methyl methacrylate) (PMMA). It was discovered several decades ago that PVDF-PMMA polymer blends with an appropriate molar ratio can crystallize in the β-phase.(132, 133) Gregorio Jr. *et al.* reported that a small concentration of PMMA (10 to 15 wt. %) in PVDF-PMMA blends leads to

preferential β-phase crystallization from solution casting.(134) Li *et al.* further investigated the crystallization behavior of PVDF-PMMA blends and reported a phase diagram indicating that β-phase can be obtained by annealing the polymer blend near its melting point.(135) PMMA promotes β-phase crystallization for steric reasons in addition to dipole-dipole interactions. Due to their similar electronic structure, PMMA chains can enter the crystalline region of PVDF and induce steric hindrance between PVDF chains.(134) Meanwhile, the dipole-dipole interaction and hydrogen bonds between the PMMA and PVDF forces the PVDF and PMMA polymer chains to align in a parallel orientation. Such interaction favors the all-trans conformation in both polymer chains, leading to the formation of β-phase. However, since PMMA is an amorphous polymer, a large fraction of PMMA will decrease the degree of crystallinity of PVDF which leads to the loss of ferroelectricity.(136)

1.3.2.4 Nanofabrication Methods

The methods discussed in this section are the electrospinning method and Langmuir-Blodgett method. Both techniques are versatile processing methods that are widely used for fabricating nanostructures comprised of polymers. However, during these processes, a high ratio of 'stretching' is induced in the PVDF which leads to phase transition and results in extremely high fraction of β-phase.

Electrospinning techniques have attracted significant attention as a convenient method to prepare polymeric nanofibers. In the process of electrospinning, electric force is used to draw charged polymer solutions or polymer melt into fibers with diameters on the order of hundreds of nanometers. The method is usually executed by applying a high voltage to charge a droplet of polymer solution or melt. When the electrostatic repulsion of the charged droplet is strong enough to counteract its surface tension, a stream of liquid jet will form from the surface of the droplet and be deposited onto a grounded collector.(137, 138) With a syringe pump or liquid dispenser to continuously feed polymer solution or melt to a charged nozzle, the polymer can be drawn by the electric field at a constant rate to form continuous nanofibers or sprayed nanowebs (Figure 1.9). Electrospinning of PVDF solution has been widely reported as a promising method for fabricating micro- and nano-scale piezoelectric devices.(139, 140) During the electrospinning process, the PVDF polymer chains are charged and stretched by the electric field to form all-trans

conformations with dipoles aligned parallelly according to the field. The effects of the electric field act as a combination of mechanical drawing and electric poling. As a result, electrospun PVDF fibers possess a high fraction of β-phase and strong piezoelectricity.(141-143) Pu *et al.* reported a nanoscale actuator based on electrospun PVDF fibers and reported a large inverse piezoelectric strain coefficient d_{33} of -57.6 pm/V.(144) Additionally, Chang *et al.* and Soin *et al.* reported PVDF nanogenerators fabricated using an electrospinning method and observed high energy conversion efficiency.(145, 146) Electrospun β-phase PVDF fibers have attracted interest in various fields including sensing, batteries, filtration, and biomedical applications.(147, 148) The development of controllable near-field electrospinning techniques in recent years also indicate its potential as a candidate additive manufacturing method for high-performance piezoelectric devices.(145, 146)

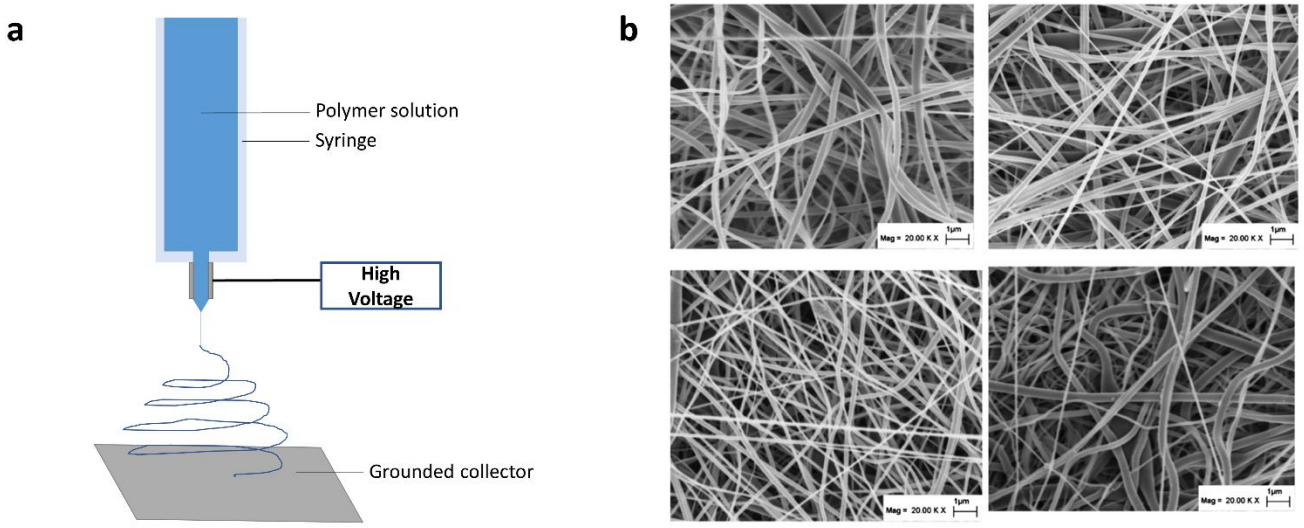

Figure 1.9 Electrospinning of PVDF. (a) Schematic diagram of electrospinning process. (b) PVDF nanofibers electrospun under different conditions. (149)

The Langmuir-Blodgett (LB) method is a monomolecular film assembly technique that is used for preparing nanosheets or ultrathin films of polymers. The LB method utilizes the hydrophilic and hydrophobic functional groups in the polymer which acts as surfactant. Once deposited on water surface, the surfactant molecules will be spread out by the surface tension of water and eventually form a monomolecular layer on the surface of the water. In the case of PVDF, the C-F groups serve as the hydrophilic groups by forming hydrogen bonds with water molecules

(Figure 1.10).(150) During the spreading process on the surface of the water, the PVDF chains are stretched by surface tension to extend biaxially. Monolayer of oriented β-phase PVDF film is thus formed on the surface of the water and can be deposited onto a solid substrate by immersing the substrate into water. Thicker β-phase PVDF films can be obtained by repeatedly depositing PVDF monolayers onto the substrate.(151, 152) Since the thickness of a single monolayer is fixed, the thickness of the deposited PVDF LB film can be precisely controlled by controlling the number of layers. Kliem *et al.* reported an LB deposition method and prepared oriented PVDF films with thicknesses of only several nanometers and β-phase fraction of almost 100%.(152) Chen *et al.* characterized the piezoelectricity of the PVDF LB film and observed a large d_{33} coefficient of -49.4 pm/V. (150) They also reported that because the PVDF molecules are highly oriented in the LB film, the electric poling process is not necessary for maximizing the piezoelectricity of the PVDF. Additionally, Zhu *et al.* reported that the LB deposition of PVDF can further improved by the use of amphiphilic nanosheets, in order to prepare highly-oriented ferroelectric PVDF LB films.(153)

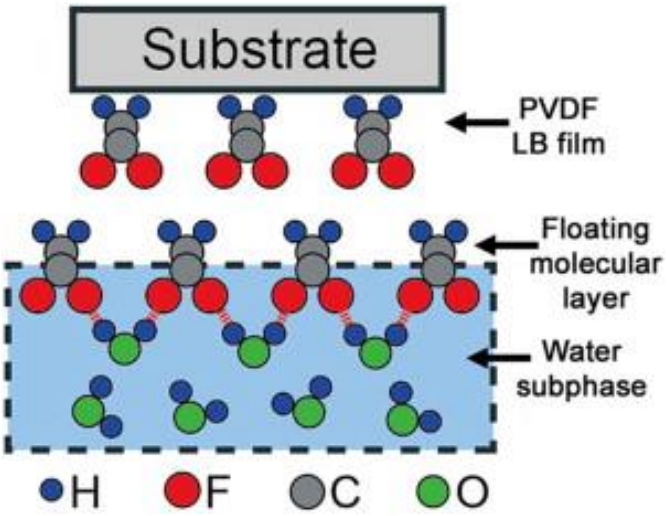

Figure 1. 10 Illustration of the preparation of oriented β-phase PVDF through LB method. (150)

Although both the electrospinning method and LB deposition method still use external force to form β-phase PVDF by stretching, they are able to prepare highly-piezoelectric nanoscale PVDF products. It can be expected that these nanofabrication methods will find great use in future development if MEMS, microrobots, and nanodevices.

1.3.2.5 Defect-Engineering Methods

The 'defect-engineering' strategy originates from the study of the head-to-tail isomerism of PVDF.(154, 155) In 1972, Farmer *et al.* reported that the head-to-head/tail-to-tail (HHTT) defects induced during the polymerization of PVDF will influence the polymorphic crystallization behavior of the PVDF.(155) It is demonstrated that with a high fraction of such 'defects', the β-phase formation is promoted. The reason of promoted β-phase formation was found to be that the regional steric effect caused by the HHTT defects increased the energy barrier of α-phase formation while causing no significant effects on the formation of β-phase.(156) Defect-engineered copolymers of PVDF such as poly(vinylidene fluoride-co-trifluoroethylene), or P(VDF-TrFE), have been developed as alternative piezoelectric polymeric materials to PVDF.(27, 28, 72, 73) The newly introduced comonomers can adjust the ferroelectric and piezoelectric properties of VDF based polymers by affecting the structure of crystalline and ferroelectric domains. The comonomers used in PVDF copolymers are larger and bulkier than the VDF units, thus introducing more steric effects to the crystalline region of the PVDF.(156) Such effects lead to a preferential crystallization in β-phase in these copolymers. As a result, P(VDF-TrFE) can crystallize into β-phase from melt and solution casting, widely broadening its processing opportunities when compared to PVDF formed using alternative methods.(20, 157-159) The mechanism of promoted β-phase formation in the P(VDF-TrFE) copolymer will be investigated in detail in chapter 2.

P(VDF-TrFE) copolymers are conventionally prepared by using the free radical copolymerization of VDF and trifluoroethylene (TrFE). The polymerization can be performed during aqueous dispersions such as suspension, emulsion, and microemulsion to yield high molecular weight products.(157, 160, 161) The composition of the polymerization system needs to be carefully controlled since residual ionic species in the final product will reduce the piezoelectricity. Iodine transfer polymerization methods and reversible addition fragmentation chain transfer (RAFT) polymerization methods have also been reported to prepare electroactive block copolymers of VDF and TrFE.(161-163) Although the copolymers have a huge advantage in the stable β-phase formation when compared to PVDF, the copolymerization is complicated and expensive which increases the cost of using PVDF copolymers in piezoelectric applications.

Furthermore, the mechanical properties and some piezoelectric coefficients of these copolymers were found to be lower than the PVDF homopolymer.(13, 164, 165)

This dissertation will design a low-cost and versatile route to prepare β-phase PVDF following the defect-engineering strategy. The molecular defects are introduced by the chemical modification method through dehydrofluorination of PVDF. The dehydrofluorination reaction takes place when PVDF is subjected to basic or high temperature conditions and modifies the backbone structure of PVDF by introducing carbon-carbon double bonds or forming crosslinks (Figure 1.6).(166, 167) The relationship between the modified molecular structure and phase composition of PVDF will be further investigated to obtain a better understanding of the crystallization behavior of fluoropolymers. Finally, an optimized dehydrofluorination method will be developed to prepare β-phase PVDF with high piezoelectricity. Additionally, the piezoelectric properties and performance of the new developed PVDF will be demonstrated.

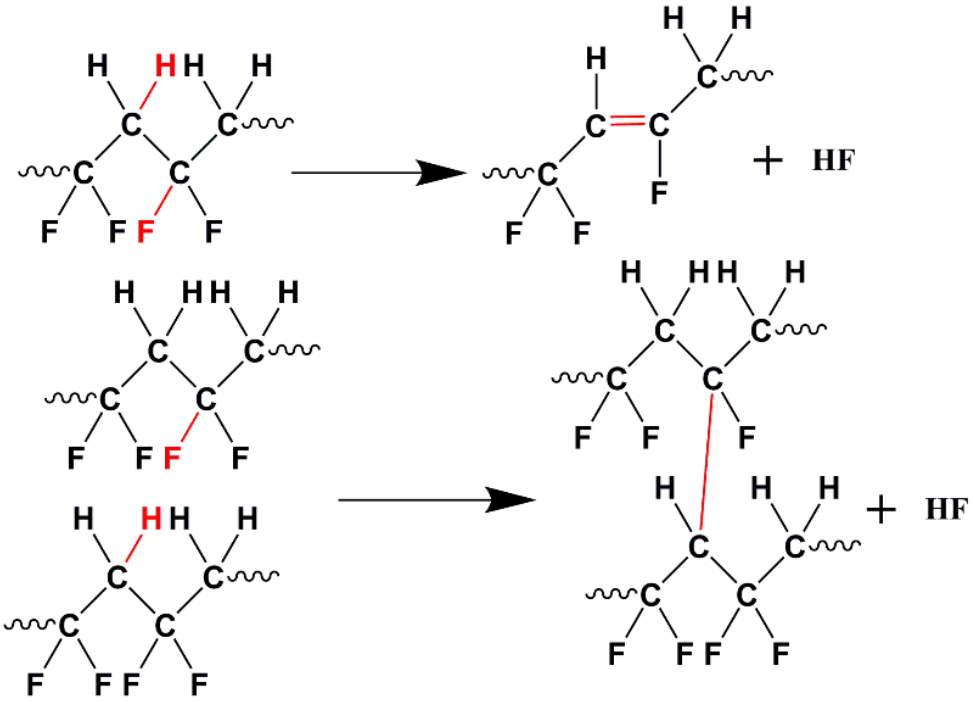

Figure 1.11. Dehydrofluorination of PVDF

1.4 Dissertation Overview

In the following section, a detailed description of the research performed in each chapter is provided:

Chapter 2 investigates the effects of dehydrofluorination on the crystallization behavior of PVDF using a molecular simulation method. It begins with a brief overview of defect-engineered P(VDF-TrFE) copolymers and its terpolymers which preferentially crystallize in β-phase. The mechanism of the crystallization behavior of P(VDF-TrFE) is discussed and investigated for the first time with a molecular simulation method. The results provide a quantitative explanation of how bulkier comonomers change the potential energy levels of each crystalline phase in PVDF and lead to preferential crystallization. Based on the same defect-engineering strategy, the model of P(VDF-fluoroethyne) copolymer, which can be experimentally prepared through dehydrofluorination, is built and investigated using the same molecular simulation method. The results demonstrate that the β-phase formation can be promoted when a certain fraction of double bonds is introduced into PVDF. These findings provide the theoretical proof for the efficacy of using dehydrofluorination to prepare β-phase PVDF.

Chapter 3 focuses on the development and optimization of the dehydrofluorination process. It begins with an introduction to the experimental process of PVDF dehydrofluorination and the chemical characterization techniques which were used in this study. Methods to calculate the dehydrofluorination extent and β-phase fraction of dehydrofluorinated PVDF is developed based on the characterization results. Furthermore, the effect of experimental parameters such as dehydrofluorination agents, concentration, and reaction time are investigated in Chapter 3. The results provide experimental proof of promoted β-phase formation in dehydrofluorinated PVDF. High ferroelectric properties are observed from the dehydrofluorinated PVDF indicating the formation of large β-phase domains. Eventually, a relationship between dehydrofluorination extent and β-phase fraction is quantified for the first time, and a set of optimized reaction conditions for manufacturing high β-phase PVDF is provided. The findings of this chapter open a new approach to large-scale manufacturing of high β-phase PVDF.

As the efficacy of dehydrofluorination-induced β-phase PVDF has been proven theoretically and experimentally in last two chapters, Chapter 4 focuses on the investigation of the piezoelectricity and thermal stability of the dehydrofluorinated PVDF. Different piezoelectric

characterization methods are performed on dehydrofluorinated PVDF to evaluate its piezoelectric performance through both direct and inverse piezoelectric effects. Giant piezoelectric strain coefficients of d_{33} = -65.59±0.71 pm/V and d_{31} = 25.12±1.13 pC/N are measured from dehydrofluorinated PVDF, which are the highest piezoelectric coefficients reported for all PVDF based polymers to date. The investigation of the thermal stability of β-phase in dehydrofluorinated PVDF further demonstrates the preferential crystallization behavior induced by dehydrofluorination. The results show that the β-phase fraction of dehydrofluorinated PVDF can be preserved through cycles of melting and cooling processes below an upper limit temperature of 210 ˚C. The results demonstrate that the developed PVDF is a worthwhile candidate with great potential for low-cost, high-performance commercial applications of piezoelectric materials.

Chapter 5 of this dissertation develops two additive manufacturing techniques for fabricating piezoelectric devices based on dehydrofluorinated PVDF. The first technique is a direct-writing method that can print 2D patterns of PVDF with precisely controlled thickness while perfectly preserving the β-phase fraction of dehydrofluorinated PVDF. Energy harvesters and bilayer actuators based on dehydrofluorinated PVDF are fabricated through the direct-writing method. The developed stretching mode energy harvester based on dehydrofluorinated PVDF shows a high power density of 21.96 mW/cc which is over 3 times higher than the same device fabricated by the state-of-the-art drawn PVDF. The second technique is the electrospin-assisted 3D printing method, which can achieve micro-level high resolution printing of PVDF 3D structures meanwhile provide *in situ* stretching and electric poling to maximize the piezoelectric performance. A breathable and wearable PVDF energy harvester is fabricated using this method and a decent voltage response is observed. The results demonstrate that high-performance piezoelectric energy harvesters and actuators can be fabricated in a convenient and efficient way by integrating dehydrofluorinated PVDF into additive manufacturing methods. Such findings provide novel approaches to the development of future piezoelectric devices.

The final chapter of this dissertation starts with a brief overview of the findings throughout the dissertation. After the overview, the contributions of this dissertation and their possible influence on future research investigating piezoelectric polymers is discussed. Additionally, the final section of this chapter describes potential future work that can be conducted.

CHAPTER 2

Study of Crystallization Behavior of Dehydrofluorinated PVDF

2.1 Chapter Introduction

This chapter focuses on the effects of dehydrofluorination on the crystallization behavior and crystalline phase composition of PVDF. The hypothesis of this chapter is that the dehydrofluorination changes some of the VDF repeating units to double bond (-HC=CF-, or fluoroethyne) units which will bring steric defects into crystalline PVDF thus impacting the phase composition. In order to build the theoretical basis and prove this hypothesis, this chapter begins with a review of previous studies of the crystallization behavior of the copolymer and terpolymers of PVDF. The influences of introducing foreign comonomers of different dipole moments and steric effects into the PVDF crystalline regions will be discussed with a focus on the crystalline structures, dielectric properties, and ferroelectric properties of the copolymer and terpolymers. A computational analysis will be designed and performed for the P(VDF-TrFE) copolymer to achieve a quantitative understanding of the mechanism of its preferential crystallization behavior. Molecular models of dehydrofluorinated PVDF will also be built and analyzed using the same computational method to predict the crystallization behavior. It will therefore be demonstrated that fluoroethyne units introduced by dehydrofluorination can increase the planar chain conformation of PVDF thus leading to more β-phase formation. These results provide a theory explaining how dehydrofluorination is able to impact the crystallization behavior of PVDF and improve the fraction of the piezoelectric phase. The key contribution of this chapter is to provide a better understanding of the crystallization behavior of PVDF and the effects of comonomers, and to provide another solution to prepare high β-phase PVDF through chemical modifications.

2.2 Promoted β-phase Formation in PVDF Copolymers and Terpolymers

In previous research, many PVDF copolymers have been synthesized and reported due to their unique electroactive properties. Commonly reported comonomers include trifluoroethylene

(TrFE), 1,1-chlorofluoroethylene (CFE), chlorotrifluoroethylene (CTFE) and hexafluoropropylene (HFP) (Figure 2.1).(168-170) These comonomers are widely used to adjust the ferroelectric and piezoelectric properties of VDF based polymers by affecting the structure of the crystalline and ferroelectric domains.(171, 172) Studying the effects of comonomers on the crystallization behavior of PVDF can help theorize the mechanism of promoted β-phase formation in dehydrofluorinated PVDF.

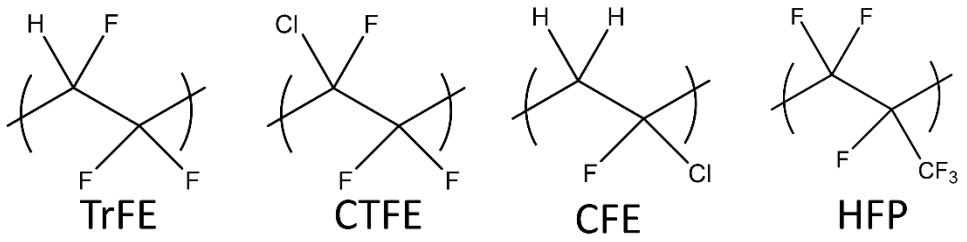

Figure 2.1. Repeating units of common comonomers of PVDF based polymers.

Among the previously mentioned copolymers, P(VDF-TrFE) copolymers have attracted the most attention and been preferred over PVDF homopolymers for many piezoelectric and ferroelectric applications.(69, 164) The P(VDF-TrFE) copolymers were first reported in the early 1980s as a better alternative material to the PVDF homopolymer due to their high ferroelectric properties.(72, 157) Unlike the PVDF homopolymer which needs mechanical stretching to achieve β-phase, P(VDF-TrFE) copolymers can crystallize into a ferroelectric phase with all-trans conformation, similar to the β-phase of PVDF, directly from melt or solvent casting.(157) This preferential formation of the ferroelectric phase of P(VDF-TrFE) provides access to various processing methods such as solvent-casting, inkjet printing, and 3D printing thus providing an advantage over traditional PVDF homopolymers.(27, 158, 173, 174) The mechanism of this crystallization behavior has yet to be thoroughly investigated, but the reason for promoted β-phase formation is anticipated to be a result of the slight structural differences in the ferroelectric phases of the P(VDF-TrFE) copolymer and PVDF homopolymer. Farmer *et al.* first reported that the replacement of hydrogen atoms by fluorine atoms in the PVDF chains would strongly influence the polymorphic crystallization behavior of PVDF.(155) Although their study focused on the effects of head-to-tail isomerism in PVDF polymerization, they provided changes in the potential energy of each chain conformation (all-trans for β-phase and TGTG' for α-phase) when -CF_2-CF_2-

segments were introduced by head-to-head/tail-to-tail defects. Their results show that the potential energy level of TGTG' conformation increases significantly with an increase in -CF_2-CF_2- segment percentage, which leads to a preferential crystallization in β-phase for the whole polymer system. Lando *et al.* claimed that this increase of potential energy in TGTG' conformation is attributed to the increased steric effects caused by the larger fluorine atoms.(175, 176) Since the distance between the fluorine atom and hydrogen atom on adjacent carbons of TGTG' conformation chain (2.30 Å) are smaller than the sum of van der Waals radius of two fluorine atoms ($R_{van\ der\ Waals}$(F)=1.47 Å) (Figure 2.2), the replacement of a fluorine atom at the position originally occupied by a hydrogen atom would induce significant strain in α-phase crystals. However, the strain induced in the all-trans conformation chains is minimal because the distance between the adjacent hydrogen atom and fluorine atom is larger (2.56 Å).(177) In the case of the P(VDF-TrFE) copolymer, the addition of TrFE units to the backbone of PVDF would also increase the steric hindrance in TGTG' conformation chains, leading to a higher potential energy level for α-phase formation. These bulky TrFE units act as defects in the crystalline region of PVDF and create a localized higher energy barrier for the formation of TGTG' conformation. The formation of α-phase domains is interrupted, while the energy level of the formation of β-phase domains is unaffected. As a result, P(VDF-TrFE) copolymers can always crystallize in a β-phase conformation in most processing methods.

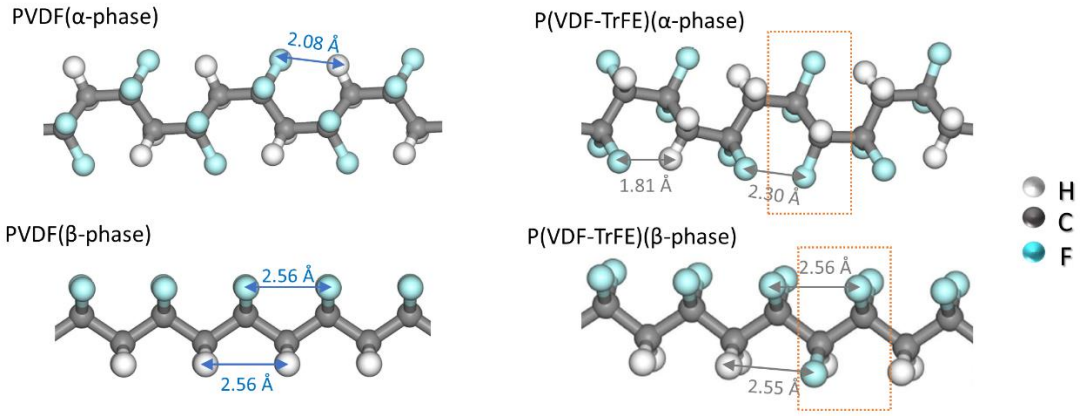

Figure 2.2. Interatomic distance changes between PVDF and P(VDF-TrFE) copolymer in both α-phase and β-phase chain conformation.

The steric effects of introducing TrFE units also lead to changes in intermolecular interactions between neighboring polymer chains in the crystalline region. Because of the introduction of large fluorine atoms, the interchain distances of the all-trans conformation phase of the copolymer is noticeably increased.(178, 179) These bulky units of TrFE act as defects in the crystalline region of PVDF, occupying more space and allowing a more flexible dipole rotation along the chain axis. The increased interchain space and chain flexibility will also contribute to the formation of polar β-phase by further lowering the intermolecular van der Waals effects. This will reduce the energy barrier created by steric hindrance so that the state of lowest intermolecular electrostatic potential energy, in which chains of dipoles are parallelly packed and oriented, can be easier to achieve. On the other hand, the increased interchain distances in the crystalline region of P(VDF-TrFE) lead to significant changes in several bulk properties such as density, elastic modulus, and melting point.(156, 159, 180) Such changes in properties can be used as evidence to reflect the effects of the comonomers. In addition to bulk material properties, the dielectric and ferroelectric properties of P(VDF-TrFE) are also significantly changed due to the comonomers.(29, 73, 157, 179) Because of the increase in the interchain distances, the energy barriers for dipole rotation along the chain axis are reduced which leads to a higher dielectric constant.(13, 168, 171) This decreased energy restriction on dipole motions also results in a low Curie temperature; previous research shows that the Curie temperature of P(VDF-TrFE) copolymers decreases significantly with increasing TrFE ratio.(157, 164)

Other comonomers such as CFE, CTFE, and HFP are also widely used to adjust the properties of the PVDF based copolymer. However, these comonomers cannot promote the β-phase formation by simply copolymerizing with PVDF. This is because CFE, CTFE, and HFP units are too big to be included in the crystalline region of PVDF in the copolymer.(30, 169, 172) Furthermore, a large fraction of these large comonomers will decrease the degree of crystallinity of the copolymer.(181, 182) However, these comonomers can be utilized by adding them to the copolymerization of VDF and TrFE, with a small molar ratio, to form a terpolymer (Figure 2.3). Since TrFE units can be crystallized together with VDF units and increase the interchain distances between crystallized chains, it is possible for large comonomers to be included into the crystalline region of P(VDF-TrFE). The interdiction of large comonomers will induce a more steric effect and further increase the interchain distances.(183) The formation of β-phase is still dominant in the crystallization, but the ferroelectric properties of the terpolymers is significantly different from

PVDF and P(VDF-TrFE) copolymers. It is reported that large comonomers like CFE and CTFE bring a 'pin' effect to the ferroelectric domains of PVDF.(170) Because of their different dipole moments and strong intermolecular interaction, these large comonomers interrupt the large ferroelectric domains and bundle a few VDF and TrFE dipoles together to form smaller domains. Such changes in ferroelectric domains provide a relaxor ferroelectric behavior to the terpolymer.(30, 168)

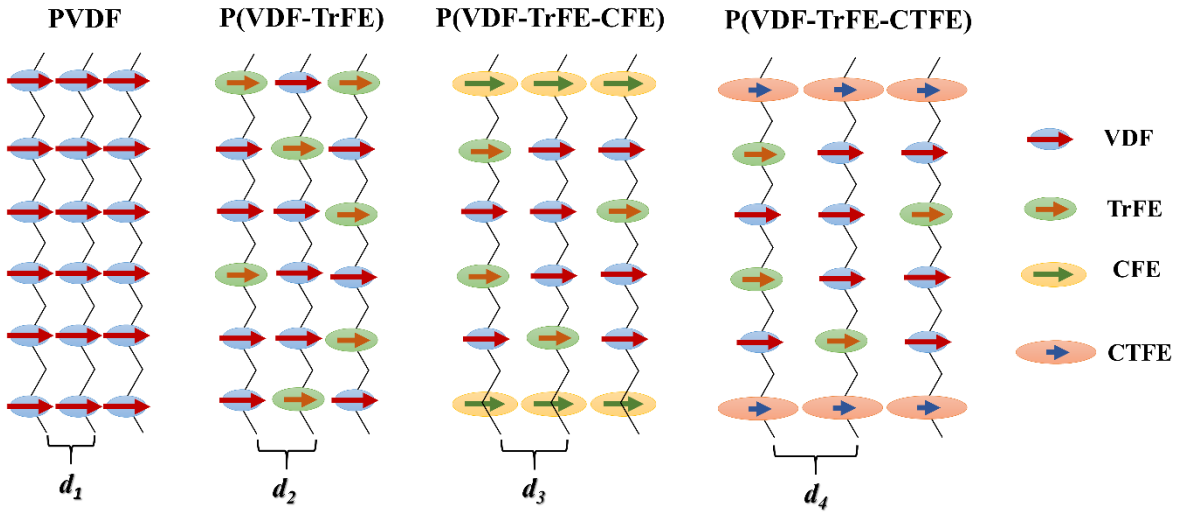

Figure 2.3. β-phase crystalline domains of PVDF's copolymer and terpolymers. The arrows represent the dipole moments. The interchain distance $d_1 < d_2 < d_3 < d_4$.

2.3 Computational Study of the Crystallization of P(VDF-TrFE) Copolymers

In order to quantify the steric hindrance brought by TrFE units and its effects on the crystallization behavior, P(VDF-TrFE) polymer chain models of TGTG' conformation (α-phase) and all-trans conformation (β-phase) with varying VDF: TrFE ratios are built. The conformational potential energy of these molecule models is calculated through molecular simulations by means of Materials Studio software. The polymer chain models are built according to the crystal parameters of α-phase and β-phase PVDF as reported by Lando *et al.* and Doll *et al.*, and a geometry optimization function from Material Studio software is applied after the TrFE units are introduced.(184, 185) Each polymer chain model contains 20 repeating units, with 0% to 50% of VDF units at random locations replaced by TrFE units. The conformational potential energy of

these polymer chains is expressed as a sum of bonded, van der Waals, and electrostatic terms as shown in the following equation (Equation 2.1) (186):

$$E_{total} = E_{bonded} + E_{vdW} + E_{es} \qquad \text{Equation 2.1}$$

where the bonded term E_{bonded} accounts for the potential energy changes due to bond stretching, bending, torsional bending, out-of-plane wagging, and bond-bond coupling, the van der Waals term E_{vdW} accounts for the potential energy changes from intramolecular van der Waals interactions, and the electrostatic term E_{es} accounts for the energy changes from electrostatic interactions. The Condensed-phase Optimized Molecular Potentials for Atomistic Simulation Studies (COMPASS) force field as incorporated in the Forcite function in Material Studio software is used to calculate the conformational potential energy of each polymer chain model.(186, 187) The parameters of the atomic partial charges are assigned by the COMPASS force field fitting to experimental and *ab initio* data. For a PVDF chain, the calculation results indicate that the all-trans conformer has higher energy than the TGTG' conformer, and the energy difference is ~20 kcal/mol (Figure 2.4a). It shows that although the all-trans conformer has a lower van der Waals term, its electrostatic term is much higher than that of the TGTG' conformer since the parallel alignment of the dipoles is not energy preferable. However, when the TrFE unit is introduced into the polymer chains, the van der Waals term of the TGTG' conformer increases significantly, indicating a largely increased steric effect. Meanwhile, the difference between the electrostatic terms of the two conformers becomes smaller when a large fraction of TrFE units replaces VDF units. As a result, the total conformational potential energy of the all-trans conformer is lower than that of the TGTG' conformer after over 10% of VDF repeating units are replaced by TrFE units, as shown in Figure 4a. The energy difference between the two conformers increases with increasing TrFE fraction. For a polymer chain with VDF: TrFE ratio of 50:50, the conformational potential energy difference is 87.5 kcal/mol, which is much higher than the energy difference between the TGTG' and all-trans conformer of pure PVDF. This indicates that the β-phase possesses high stability in the P(VDF-TrFE) copolymer with a TrFE fraction above 10%, and the formation of β-phase from these copolymers by most processing methods is energy-wise preferential. The simulation results are consistent with previously reported experimental research on P(VDF-TrFE) copolymers which conclude that the coexistence of α-phase and β-phase is only observed in copolymers with a low fraction of TrFE. (178, 179)

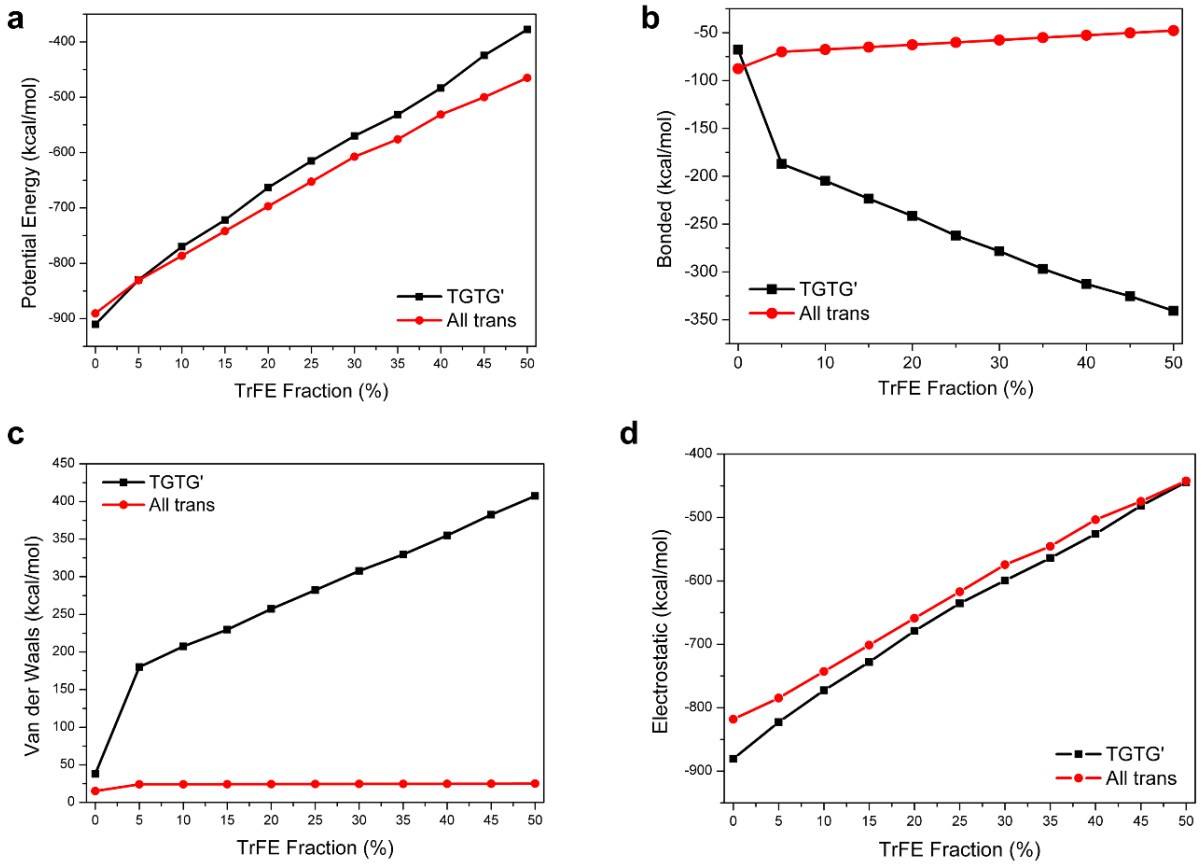

Figure 2.4. Conformational potential energy of P(VDF-TrFE) with varying TrFE fraction: (a) total potential energy, (b) bonded term E_{bonded}, (c) van der Waals term E_{vdW}, and (d) electrostatic term E_{es}.

The mechanism of the preferential crystallization in the P(VDF-TrFE) copolymer can be further confirmed by investigating the contributions from the three energy terms. The introduction of TrFE units leads to a tightly packed structure (more space is occupied) in α-phase, which leads to a decreased bonded term, E_{bonded}, in a TGTG' conformer model (Figure 2.4b). However, this tight packing causes significant steric effects in the whole molecule. The van der Waals term, E_{vdW}, of the TGTG' conformer is largely increased when TrFE units replace VDF units (Figure 2.4c). On the other hand, the TrFE units do not have significant impacts on the steric structure of the β-phase because the extra fluorine atom is placed on the hydrogen side of the backbone which has low space-occupancy. As a result, both the bonded term, E_{bonded}, and van der Waals term, E_{vdW}, in the all-trans conformer are almost unaffected by the increasing fraction of TrFE units. The energy difference between the E_{vdW} of the two conformers is much greater than the energy

difference between the two E_{bonded} of the two conformers, indicating intramolecular van der Waals interactions are the major factor in determining the potential energy levels of the molecular conformations. The electrostatic term, E_{es}, is increasing in both conformers along with increased TrFE units because of the addition of new negatively charged fluorine atoms (Figure 2.4d). The E_{es} term of an all-trans conformer is always higher than that of a TGTG' conformer in any TrFE fractions because the oriented dipoles in the all-trans conformer lead to higher potential energy. However, since the introduced TrFE units possess lower dipole moments than the VDF unit, the difference between the electrostatic terms is slightly decreased along with the increased TrFE fraction. As a result, the total conformational potential energy of the all-trans conformation becomes lower than that of the TGTG' conformation with the introduction of the TrFE unit, and this change in potential energy is significantly affected by the intramolecular van der Waals interactions. Such results quantitatively demonstrate the mechanism of the preferential crystallization in P(VDF-TrFE) copolymers and further validate the steric defect theory reported previously. Additionally, this molecular simulation method provides a new strategy in designing modified PVDF based fluoropolymers with high β-phase.

2.4 Computational Prediction of the Crystallization Behavior of Dehydrofluorinated PVDF

The dehydrofluorination method, which introduces double bonds to promote the β-phase formation in PVDF, follows the defect-engineering concept brought up in the research of P(VDF-TrFE) copolymers. The introduced fluoroethyne units satisfy two requirements that can be summarized from previous research to induce high β-phase formation and high piezoelectricity: first, the double bond containing unit is bulkier than VDF, so it may induce extra steric effects, and second, the size of the fluoroethyne unit is close to VDF units, so it will not be excluded from the crystalline region of PVDF. In order to predict the crystallization behavior of dehydrofluorinated PVDF and prove the efficacy of this double bond introducing method, fluoroethyne-containing PVDF polymer chain models of TGTG' conformation (α-phase) and all-trans conformation (β-phase) with varying fluoroethyne ratios are built. The crystal parameters of α-phase and β-phase PVDF reported by Lando *et al.* and Doll *et al.* are used to build the PVDF backbone.(184, 185) Similar to the P(VDF-TrFE) models, each polymer chain model contains 20 repeating units, and the double bonds are introduced into the PVDF backbone by replacing VDF

units with fluoroethyne units at random positions along the polymer chain. The geometry optimization function from Material Studio software is then applied after fluoroethyne units are introduced. Considering the trans-cis isomerism of carbon-carbon double bonds, four sets of polymer chain models are built to investigate all possible regional chain conformations (Figure 2.5): cis conformation double bonds within α-phase (TGTG'-cis), trans conformation double bonds within α-phase (TGTG'-trans), cis conformation double bonds within β-phase (alltrans-cis), and trans conformation double bonds within β-phase (alltrans-trans). Among these four scenarios, TGTG'-trans and TGTG'-cis lead to the formation of α-phase, while only alltrans-trans leads to the formation of β-phase. Decreased interatomic distances between the hydrogen/fluoride atom on the fluoroethyne unit and the fluoride/hydrogen atom on the adjacent VDF unit are observed from both α-phase conformers (TGTG'-trans and TGTG'-cis, from 2.08 Å to 1.90 Å and 1.85 Å, respectively). This indicates that the introduction of double bonds can induce extra steric effects into the α-phase of PVDF. However, such interatomic distances in β-phase conformers are increased (Alltrans-trans and all trans-cis, from 2.56 Å to 2.63 Å and 2.62 Å, respectively), indicating less steric effects after the introduction of double bonds.

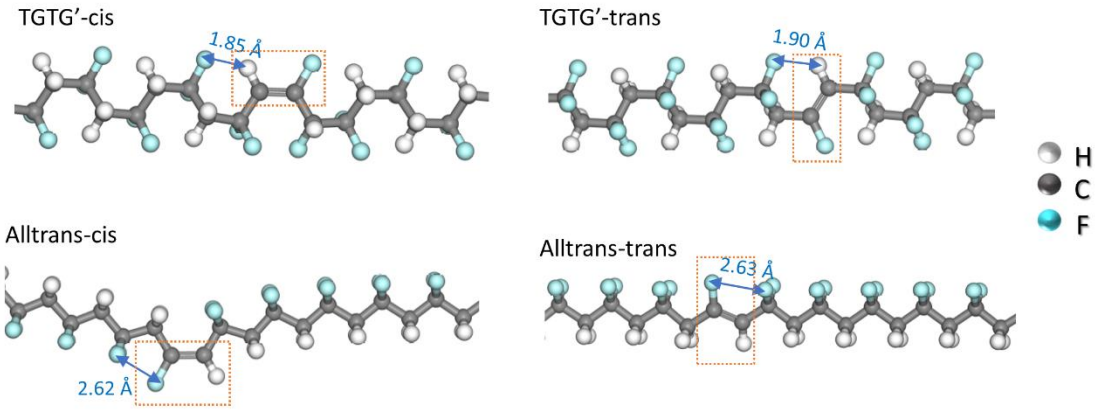

Figure 2.5. The four regional chain conformations of double bonds containing PVDF.

The potential energy surfaces of the polymer chain models are again assigned by the COMPASS force field as incorporated in the Materials Studio software.(186) The resulting conformational potential energy of the four models are shown in Figure 2.6. The alltrans-cis conformer possesses the highest potential energy due to a shift of the dipole direction in the all-trans conformation chain caused by the double bond in the cis conformation. This leads to high

energy level in both E_{vdW} and E_{es} terms. Among the remaining three models, the alltrans-trans conformer becomes the most energy preferable model after 10% of fluoroethyne units is introduced. The total conformational potential energy of the alltrans-trans conformer containing 10% double bonds is 2.451 kcal/mol lower than the TGTG'-cis conformer and 26.404 kcal/mol lower than the TGTG'-trans conformer with same fraction of double bonds. At a fluoroethyne: VDF ratio of 50:50, the energy differences between the alltrans-trans and the TGTG'-cis conformer and between the alltrans-trans and the TGTG'-trans conformer are 169.891 kcal/mol and 74.832 kcal/mol respectively. Thus, the potential energy differences between the two phases is even larger than that of the P(VDF-TrFE) copolymers discussed above, indicating that the method of introducing double bonds is very efficient in promoting β-phase formation. PVDF containing the double bond is expected to exhibit a preferential crystallization to β-phase from melt and solvent casting in addition to other processing methods. The major factor leading to this change in crystallization behavior is still the van der Waals interaction which shows that the E_{vdW} terms of TGTG'-trans and TGTG'-cis conformers are higher than the E_{vdW} term of the alltrans-trans conformer. The E_{vdW} terms are also increasing with increased fraction of fluoroethyne units due to increasing steric hindrance. Meanwhile, the E_{vdW} term of the alltrans-trans conformer is decreased after the introduction of fluoroethyne units, indicating reduced steric effects from the double bonds. The bonded term, E_{bonded}, is observed to be increasing with increasing fraction of fluoroethyne units in all conformers as a result of the bulky double bonds inducing more restrictions in bond motion. However, unlike P(VDF-TrFE), E_{bonded} of the alltrans-trans conformer is lower than that of the TGTG' conformers because of the planar conformation of the double bond and the whole polymer chain. Thus, the energy differences between E_{bonded} terms further contribute to the preferential crystallization of β-phase.

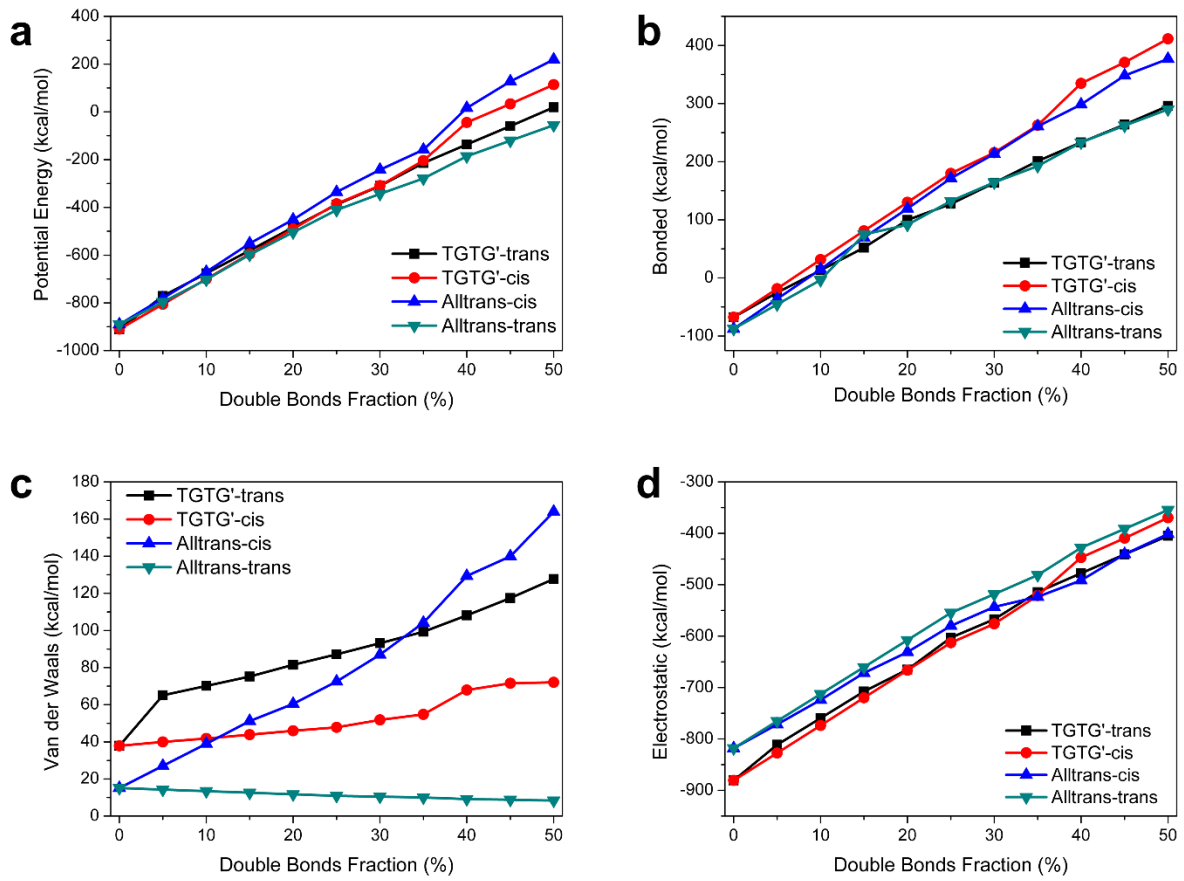

Figure 2.6. Conformational potential energy of the four double bonds containing PVDF models with different carbon-carbon double bond fractions. (a) Total potential energy, (b) bonded term, E_{bonded}, (c) van der Waals term, E_{vdW}, and (d) electrostatic term, E_{es}.

To simulate the intermolecular interactions of dehydrofluorinated PVDF chains in the crystalline region, a set of supercell models is built, and their potential energy is calculated and compared. To build the supercell model, the crystalline unit cell of both α-phase and β-phase are first built according to the atomic coordination parameters reported by Lando *et al.* and Doll *et al.*(184, 185) Each unit cell contains two polymer chains, and each chain contains two repeating units. The supercell model is created by repeating the unit cell 10 times along the chain axis to build a larger crystalline unit cell containing two polymer chains of 20 repeating units (Figure 2.7). The introduction of double bonds is done by replacing VDF units with fluoroethyne units at random positions in the supercell model. The introduced fluoroethyne unit follows the regional

chain conformation cases except in the alltrans-cis scenario because the cis conformation double bond cannot fit into the β-phase unit cell. The COMPASS force field in the Materials Studio software is again used to assign the parameters of the atomic partial charges of these supercell models.(186) Finally, the potential energy of the supercell model is calculated through the Forcite module in Materials Studio. The supercell model allows this calculation to include both the effects of intermolecular interactions within the unit cell as well as the interactions with the symmetric unit cells adjacent to the boundaries of the supercell.

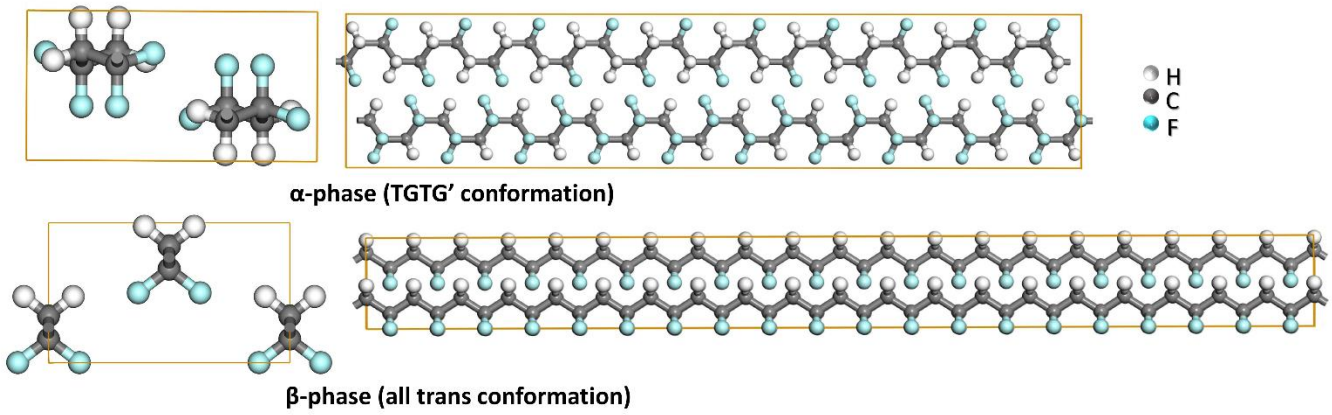

Figure 2.7. Supercell model of α-phase (top) and β-phase (bottom) PVDF.

The total potential energy as well as the E_{bonded}, E_{vdW}, and E_{es} terms of the supercell models are shown in Figure 2.8. The trends in the energy changes are found to be similar to the results of the single chain simulation discussed previously. The total potential energy of the TGTG'-trans and TGTG'-cis are both lower than that of the alltrans-trans at a low fraction of double bonds. However, the alltrans-trans model becomes the most energy preferential conformation when the fraction of double bonds is above 25% as it possesses an energy level that is 65.34 kcal/mol lower than the TGTG'-trans and 333.03 kcal/mol lower than the TGTG'-cis conformations. The energy differences increase as additional double bonds are introduced, indicating the formation of β-phase is more preferential in regard to potential energy. In this supercell simulation, both α-phase models (TGTG'-trans and TGTG'-cis) exhibit much higher E_{bonded} and E_{vdW} terms in comparison to the β-phase model. The E_{es} term of the alltrans-trans model is significantly higher than that of the α-phase models, but the energy differences between the E_{es} terms are decreased by the introduction of double bonds. When considering the intermolecular interactions of multiple polymer chains in

the crystalline region of PVDF, the electrostatic interactions become the major factor in determining the energy preferential phase in PVDF. The energy difference between the alltrans-trans model and the TGTG'-trans model decreases from 553.07 kcal/mol for pure PVDF to 113.968 kcal/mol for PVDF containing 50% double bonds. All three terms (E_{vdW}, E_{bonded}, and E_{es}) contribute to the low potential energy of β-phase in PVDF with an increasing fraction of double bonds. These simulation results further confirm the theoretical efficacy of the presented method using double bonds to promote the formation of β-phase in PVDF.

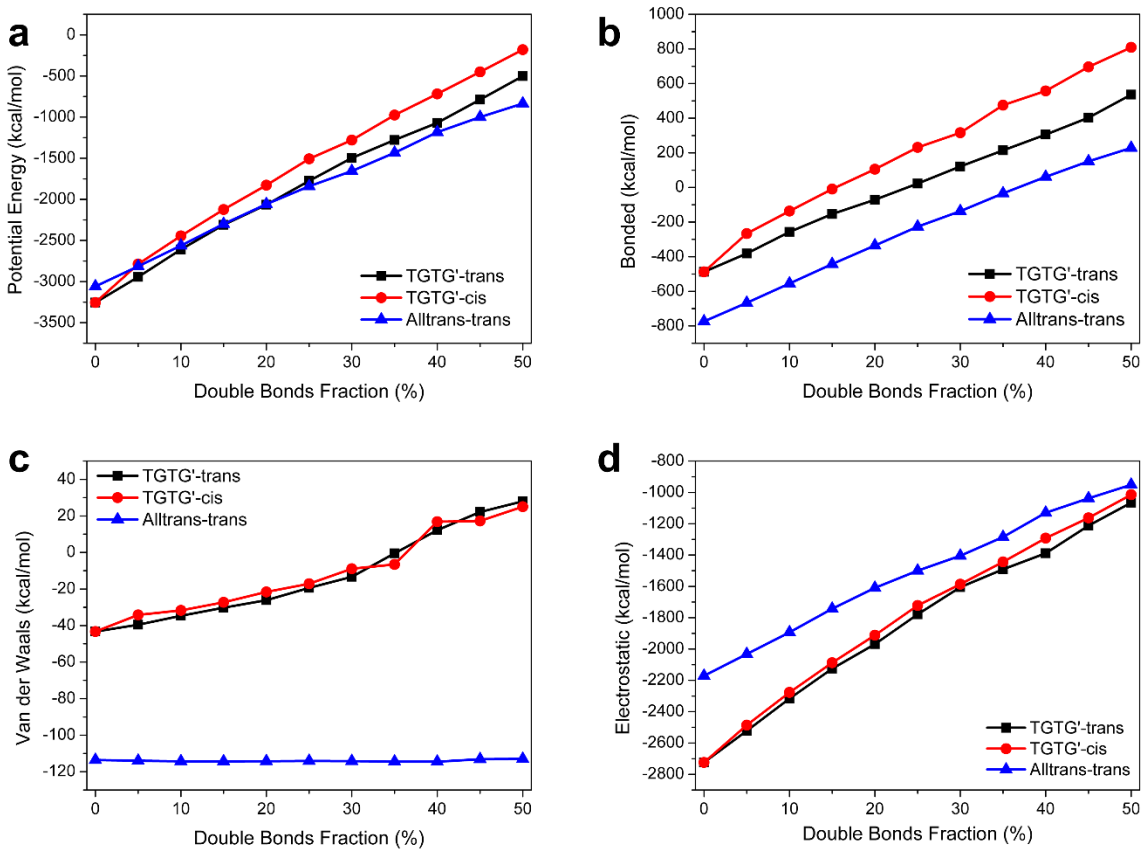

Figure 2.8. Conformational potential energy of the three double bonds containing PVDF supercell models with different carbon-carbon double bond fractions. (a) Total potential energy, (b) bonded term, E_{bonded}, (c) van der Waals term, E_{vdW}, and (d) electrostatic term, E_{es}.

2.5 Chapter Summary

In this chapter, the crystallization behavior and mechanism of the defect-engineered PVDF copolymer and terpolymers are investigated. As has been claimed in previous research, the

preferential β-phase formation in P(VDF-TrFE) and other PVDF copolymers is induced by the steric defects brought by larger and stiffer comonomers. In this work, this conclusion is proven quantitatively for the first time by a molecular simulation of the factors contributing to the conformational potential energy of PVDF. The newly developed simulation method successfully demonstrates that the potential energy changes of both α-phase and β-phase in P(VDF-TrFE) is mainly controlled by the changes in intramolecular van der Waals interaction due to the TrFE units. The method further predicts that β-phase formation will be dominant in P(VDF-TrFE) with a TrFE fraction above 10%, which is consistent with reported experimental data.

The crystallization behavior of dehydrofluorinated PVDF is analyzed theoretically and predicted by the molecular simulation method. Intramolecular models and intermolecular models of PVDF crystals containing dehydrofluorination-induced double bonds are built and analyzed. The simulation results of both models indicate the preferential crystallization of β-phase in dehydrofluorinated PVDF with a sufficient double fraction above 10~20%. Detailed investigation shows that the introduction of double bonds effectively increases the van der Waals potential energy of α-phase while maintaining the conformational potential energy of β-phase at a lower level. These results theoretically prove the efficacy of dehydrofluorination in promoting the formation of β-phase in PVDF and demonstrate the mechanism of this change in crystallization behavior. In the next chapter, the efficacy of dehydrofluorination method will be further demonstrated through experimental approaches. A series of dehydrofluorinated PVDF samples are prepared using different dehydrofluorination agents and reaction conditions. Their crystalline structure and dielectric properties will be investigated to correlate their phase composition with the extent of dehydrofluorination.

CHAPTER 3

Development and Optimization of Dehydrofluorination Process for High β-phase PVDF

3.1 Chapter Introduction

The following chapter focuses on the optimization of the dehydrofluorination process of PVDF to maximize the β-phase fraction obtained through the proposed chemical modification method. In order to develop a slowly-induced, controllable dehydrofluorination method, the effects of experimental parameters such as dehydrofluorination agents, agent concentration, and reaction time are investigated in a series of controlled experiments. The extent of dehydrofluorination and the fraction of carbon-carbon double bonds are characterized and used as criteria to control the experimental parameters of the modification process. In this chapter, the phase compositions of dehydrofluorinated PVDF are investigated by chemical and ferroelectric characterization methods. The results provide experimental evidence for the conclusions obtained from previous molecular simulations, showing that the dehydrofluorination process can effectively promote the β-phase formation in PVDF. The fraction of β-phase in the treated PVDF is measured and correlated to the extent of dehydrofluorination. The correlation between β-phase fraction and double bond fraction of PVDF is also found to be consistent with the predictions from the molecular simulation study. Ferroelectric properties of dehydrofluorinated PVDF are also investigated to further confirm the formation of large β-phase domains. The results are then used to develop an optimized dehydrofluorination process that maximizes the piezoelectric and dielectric properties of PVDF.

3.2 Preparation and Characterization of Dehydrofluorinated PVDF

As previously mentioned, the dehydrofluorination reaction takes place when PVDF is subjected to a basic or high temperature environment. Mostly, dehydrofluorination leads to the formation of carbon-carbon double bonds on the backbone of the PVDF polymer chain by

removing the hydrogen and fluoride atoms bonded on adjacent carbon atoms which form a molecule of hydrogen fluoride (HF). In some cases where massive and rapid dehydrofluorination occurs, nonadjacent dehydrofluorinated carbon atoms occasionally bond to form a crosslink between PVDF polymer chains.(167, 188) To induce dehydrofluorination uniformly in PVDF, the reaction is usually done in a low concentration solution of PVDF. In this study, we found that the dehydrofluorination can be conveniently terminated by mixing the reaction solution with water to precipitate PVDF from the solution. A typical dehydrofluorination reaction is conducted as follows (Figure 3.1): PVDF is first dissolved in N, N-dimethylformamide (DMF) at room temperature with a weight fraction in the range of 5% to 15 %. Then a dehydrofluorination agent is added into the PVDF/DMF solution. The concentration of the dehydrofluorination agent is controlled by the molar ratio between the agent and the repeating units in the solution (Agent: VDF ratio). After thorough vortex mixing, the solution is kept at room temperature. The reaction time depends on the type of dehydrofluorination agents and can range from a few minutes to weeks. After the reaction, the PVDF solution is slowly mixed into distilled water to terminate the reaction by precipitating PVDF from the solution. The precipitates are collected and washed using distilled water three times to completely remove the residual dehydrofluorination agent. The washed PVDF is then dried under vacuum at 80 ºC overnight. The prepared PVDF can be dissolved into a DMF solution again to prepare thin films or can be used directly for other processing methods.

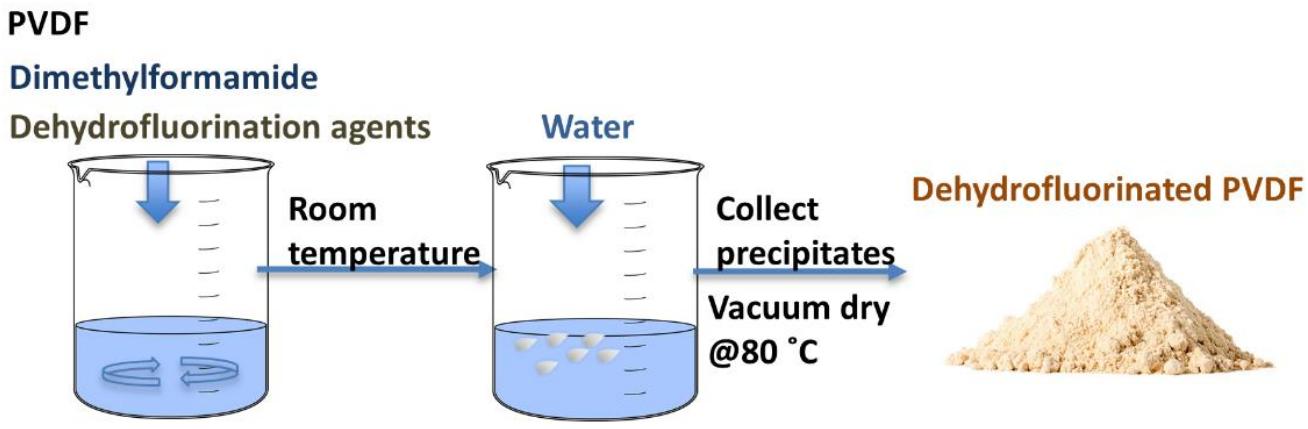

Figure 3.1. Scheme of the experimental process of PVDF dehydrofluorination

In order to measure the extent of reaction and phase composition of the dehydrofluorinated PVDF, thin films of dehydrofluorinated PVDF are prepared. The PVDF solution is spread uniformly onto glass substrates through doctor blading or a direct writing method. The samples are then kept under vacuum at 80°C for solvent evaporation. An optional annealing process is performed on the dried film to increase the crystallinity of the PVDF film. The annealing process is conducted by heating the PVDF film while still on the glass substrate up to 200°C, then holding for 20 minutes before slowly cooling down to room temperature over 5 hours (cooling rate ~0.5 °C/min).

The extent of dehydrofluorination is characterized by combustion elemental analysis. Combustion elemental analysis is a method used to determine the elemental composition of a pure organic compound by combusting the sample under specific conditions where the combustion products can be analyzed quantitatively. In this work, the weight fraction of the carbon, hydrogen and fluoride elements contained in the PVDF are measured by combustion analysis. The combustion experiments are conducted by Micro-Analysis, Inc. The fractions of carbon and hydrogen are then measured according to the ASTM standard D5291. The fraction of fluoride is measured by converting the fluoride to the ionic form by oxygen flask combustion, followed by ion chromatography. During dehydrofluorination, the percentage of the fluoride element is supposed to decease noticeably because of the loss of HF molecules. This change in composition will be measured by combustion analysis and can be used to calculate the reaction extent. The extent of dehydrofluorination, *%DHF*, is given by the following equation based on the fraction of lost fluoride:

$$\%DHF = \frac{\%F_0 - \%F}{\%F_0 - \%F_u} \times 100\% \qquad \text{Equation 3.1}$$

where *%DHF* is the percentage of dehydrofluorinated VDF units in PVDF, *%F* is the weight fraction of fluoride in the tested sample measured from the combustion analysis, $\%F_0$ is the weight fraction of fluoride in untreated PVDF, which is supposed to be 59.375%, and $\%F_u$ is the weight fraction of the PVDF in which all repeating units have been dehydrofluorinated to carbon-carbon double bonds, which is supposed to be 43.182%. It should be noted that according to this equation, *%DHF* reaches 100% when only half of the fluoride atoms are lost due to

dehydrofluorination. It is possible for a *%DHF* value above 100%, which indicates that some repeating units are dehydrofluorinated twice to form carbon-carbon triple bonds.

The fraction of carbon-carbon double bonds induced by dehydrofluorination is characterized by X-ray photoelectron spectroscopy (XPS). XPS is a surface-sensitive quantitative chemical characterization technique that measures the elemental composition and electronic state of elements within the tested material. XPS can accurately measure the kinetic energy and number of electrons that escape from the surface of the material under X-ray irradiation, with a measurement depth of ~10 nm. The XPS measurement of PVDF is performed by a Kratos Axis Ultra XPS. The C1s spectra obtained by specific XPS scanning in the carbon region provide the states of carbon bonds within the dehydrofluorinated PVDF (Figure 3.2). The fraction of carbon-carbon double bonds can thus be obtained, which is important to the phase transition of dehydrofluorinated PVDF. Ideally, when *%DHF* is less than 100% (carbon-carbon triple bonds are not formed), the fraction of double bonds should be close to the extent of dehydrofluorination.

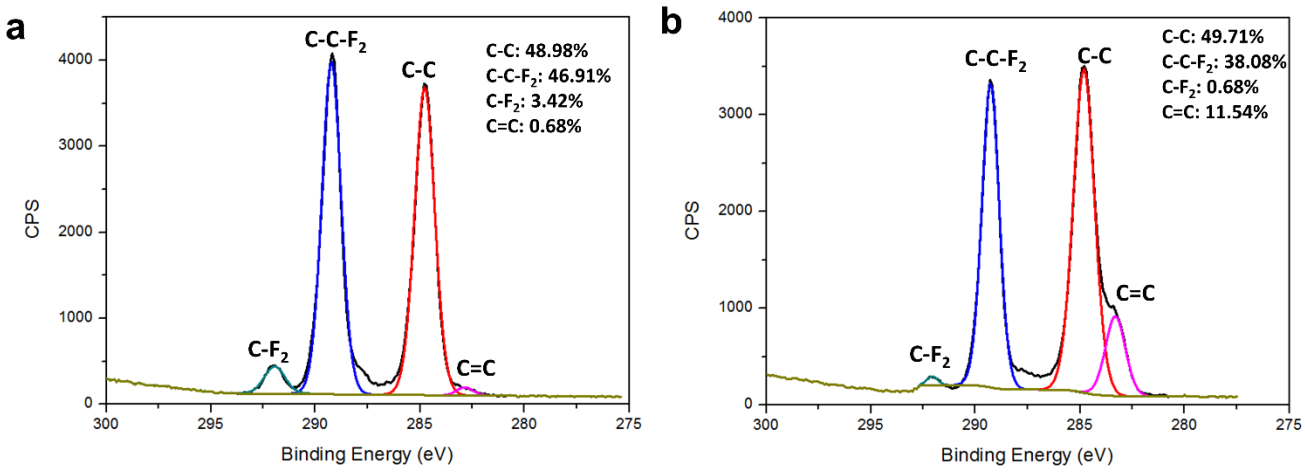

Figure 3.2. XPS C1s scanning of (a) untreated PVDF and (b) dehydrofluorinated PVDF.

Four major chemical states of carbon bonds can be observed in the XPS C1s spectra as listed in Table 3.1. In the optimization of dehydrofluorination process, a relationship between *%DHF* and the fraction of double bonds is built to indicate an effective dehydrofluorination extent.

Table 3.1. Bond type and binding energy of carbon peaks in XPS C1s spectra of PVDF

Bonds	*Binding energy*
C-F_2	291.9 eV
C-C-F_2	289.1 eV
C-C	284.7 eV
C=C	283.0 eV

The phase composition of PVDF is characterized by Fourier transform infrared spectroscopy (FTIR) and X-ray diffraction analysis (XRD). FTIR is a semi-quantitative chemical composition technique that can provide information such as chemical bonds, functional groups, and chain conformations. FTIR measures the infrared absorption spectrum of a sample by recording the intensity changes of an infrared light of varying wavelength passing through the tested sample. Absorption occurs when the frequency of IR matches the vibrational frequency of a bond, allowing it to be identified and quantified. FTIR is suitable for use as a convenient and fast method to validate the existence of β-phase inside of a PVDF sample. Because of the large differences between the chain conformations of different crystalline phases of PVDF, the evidence and relative fraction of β-phase can be confirmed by obvious changes in their IR spectra. FTIR measurement of the PVDF is performed by a Nicolet iS60 spectrometer (Thermo Scientific) with a SMART iTR accessary in the wave number range of 550~4000 cm^{-1}. Typical FTIR spectra of α-phase dominated and β-phase dominated PVDF are shown in Figure 3.3 and the wavenumbers of characteristic peaks of both phases are listed in Table 3.2. Both α-phase and β-phase usually coexist in PVDF films, and the fraction of β-phase in the crystal part of PVDF can be quantified by FTIR measurements. In such a quantification method, the fractions of α-phase and β-phase are calculated based on the absorption at their characteristic band: 763 cm^{-1} for α-phase and 840 cm^{-1} for β-phase.(87) Assuming the infrared absorption of PVDF follows the Beer-Lambert law, the absorbance of the α-phase and β-phase is given by:

$$A_\alpha = \log\left(\frac{I^0_{763cm^{-1}}}{I_{763cm^{-1}}}\right) = c \cdot K_{763cm^{-1}} \cdot X_\alpha \cdot l \qquad \text{Equation 3.2}$$

$$A_\beta = \log\left(\frac{I^0_{840cm^{-1}}}{I_{840cm^{-1}}}\right) = c \cdot K_{840cm^{-1}} \cdot X_\beta \cdot l$$

Equation 3.3

where X_α and X_β are the degree of crystallinity of the specific phase of PVDF, A_α is the absorbance of the α-phase at 763 cm^{-1}, A_β is the absorbance of the β-phase at 840 cm^{-1}, l is the thickness of the sample, c is the average monomer concentration, I^0 and I are the incident intensity and transmitted radiation intensity at specific wavenumber respectively, K is the absorption coefficient at the specific wave number, and X_α and X_β are the degree of crystallinity of the specific phase of PVDF. Thus, the relative fraction of β-phase in a PVDF sample containing both phases can be calculated using:

$$f(\beta) = \frac{X_\beta}{X_\alpha + X_\beta} = \frac{A_\beta}{(K_{840cm^{-1}} / K_{763cm^{-1}})A_\alpha + A_\beta}$$

Equation 3.4

where K_{840cm}^{-1}= 7.7x10^4 cm^2/mol and K_{840cm}^{-1}= 6.1x10^4 cm^2/mol.(25, 96) The quantified β-phase is used as major evidence to prove the promoted β-phase formation in the dehydrofluorinated PVDF.

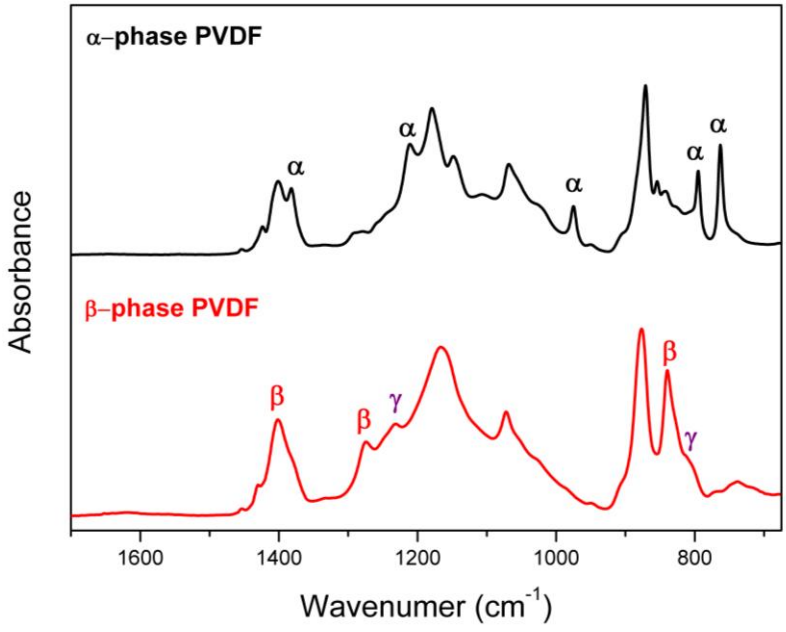

Figure 3.3. FTIR spectra of α-phase dominated PVDF and β-phase dominated PVDF.

Table 3.2. FTIR wavenumber and assigned functional group vibrational mode in different phases of PVDF.(87)

Phase	Band wavenumber (cm^{-1})	Functional group and vibrational mode
α-phase	615	CF_2 bending
	763	CF_2 skeletal bending
	795	TGTG' conformation CH_2 rocking
	855	CH out-of-plane deformation
	976	CH out-of-plane deformation
	1220	CF out-of-plane deformation
	1380	CH_2 bending
β-phase	840	T_4 conformation CH_2 rocking
	1279	CF out-of-plane deformation
	1400	CH_2 bending
γ-phase	834	T_3G conformation CH_2 rocking
	1234	CF out-of-plane deformation

X-ray diffraction (XRD) is a common technique used to determine the crystal structure and the degree of crystallinity. XRD uses a monochromatic x-ray beam to scatter off the sample's lattice structure and measures the angle and intensity of the scattered beam. This scattering phenomenon is defined as diffraction and is governed by Bragg's law:

$$n\lambda = 2d_{hkl}sin\theta \qquad \text{Equation 3.5}$$

where d_{hkl} is the lattice spacing between the diffracting planes, λ is the wavelength, and θ is the angle of the incident beam. Experimentally, an x-ray of known wavelength is transmitted at a known incident angle so that *d*, the lattice parameter, can be measured. Typically, data is presented as plot of 2θ versus intensity, where peaks characteristic to the sample material will exist at specific diffraction angles. XRD is another necessary characterization method in this research to measure the phase composition and crystalline structure of dehydrofluorinated PVDF. The XRD measurements of the PVDF are performed on a Rigaku Ultima IV X-ray diffractometer equipped with a Cu Kα X-ray tube source (λ= 0.154 nm). Figure 3.4 presents a comparison between diffraction patterns of α-phase PVDF and β-phase PVDF. The peaks at 17.6˚, 18.4˚ and 19.9˚ are ascribed as the α-phase according to JCPD No.42-1650, while the peaks at 18.6˚ and 20.6˚ represent the β-phase according to JCPD No.42-1649. The peaks at 18.6˚ and 20.3˚ represent γ-phase according to JCPD No. 38-1638. Note that the peaks corresponding to β-phase and γ-phase are usually overlapping because of similar short-term conformation and lattice parameters. In the

XRD pattern of dehydrofluorinated PVDF, the position of α-phase and β-phase peaks are often not exactly the same as the untreated PVDF, indicating changes of interchain distances during the modification. The FTIR spectra and XRD patterns of defluorinated PVDF samples prepared in the last task are expected to show a correlation between β-phase fractions and the experimental parameters. This will provide better understanding of the mechanism and kinetics of dehydrofluorination. An optimized dehydrofluorination procedure is expected to be formulated, which can efficiently introduce the highest fraction of β-phase to PVDF at a low cost.

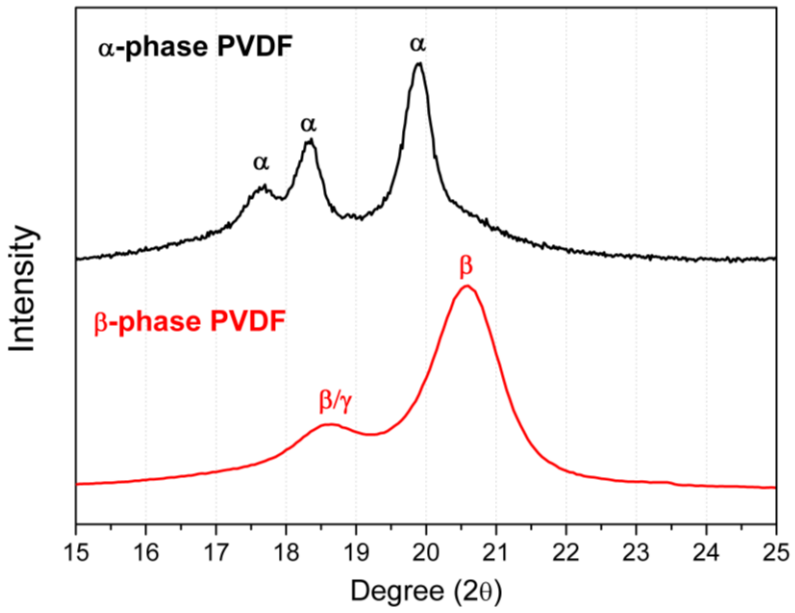

Figure 3.4. XRD pattern of α-phase dominated PVDF and β-phase dominated PVDF.

3.3 Effect of Dehydrofluorination Agents

As mentioned previously, the dehydrofluorination reaction occurs when PVDF is under either a basic or high temperature condition. Thus, basic chemicals are often used as dehydrofluorination agents to introduce carbon-carbon double bonds in PVDF. These basic chemicals can be divided into three categories: strong ionic bases, such as sodium hydroxide (NaOH) and potassium hydroxide (KOH); ionic basic salts, such as sodium carbonate (Na_2CO_3) and sodium bicarbonate ($NaHCO_3$); and organic bases, which are mostly amines.(166, 188-190) In previous research efforts, strong ionic bases were used to induce fast and high extent dehydrofluorination, which usually led to overreaction. In this case, an increase of undesirable

crosslinks and excess degradation occurs, leading to hindered crystallization of PVDF and reduced dielectric performance.(166, 190) Additionally, since these ionic bases cannot be dissolved in organic solvents such as DMF, dehydrofluorination cannot be uniformly induced to the PVDF solution, causing non-uniform properties in the product. Ionic basic salts such as $NaHCO_3$ can induce dehydrofluorination in a much slower rate in comparison to strong bases because of their lower basicity. However, the low solubility of these salts in organic solvents also prevents these salts from inducing dehydrofluorination uniformly. The extent of dehydrofluorination is difficult to control when the dehydrofluorination agent is an immiscible solid base. Thus, the attention of this research is more focused on organic bases which are in liquid form or have high solubility in PVDF solution.

In this work, weak organic bases are used as dehydrofluorination agents instead of strong ionic bases and basic salts to slowly and uniformly induce the dehydrofluorination of PVDF in PVDF/dimethylformamide (DMF) solution. Primary and tertiary amines that are miscible with DMF are studied for their performance as dehydrofluorination agents. The investigated amines include ethylene diamine (EDA), trimethylamine (TEA), 1,4-diazabicyclo [2.2.2] octane (DABCO), and 1,8-diazabicyclo [5.4.0] undec-7-ene (DBU). Among these dehydrofluorination agents, EDA is a common primary amine with a basicity (pK_a=10.7) close to bicarbonate salts (pK_a=10.25). DABCO and TEA are tertiary amines with low basicity (pK_a=8.8 for DABCO and pK_a=9.0 for TEA in DMF).

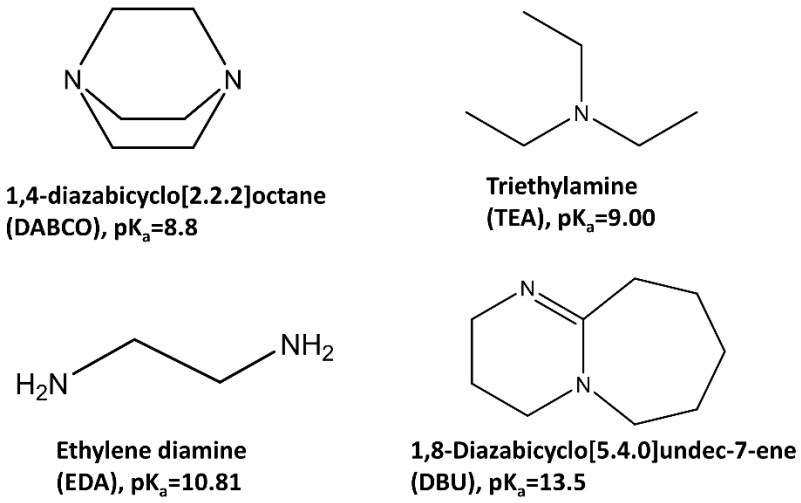

Figure 3.5. Amine dehydrofluorination agents investigated in this study.

It is expected that these amines will induce dehydrofluorination at a reduced reaction rate so that the extent of dehydrofluorination can be precisely controlled through the reaction period. The experimental results show that the reaction rate is largely dependent on the basicity of the PVDF solution. As shown in Figure 3.6, at the same concentration (agent: VDF ratio =1 :10), high pK_a dehydrofluorination agents such as EDA and DBU can induce a high extent of dehydrofluorination in minutes or hours, while low pK_a dehydrofluorination agents take multiple days to achieve a low extent of dehydrofluorination. To achieve an extent of dehydrofluorination of *%DHF*=~10%, it takes a period of 8 hours for EDA catalyzed dehydrofluorination with a concentration of EDA: VDF= 1:10. For same concentration of DABCO and TEA, the reaction time to achieve 20% dehydrofluorination is 20 days and 30 days, respectively. However, for strong organic bases like DBU (pK_a=13.5), the extent of reaction is much more difficult to control. Due to both the fact that its basicity is in the range of strong ionic bases and the fact that it is highly miscible in organic solvents, DBU has been widely used as catalyst in dehydrohalogenation reactions. Yet in this case, the strong basicity leads to rapid dehydrofluorination. It is observed that at a same concentration of DBU: VDF= 1:10, DBU induces fast and non-uniform dehydrofluorination in PVDF, leading to inconsistent elemental compositions on different spots of a same sample.

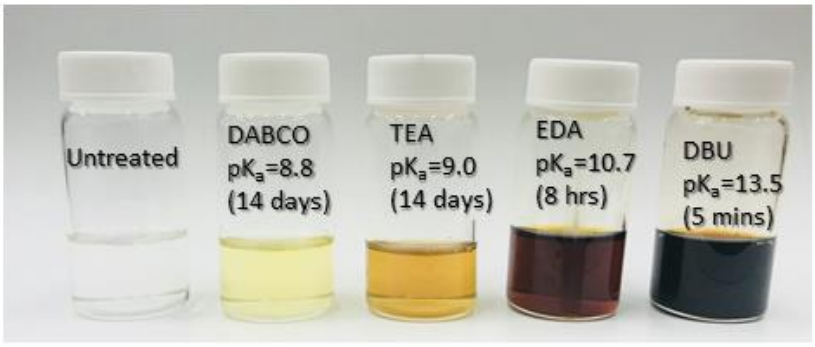

Figure 3.6. PVDF dehydrofluorination induced by different amines with same concentration of agent: VDF=1:10.

However, there are no side-effects observed from different dehydrofluorination agents except the significant difference in reaction rate. Phase composition characterization of the PVDF

dehydrofluorinated by different amines is performed by FTIR and is shown in Figure 3.7. When %DHF ≥ 10%, all dehydrofluorinated PVDF samples are dominated by β-phase with the β-phase fraction in the range of 75%~85%. These results indicate that once a sufficient dehydrofluorination extent is achieved, the formation of β-phase will be promoted. Additionally, there is no evidence of other chemical changes which can be extracted from the FTIR spectra of the dehydrofluorinated PVDF samples. Thus, it can be concluded that the dehydrofluorination of PVDF can be induced and utilized to promote β-phase formation by any of the dehydrofluorination agents investigated above, including primary and tertiary amines. The reaction rate of dehydrofluorination is only decided by the basicity of the dehydrofluorination agent, and the efficiency of promoting β-phase formation is solely dependent on the extent of dehydrofluorination. Such conclusions demonstrate that dehydrofluorination can be a versatile and convenient method for preparing high quality β-phase PVDF. The wide choices in catalysts and the flexibility in reaction process are expected to have great potential for scalability in manufacturing. In order to control the extent of dehydrofluorination in an accurate and time-efficient manner, the reaction parameters of EDA catalyzed dehydrofluorination is investigated in further detail in the next section of this study. Furthermore, an optimized procedure of dehydrofluorination and sample preparation will be established to maximize the β-phase fraction of PVDF.

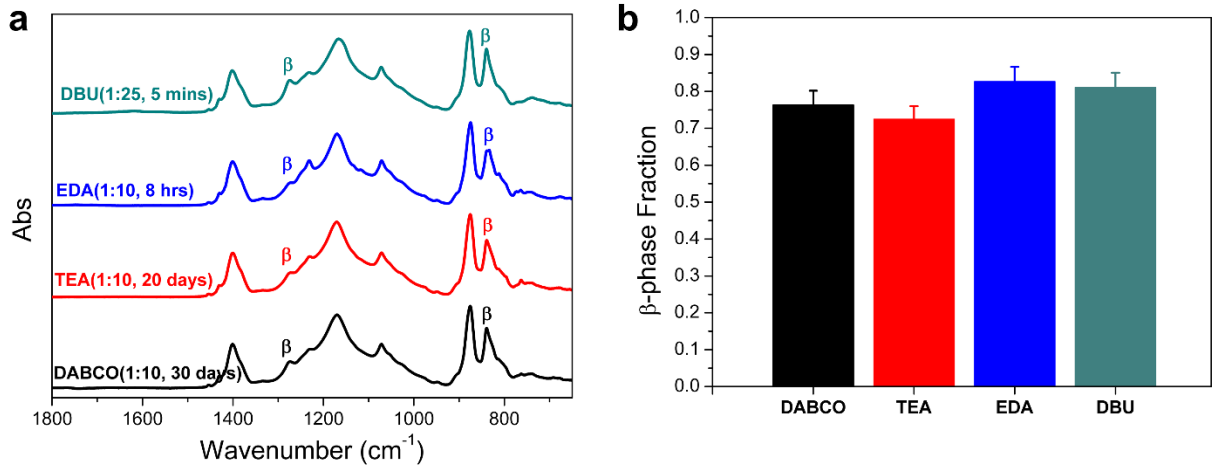

Figure 3.7. Effect of different dehydrofluorination agents. (a) FTIR spectra of dehydrofluorinated PVDF treated by different dehydrofluorination agents and (b) the β-phase fraction in these samples.

3.4 Optimization of EDA Catalyzed Dehydrofluorination Procedure

The optimization of the dehydrofluorination procedure primarily aims to achieve two goals: one is to find out the extent of dehydrofluorination that can induce the highest piezoelectric performance in PVDF, and the other is to establish a set of reaction parameters that can stably produce PVDF with the desired extent of dehydrofluorination. In order to achieve these goals, the first step is to characterize the extent of dehydrofluorination in EDA treated PVDF. Since EDA is a weak organic base that can slowly induce a high extent of dehydrofluorination within hours of initiating the reaction, reaction time is used as the major parameter to control the extent of dehydrofluorination. In this study, EDA catalyzed dehydrofluorination is conducted using a 7 wt. % PVDF/DMF solution at room temperature, with EDA: VDF=1: 10. The effect of reaction time is investigated in the range of 0 to 48 hours. The extent of dehydrofluorination at different reaction times is monitored by combustion elemental analysis, as shown in Table 3.3 and Figure 3.8. The XPS C1s spectra provide a clear insight to the dehydrofluorination process. As the reaction time increases, the C-F_2 peak decreases while the C=C peak increases significantly. This shows that the *%DHF* value and fraction of double bonds in EDA treated PVDF are both increasing with reaction time. The C=C fraction values are very close to the *%DHF* values calculated above when the reaction time is within 12 hours, indicating that the majority of the EDA induced dehydrofluorination leads to double bond formation in the early stages of reaction. However, in the case of a very long time (48 hours), the C=C fraction only reaches 36.42% while the *%DHF* value reaches 69.05%. This difference might indicate an increase of crosslink formation in the late stages of the dehydrofluorination of PVDF. As predicted by the molecular simulation results in Chapter 2, the β-phase formation becomes preferential when double bond fraction is above 10%. This double bond fraction corresponds to a *%DHF* value of ~10% and a reaction time of about 8 hours.

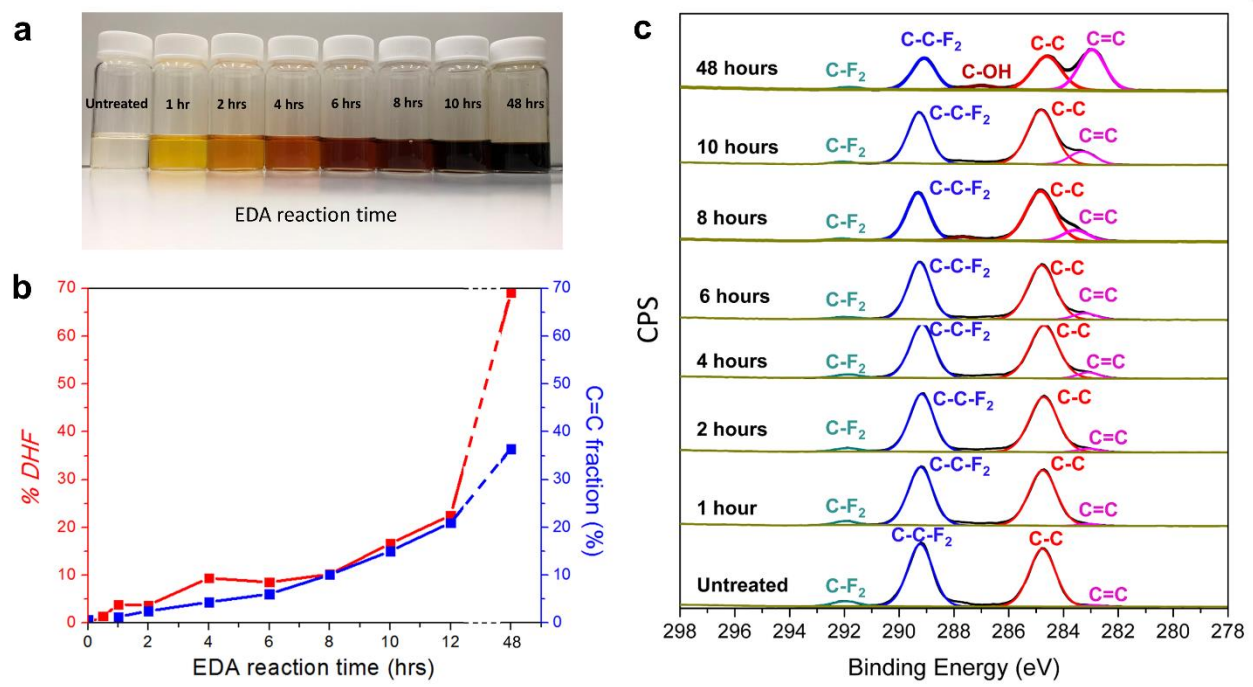

Figure 3.8. Characterization of dehydrofluorination extent. (a) EDA treated PVDF with different reaction time in 7 wt. % PVDF/DMF solution. (b) The calculated %DHF and double bonds fractions versus reaction time plot for EDA treated PVDF (c) XPS C1s spectra of EDA treated PVDF with different reaction times.

Table 3.3 Results of combustion elemental analysis of EDA treated PVDF

Reaction time(hrs)	**Wt. % (C)**	**Wt. % (H)**	**Wt. % (F)**	***%DHF***	**C=C fraction (%)**
0	36.76	3.39	59.22	0	0.68
0.5	36.94	3.3	58.98	1.48	--
1	37.3	3.15	58.59	3.88	1.36
2	37.11	3.43	58.61	3.76	2.54
4	37.3	3.36	57.69	9.43	4.4
6	37.51	3.37	57.83	8.56	6.11
8	37.95	3.18	57.56	10.23	10.11
10	38.46	3.32	56.52	16.65	15.07
12	38.45	3.24	55.56	22.56	21.01

48	38.29	3.85	48.02	69.05	36.42

Since the piezoelectric performance of PVDF is mainly determined by the β-phase fraction, the phase composition is the most important criteria in the optimization of the dehydrofluorination procedure. As shown in the FTIR spectra (Figure 3.9), the EDA treated PVDF shows an increasing fraction of β-phase as the reaction time increases. In the first 4 hours of the reaction, the FTIR show that the EDA treated PVDF samples are dominated by α-phase, yet the intensity of the α-phase peaks is slightly decreased. In the following four hours of the reaction, the peaks of the β-phase PVDF appear and grow rapidly. The fraction of β-phase increases from 40.76% in the untreated PVDF, to 83.74% after 8 hours of dehydrofluorination. At this point, the EDA treated PVDF shows a dehydrofluorination extent of *%DHF*=10.23%. Further increase in dehydrofluorination extent does not show significant effects on the fraction of β-phase in the dehydrofluorinated PVDF. The fraction of β-phase reaches a saturation after a reaction time of 8 hours and remains in the range of 80~85% up to a reaction time of 30 hours, where the dehydrofluorination extent is 49.1±4.5%. This result is consistent with the molecular simulation results discussed in the previous chapter. When a sufficient extent of dehydrofluorination is achieved in PVDF, the potential energy level of β-phase formation becomes lower than that of α-phase formation. This would affect the crystallization behavior of the PVDF and rapidly change the dominating phase in dehydrofluorinated PVDF. Further increase in β-phase fraction is limited by the structural defects located on the grain boundaries of the semi-crystalline polymer, as well as the coexistence of small fractions of γ-phase, as seen in FTIR spectra.

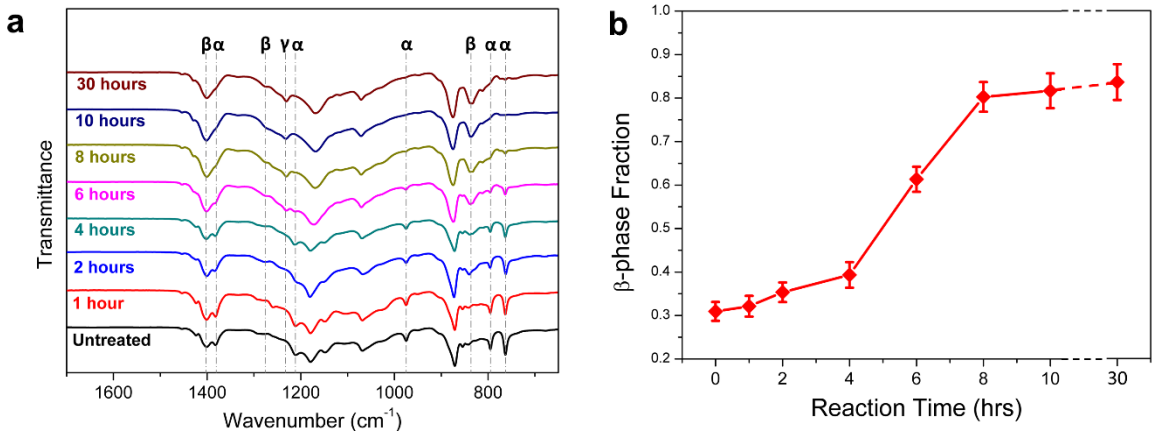

Figure 3.9. (a) FTIR spectra and (b) calculated β-phase fraction of EDA treated PVDF.

The crystalline phase composition of the EDA treated PVDF films is further investigated through X-ray diffraction (XRD) analysis. As illustrated in Figure 3.10, untreated PVDF is dominated by α-phase which is recognized by the peaks at 17.6°, 18.4° and 19.9°. By increasing the EDA treating time, the α-phase peaks at 17.6° and 18.4° are gradually replaced by a new peak at 18.6° which is ascribed to both β-phase and γ-phase, while the peak at 19.9° shifts toward higher 2θ values indicating increased β-phase and γ-phase. After a reaction time of 8 hours, the XRD pattern of dehydrofluorinated PVDF shows a weak peak at 18.6° and a strong peak at ~20.5°, which indicate a combination of β-phase and γ-phase. The peak at ~20.5° is a summation of β-phase at 20.6° and γ-phase peak at 20.3°. Both FTIR and XRD results show the presence of γ-phase in dehydrofluorinated PVDF which is not found in untreated PVDF. The reason of γ-phase formation is due to the T_3GT_3G' conformation of γ-phase PVDF acting as a metastable energy state during the phase transition between α-phase and β-phase. Similar to the FTIR analysis, the XRD results indicate that the content of β-phase significantly increases in dehydrofluorinated PVDF. These results demonstrate that β-phase becomes the dominant phase in PVDF films with a %DHF above 25%. This is consistent with the results from the molecular simulations which indicates that β-phase formation is preferential after such fraction of double bonds is introduced by dehydrofluorination.

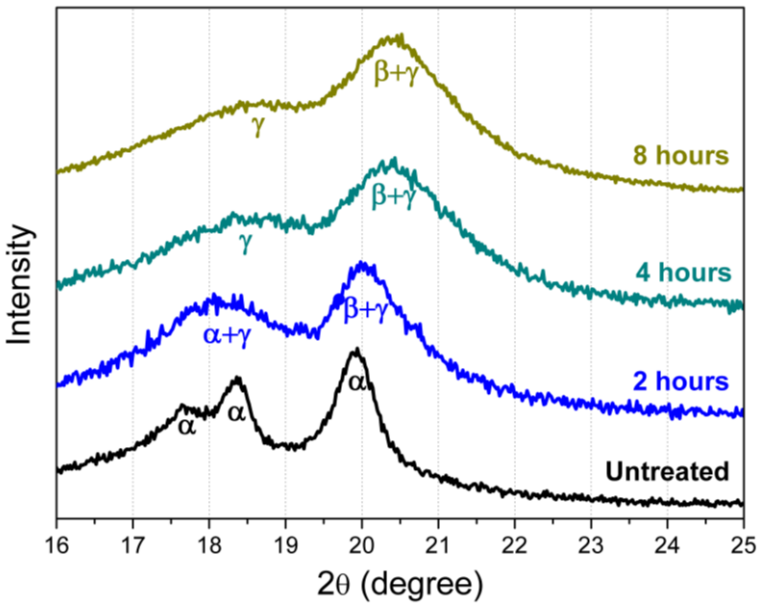

Figure 3.10. XRD patterns of EDA treated PVDF with different reaction time.

However, the fraction of β-phase is not the only factor that determines the piezoelectric performance of PVDF. As discussed in the last chapter, the defect-engineering method adopted in PVDF copolymerization will lead to changes in other electric properties such as Curie temperature, dielectric constant, and breakdown strength. These changes are also expected in dehydrofluorinated PVDF. The dielectric constant of dehydrofluorinated PVDF is measured by an Agilent E4980A precision LCR meter, as shown in Figure 3.11a. The dielectric constant of PVDF increases with increasing dehydrofluorination extent, from 8.8 to 14.7 at 1 kHz when *%DHF* increases to over 50%. Such an increase in the dielectric constant is caused by the increased flexibility of the dipole rotation along the chain axis, which is due to the increased interchain distances. However, the changes in dielectric constant are much smaller than those associated with PVDF copolymers, indicating the change in the interchain distance of β-phase is negligible. Such changes in lattice structure can only be observed by XRD analysis in stretched PVDF samples with very high *%DHF*. Another significantly affected property is the electrical breakdown strength. As shown in Figure 3.11b, the breakdown strength of dehydrofluorinated PVDF drops significantly after over 8 hours of reaction. This result is attributed to overreaction since a high fraction of dehydrofluorination induces double bonds and crosslinks, leading to low breakdown strength. Low electrical breakdown strength will limit PVDF in applications at high

voltage and its performance as actuators, and thus should be avoided during the modification process.

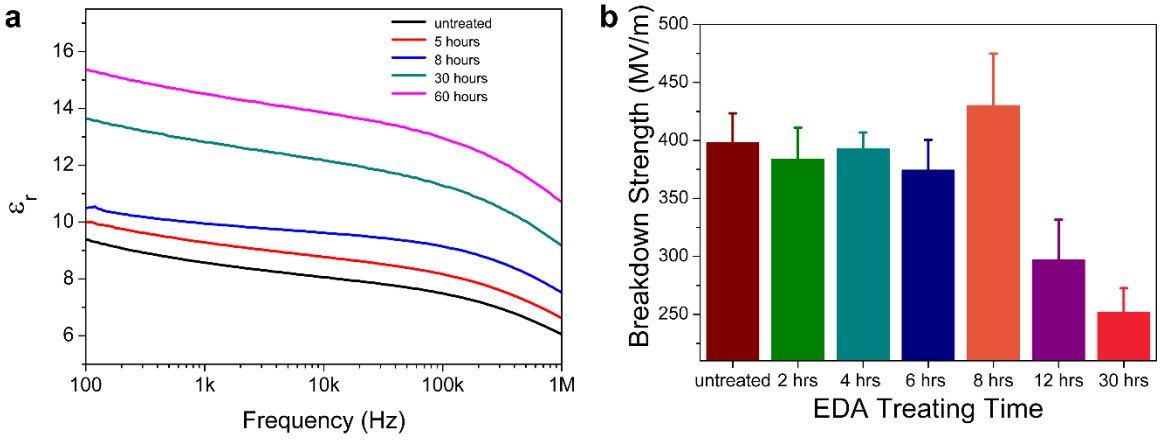

Figure 3.11. a) Dielectric constants and (b) electric breakdown strength of EDA treated PVDF with different reaction time.

As a conclusion, the optimized reaction procedure and conditions for the EDA catalyzed dehydrofluorination are as follows: adding EDA to a 7wt. % PVDF/DMF solution by a molar ratio of EDA: VDF=1: 10 and reacting at room temperature for 8 hours. Such a treatment yields a dehydrofluorination extent *%DHF*= ~25%, which is optimal for β-phase formation and electric performance. Unlike mechanically drawn PVDF, the β-phase in dehydrofluorinated PVDF is induced by intrinsic chemical modification. This unique characteristic leads to uniform mechanical and electrical properties in the dehydrofluorinated PVDF, as well as thermal stability since the phase composition remains unchanged through most heat treatments.

3.5 Study of Ferroelectricity of Dehydrofluorinated PVDF

Ferroelectricity is a property of certain materials that possess a spontaneous electric polarization that can be reversed by the application of an external electric field. Ferroelectric materials exhibit a hysteresis effect under oscillating electric field, which can reflect the size and structure of dipole domains within the material. Ferroelectric materials also exhibit piezoelectric behavior because of the requirement of symmetry in the crystal structure. However, piezoelectric materials do not necessarily exhibit ferroelectric behavior. Since β-phase is the only ferroelectric

phase in PVDF, strong ferroelectric properties are often indicative of the existence of high β-phase fraction. Furthermore, the remnant polarization and coercive field of PVDF can reflect the size of the oriented crystalline domains of β-phase, which can hardly be measured through chemical characterization methods such as FTIR. In an α-phase dominated PVDF sample, only a small number of free dipoles in the amorphous part of PVDF can be aligned and reversed by external electric fields. Thus, the sample will exhibit a dielectric polarization behavior (Figure 3.12). Ferroelectric relaxor behavior can be found when small domains of aligned dipoles are present in PVDF, which exhibits a high saturation point but a low remnant polarization. Relaxor behavior can be widely found in PVDF terpolymers such as P(VDF-TrFE-CTFE) and P(VDF-TrFE-CFE).(170) Only in PVDF containing large domains of aligned dipoles, like the β-phase structure, a strong ferroelectric response with high remnant polarization can be observed.

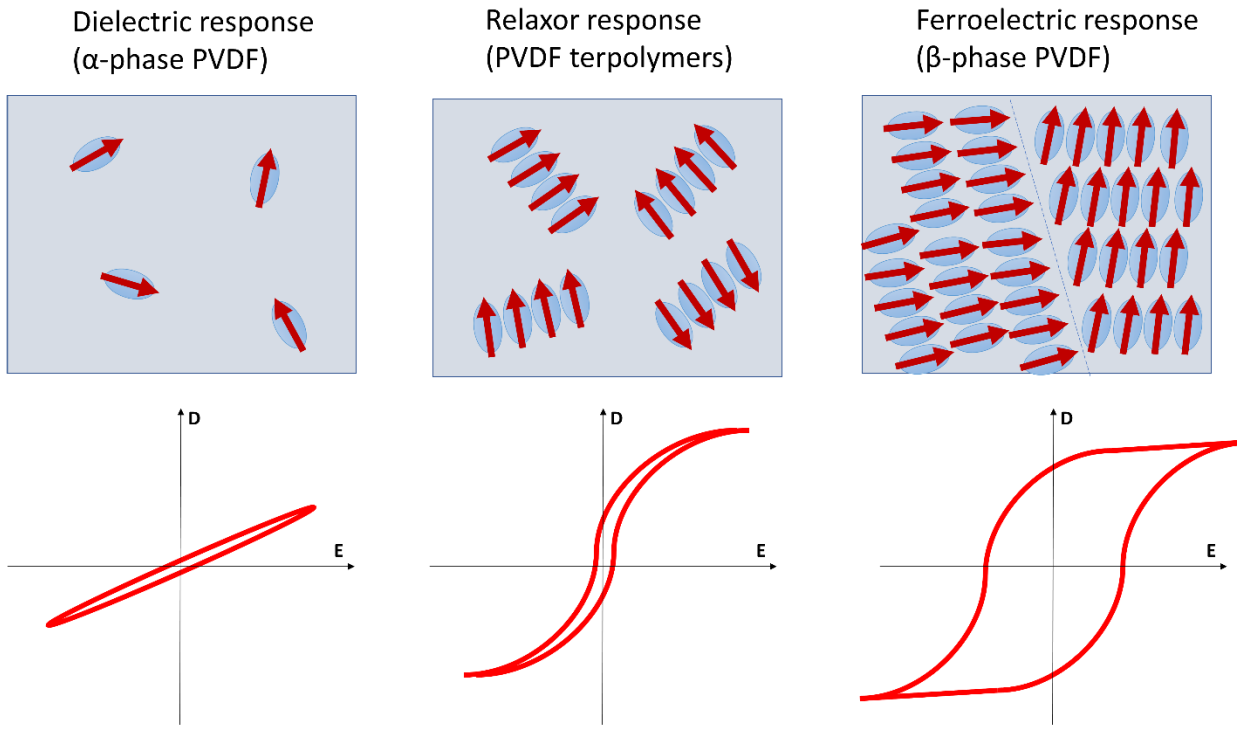

Figure 3.12. Domain structures and polarization responses of α-phase PVDF, PVDF terpolymer and β-phase PVDF.

In this study, the ferroelectric property of dehydrofluorinated PVDF is evaluated by measuring the ferroelectric hysteresis loop through a Sawyer-Tower circuit (Figure 3.13). A voltage signal with a frequency of 10 Hz is applied to the circuit to create an AC electric field with an amplitude

of 300 MV/m on the tested sample. The tested PVDF sample is prepared by the doctor blading method into a thin film with a thickness of 10 μm. Thin layers of gold (Au) are coated on both sides of the film as electrodes using a sputter coater. The polarization, or electric displacement, is calculated by the following equation:

$$D = \frac{C_f V_f}{A}$$

where D is the polarization, C_f is the capacitance of the reference capacitor, V_f is the voltage measured across the reference capacitor, and A is the area of the tested sample. The hysteresis loop is obtained by plotting the polarization versus the electric field.

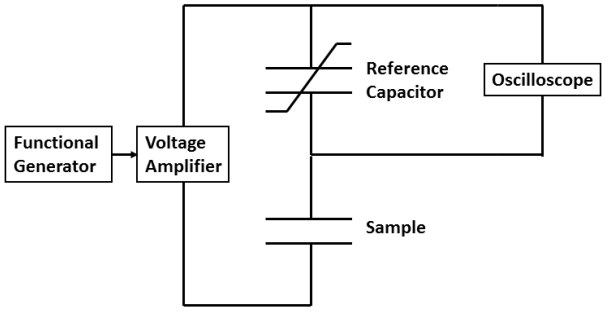

Figure 3.13. Sawyer-Tower circuit for ferroelectric measurements.

The ferroelectric polarization loops of dehydrofluorinated PVDF with different EDA treatment reaction times, as well as untreated PVDF are shown in Figure 3.14. As the reaction time increases, the polarization behavior of the PVDF transits from mostly dielectric polarization to high ferroelectric polarization with an obvious hysteretic behavior. The remnant polarization of PVDF increased from 0.25±0.05 μC/cm² for untreated PVDF to 6.31±0.15 μC/cm² for dehydrofluorinated PVDF with an 8-hour EDA reaction time (*%DHF*= ~27%). This large increased ferroelectric behavior is indicative of an increased fraction of β-phase in the dehydrofluorinated PVDF. The trend of increasing remnant polarization with increasing dehydrofluorination extent is found consistent with the trend of increasing β-phase faction obtained from the FTIR analysis shown in Figure 3.9. The correlation between dehydrofluorination extent and ferroelectricity further proves the efficacy of the dehydrofluorination method in promoting β-phase formation in PVDF. The large increased remnant polarization and high coercive field also indicate the existence of large crystal domains

of β-phase in properly dehydrofluorinated PVDF. With the fact that the coercive field is decreased at low extent of dehydrofluorination, it can be inferred that the size of crystal domains of α-phase in PVDF are first reduced by the effect of dehydrofluorination and that crystal domains of β-phase grow bigger with increased extent of dehydrofluorination. The coexistence of small domains of different phases of PVDF when low extent of dehydrofluorination is induced is consistent with the XRD pattern of EDA treated PVDF with a short reaction time.

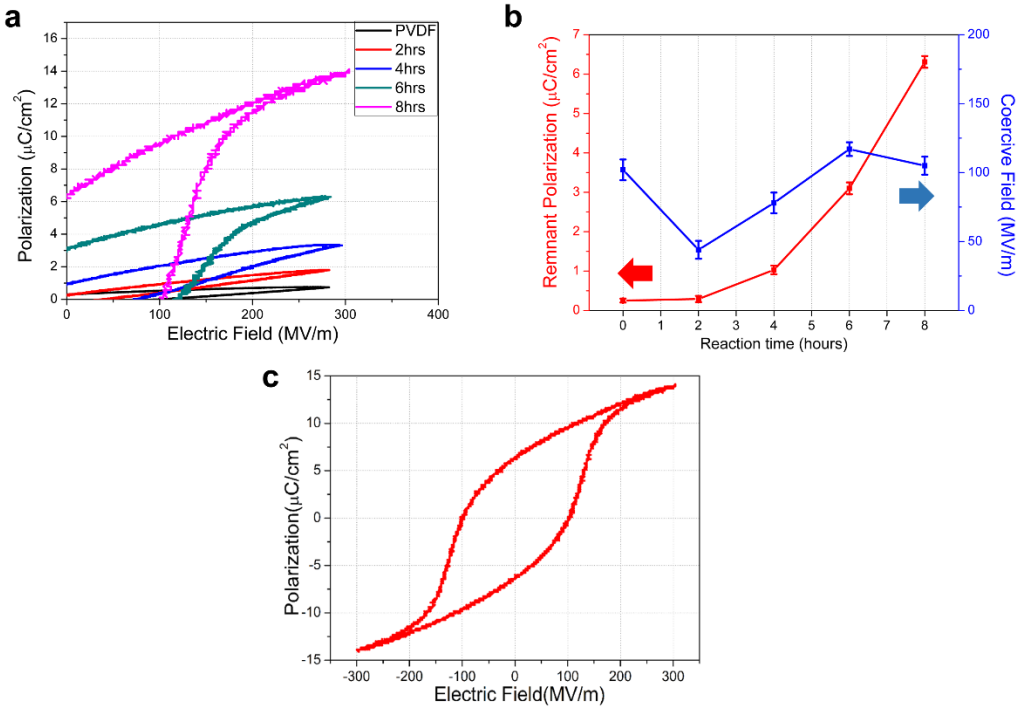

Figure 3.14. Ferroelectricity measurement of dehydrofluorinated PVDF. (a) Polarization versus electric field plots of dehydrofluorinated PVDF with different reaction time, as well as untreated PVDF. (b) Remnant polarization and coercive field versus reaction time. (c) Full ferroelectric hysteresis loop of dehydrofluorinated PVDF with a reaction time of 8 hours.

3.6 Chapter Summary

In this chapter, the experimental procedure of PVDF dehydrofluorination is investigated and the efficacy of the dehydrofluorination method in promoting β-phase formation is proven through chemical and electrical characterization techniques. The dehydrofluorination of PVDF is induced conveniently in a room temperature reaction in solution, being catalyzed by different dehydrofluorination agents. It is demonstrated that by inducing a proper extent of

dehydrofluorination, the β-phase fraction in PVDF can be increased approximately from 40% to 80%. It is also demonstrated that the dehydrofluorination of PVDF can be induced by different dehydrofluorination agents including primary and tertiary amines. Amines including EDA, DABCO, TEA, and DBU are investigated regarding their performance in catalyzing dehydrofluorination of PVDF. It is found that the rate of dehydrofluorination is controlled by the basicity of the reaction solution, which is determined by the concentration and pK_a value of the dehydrofluorination agents. However, once the extent of dehydrofluorination (%DHF) reaches 25%, the formation of β-phase is effectively promoted regardless of which dehydrofluorination agent is used. The increasing β-phase fraction with increasing dehydrofluorination extent is observed from FTIR and XRD analysis. Strong ferroelectric effects are observed in dehydrofluorinated PVDF, indicating the existence of large β-phase crystal domains.

This chapter presents an optimized procedure for an EDA catalyzed dehydrofluorination reaction to maximize the piezoelectric performance of modified PVDF. In addition, an optimum dehydrofluorination extent (%*DHF)* is found to be ~25% with an optimum *%(C=C)'* value of 20%, where the dehydrofluorinated PVDF can achieve high β-fraction without degrading other dielectric properties. In the following chapters, β-phase PVDF films and devices are prepared according to the procedure established in the current chapter, in order to evaluate the performance of the dehydrofluorinated PVDF in various applications. This work is the first to report the method of preparing high β-phase PVDF through controlled dehydrofluorination. The fundamental findings in this chapter are valuable in designing large-scale manufacturing methods for high piezoelectric PVDF.

CHAPTER 4

Study of Electromechanical Coupling Properties and Thermal Stability of Dehydrofluorination Induced β-phase PVDF

4.1 Chapter Introduction

In the last two chapters, the efficacy of the dehydrofluorination method in promoting β-phase PVDF formation has been demonstrated in both theoretical and experimental methods. The novel developed dehydrofluorination induced β-phase PVDF is expected to have exceptional advantages over the traditional drawn PVDF. The intrinsically increased β-phase fraction can lead to further improved electromechanical coupling efficiency and giant piezoelectric responses. Thus, one of the major tasks of this chapter is to characterize the piezoelectric properties of the dehydrofluorinated PVDF. However, since PVDF is a soft material, traditional piezoelectric measurement methods for piezoelectric ceramics are not suitable for an accurate measurement of PVDF. In this chapter, several new piezoelectric characterization methods are designed and investigated to accurately measure the piezoelectric coefficients of the dehydrofluorinated PVDF. The piezoelectric properties of PVDF are demonstrated through both direct effect in which PVDF transfers mechanical energy to electrical energy, and inverse effect in which PVDF transfers electrical energy to mechanical energy. The results reflect the high performance of dehydrofluorinated PVDF in various applications such as sensing, energy harvesting and actuating.

Additionally, since the β-phase is induced by chemical modification instead of mechanical processing, improved thermal stability is expected for the developed dehydrofluorination induced β-phase PVDF. With no worries of phase transition due to thermal relaxation, the dehydrofluorinated PVDF is supposed to maintain its β-phase at higher use temperatures and recrystallize directly into β-phase after it is manufactured through various heat processing methods. Such thermal stability of the dehydrofluorinated PVDF is also investigated in this chapter. The effects of the dehydrofluorination process to the thermal properties of PVDF are analyzed through a series of experiments and the limitations in heat processing of the dehydrofluorinated PVDF are also demonstrated.

4.2 Piezoelectric Coefficients Measurements of the Dehydrofluorinated PVDF through Direct Effect

Direct piezoelectric effect is the energy conversion effect where a piezoelectric material transfers mechanical energy input to electrical energy output. The input mechanical energy is usually applied to the material in forms of compression, stretching and vibration, to induce deformation of the piezoelectric material. The electrical energy is generated in the form of surface charge, which can be measured as a voltage across the material. By measuring the pressure applied onto the piezoelectric material and the charge displacement generated on the surface, the piezoelectric coefficients can be calculated. Before discussing the experimental measurements of the piezoelectric coefficients of PVDF, a brief review of the mathematical description of piezoelectricity and the piezoelectric coefficients in direct effect are provided as follows.

In the measurement of direct piezoelectric effect, a uniaxial external stress field is usually applied onto a sample while the external electric field is usually zero, giving a simplified equation of the d_{ij} coefficient:

$d_{ij} = \left(\frac{\partial D_i}{\partial T_j} \right)^E$ with a unit of pC/N, representing the charge generated per unit force.

The measuring techniques of the d_{ij} coefficient mostly work in two ways: measuring the d_{33} coefficient by measuring the charge displacement across the sample in the same direction of the applied stress; or measuring the d_{31} coefficient by measuring the charge displacement across the sample in the direction perpendicular to the applied stress.

4.2.1 Berlincourt circuit method for the piezoelectric d_{33} coefficient measurement

Berlincourt circuit is a widely used method for measuring the piezoelectric d_{33} coefficient of piezoelectric ceramics, and also one of the most famous methods for measuring the direct piezoelectric effect.(191, 192) A schematic diagram of a typical Berlincourt circuit d_{33} meter is shown in Figure 4.1. During the measurement, the sample is clamped between two electrodes with a preload force. A low amplitude oscillating force is applied to the sample, which periodically

changes the stress on the thickness direction of the sample. The surface voltage changes and capacitance of the tested sample is measured between the two electrodes to calculate the amount of charge generated on the sample surface. In this study, the PVDF film is clamped between the two electrodes with a preload of 1 N. The sinusoidal force signal is applied by a piezoelectric stack actuator (Piezosystem jena 101442). The capacitance of the tested PVDF sample is measured by an Agilent E4980A LCR meter and the generated voltage between the two electrodes is measured by a unity gain voltage follower (LTC6240CS8) with an input impedance of 1TΩ and a capacitance of 3.5 pF. All measured signals are collected and processed by a National Instrument DAQ system (NI USB-4431).

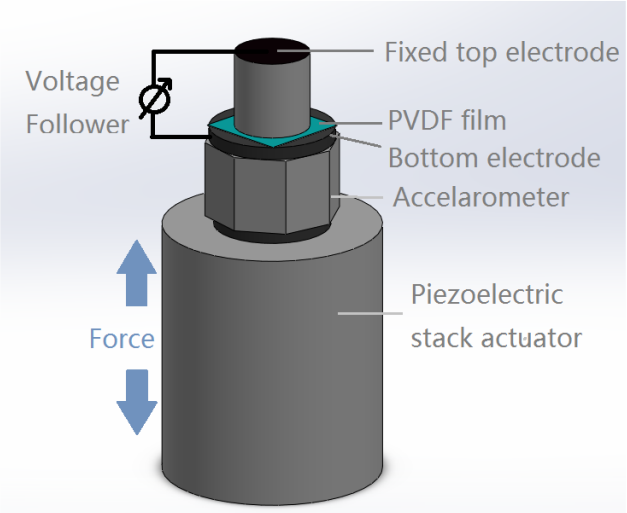

Figure 4.1. Schematic diagram of a typical Berlincourt circuit d_{33} meter.

Prior to the testing, the PVDF samples are electrically poled by corona at 12 kV at an elevated temperature of 125 °C to improve the alignment of permanent dipole moments. Both the untreated PVDF sample and the dehydrofluorinated β-phase PVDF sample are prepared and electrically poled for the d_{33} measurement. During the measurement, sinusoidal force signals are applied to the samples with a frequency of 20 Hz and various amplitudes, and the generated voltage signal from the PVDF samples were collected. Figure 4.2a shows a representative input force and output voltage signal of the PVDF films. Generated electrical charge from the PVDF films under various mechanical forces is calculated with the capacitance at 20 Hz. The root mean square (RMS)

value of the generated charge is plotted as a function of the RMS value of the applied force signals in Figure 4.2b. The d_{33} piezoelectric strain coefficients of the two PVDF samples are calculated from the slope of the linear fit of the charge versus force plot (Figure 4.2b). The d_{33} value of the dehydrofluorinated PVDF film is calculated to be -39.95±2.42 pC/N while that of the untreated PVDF film is found to be only -8.73±0.23 pC/N. The d_{33} value of the dehydrofluorinated films are about 4.5 times higher than that of the untreated PVDF films. The large piezoelectric strain coefficient of the dehydrofluorinated PVDF films is higher than that of any previously reported PVDF, clearly demonstrating their capability of high electromechanical response.(26, 83, 93, 97) This outstanding piezoelectric property reveals the underdeveloped potential of PVDF and thus opening great prospects for dehydrofluorinated PVDF in energy harvesting and sensing applications.

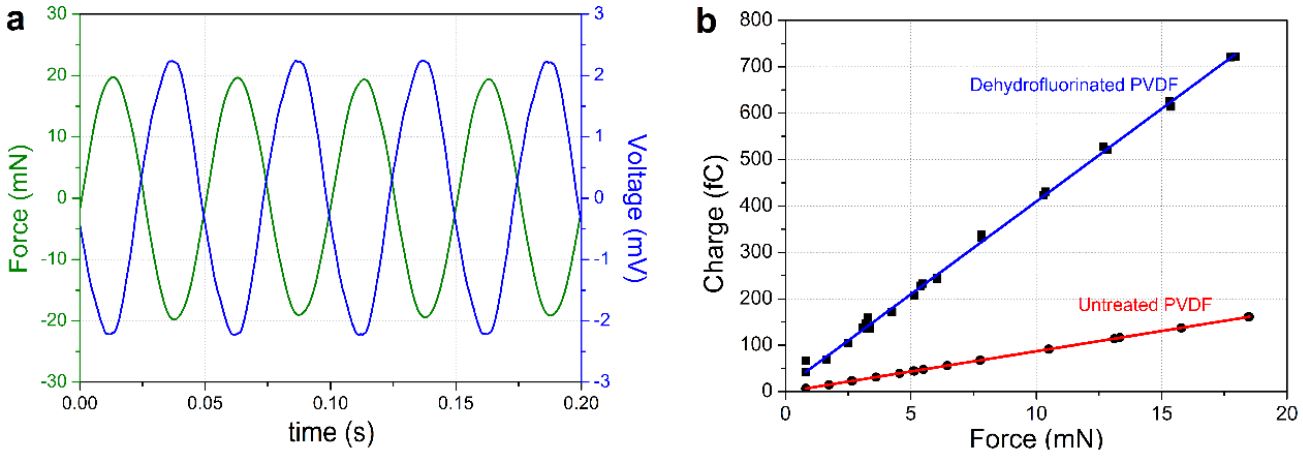

Figure 4.2. d_{33} measurement of the PVDF films by the Berlincourt circuit: (a) Input force signal and received voltage signal from the PVDF samples, (b) Charge versus force plot of the untreated PVDF sample and the dehydrofluorinated PVDF sample. The slope of the plot is obtained by linear fitting.

Although the giant d_{33} value of the dehydrofluorinated PVDF obtained from the Berlincourt circuit measurement is higher than the d_{33} coefficient of any previously reported PVDF, the accuracy of the Berlincourt method is questionable. When measuring soft materials, the results are significantly affected by a slight difference of the preload because of the deformation of the sample. It is also reported that piezoelectric coefficients of soft materials measured by the Berlincourt method usually have large instrument error over different equipment.(193) The

piezoelectric properties of the PVDF measured by Berlincourt method are reliable for comparison purpose, but not accurate enough for providing an absolute value of piezoelectric strain coefficient. A more accurate and reliable method for measuring direct piezoelectric effect for soft materials is still needed.

4.2.2 Dynamic mechanical analysis (DMA) method for piezoelectric d_{31} coefficient measurement

A novel method designed for measuring the direct piezoelectric effect of soft materials is developed in this study. This method is based on a dynamic mechanical analysis (DMA) system. DMA is widely used for the characterization of time and temperature dependent properties of polymeric materials. A tension frame on the DMA instrument can apply an accurately controlled uniaxial strain to the sample, meanwhile recording the dynamic force applied to the sample. By stretching the PVDF film sample along the longitude direction and measuring the generated voltage across the thickness, a piezoelectric d_{31} coefficient is obtained. Since the strain of the samples are accurately controlled by the DMA, the instrument error resulting from the preload difference is largely reduced. Thus, this DMA method is expected to provide an accurate measurement for the absolute piezoelectric coefficient of PVDF and other soft materials through direct piezoelectric effects.

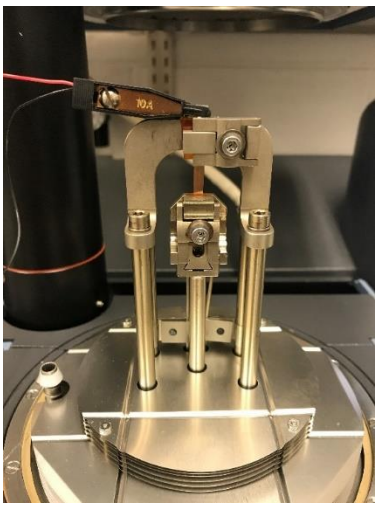

Figure 4.3. Experimental setup of the DMA measurement of direct piezoelectric effect.

In this study, the measurement is performed on a TA instruments DMA Q800 with a tension frame attachment. The tested samples are PVDF films with dimensions of approximately 20 mm × 4 mm × 10 μm. All PVDF films are corona poled at 125˚C at 12 kV and then sputtered with gold on both surfaces as the electrodes. The sample is clamped and wired on the DMA as shown in Figure 4.3. Unidirectional strain with various frequency and amplitudes are applied to the PVDF sample to generate a biased AC voltage signal. The generated voltage and current are then measured by a Keysight B2985A electrometer and collected by a National Instrument DAQ system (NI USB-4431). The piezoelectric strain coefficient, d_{31}, of each sample can be calculated with the open circuit voltage measured from the electrometer and the applied force measured from the DMA, by the following equation:

$$d_{31} = \frac{CV_{pp}t}{Fl}$$

where C is the capacitance of the sample, V_{pp} is the peak-to-peak value of the open circuit voltage, F is the peak force stimulus used to induce the strain of the sample, and l and t are the length and thickness of the sample, respectively. To calibrate the DMA method, a conventional uniaxial drawn PVDF (obtained from TE Connectivity, Inc.) with a known d_{31}=23.0 pC/N is also tested. During the calibration test, the conventional PVDF sample is subjected to 0.5% strain harmonic excitation at a frequency of 100 Hz. The generated open circuit voltage and the short circuit current are measured as shown in Figure 4.4a. The root mean square (RMS) value of the open circuit voltage from the conventional PVDF sample is measured to be 9.00 V, with an RMS short circuit current of 3.34 μA. Such results yield a d_{31} coefficient of 21.90±0.31 pC/N for the commercial uniaxial drawn PVDF devices, which is close to the reported value on the product datasheet (Reported d_{31} =23.00±0.50 pm/V from inverse effect measurements). The frequency dependence of this DMA method is also investigated by applying strain signals at different frequencies on the sample. As shown in Figure 4.4b, the RMS value of the generated voltage is not influenced by the changing frequency. Instead, it shows an almost constant ratio between the input force and output voltage. These results yield similar piezoelectric coefficients of approximately 22 pC/N, validating the accuracy of this DMA method in a wide range of measuring frequencies.

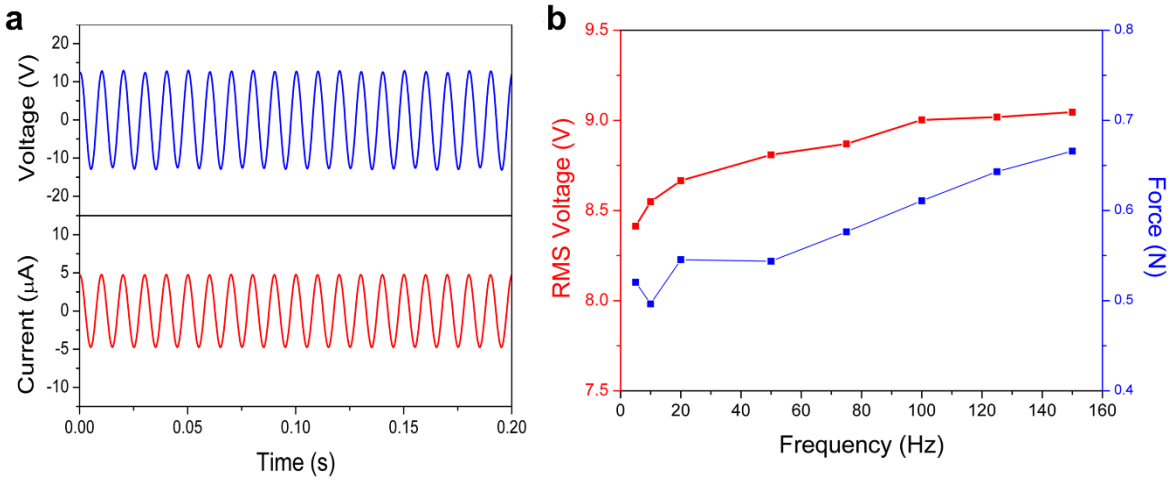

Figure 4.4. DMA measurement on conventional drawn PVDF. (a) Open circuit voltage and short circuit current generated by the conventional uniaxial drawn PVDF sample. (b) RMS open circuit voltage and applied force from the conventional uniaxial drawn PVDF sample at different frequencies.

The high β-phase PVDF treated by EDA with a reaction time of 8 hours (*%DHF=10%*) is used to prepare the dehydrofluorinated PVDF thin film samples. The samples are prepared by solution casting the dehydrofluorinated PVDF onto a glass substrate and then dried. The dried films are then corona poled at an elevated temperature, and gold is subsequently sputtered on both surfaces to function as top and bottom electrodes. A maximum peak to peak voltage of 40.26 V with an RMS value of 13.97 V was obtained when the dehydrofluorinated PVDF devices were subjected to 0.5% strain harmonic excitation at a frequency of 100 Hz (Figure 4.5). Meanwhile, a high peak to peak short circuit current of 15.74 μA with an RMS value of 5.53 μA was also measured. The dehydrofluorinated PVDF devices generate over a 55% larger voltage and current response compared to the conventional PVDF devices. A plot of the generated RMS open circuit voltage versus the frequency of strain is shown in Figure 4.5b, demonstrating that the results are not influenced by frequency. The dehydrofluorinated PVDF sample yields a d_{31} coefficient of 25.12±1.13 pC/N, higher than that of any other previously reported PVDF, which falls in the range of 20 pm/V to 23 pm/V.(9, 13, 83, 97, 194) The result demonstrates that the dehydrofluorinated process can generate large piezoelectric coupling in the PVDF without drawing, further demonstrating the efficacy of the chemical modification for the highly polar PVDF material. In order to correlate the piezoelectric property of dehydrofluorinated PVDF with their *%DHF*, the

d_{31} coefficients of the PVDF samples with different reaction times are also measured by DMA method, as shown in Figure 4.6. The d_{31} coefficient increases with increasing *%DHF* because of the increasing fraction of β phase induced by dehydrofluorination. The d_{31} coefficient reaches a peak value of ~25 pC/N when *%DHF* is 10%, after that the value starts to decrease with further dehydrofluorination. This result confirmed that the optimum extent of dehydrofluorination is *%DHF*=10% by a reaction time of 8 hours with EDA. The decreased piezoelectric properties at high extent of dehydrofluorination is due to the dropping dielectric properties that are caused by further dehydrofluorination.

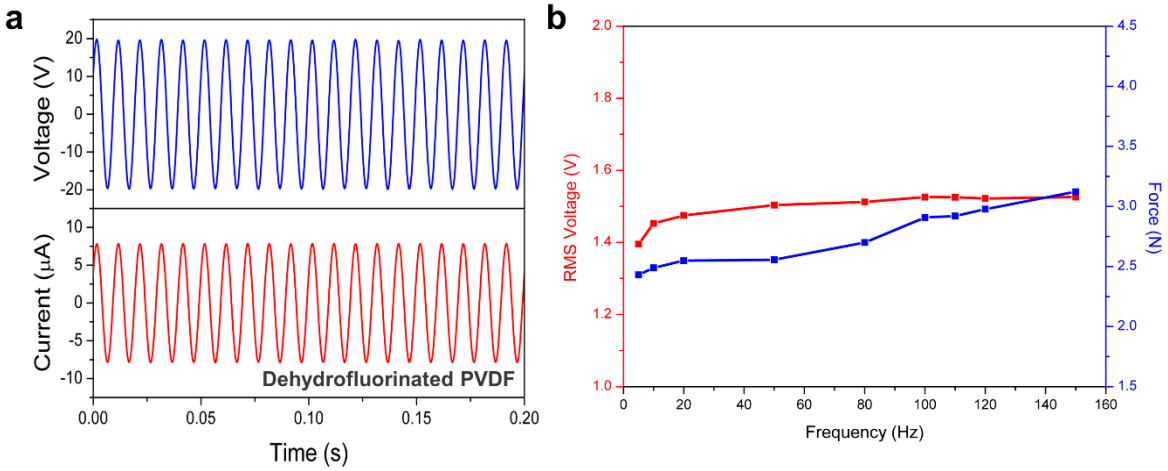

Figure 4.5. DMA measurement on dehydrofluorinated PVDF. (a) Open circuit voltage and short circuit current generated by the dehydrofluorinated PVDF sample. (b) RMS open circuit voltage and applied force from the dehydrofluorinated PVDF sample at different frequencies.

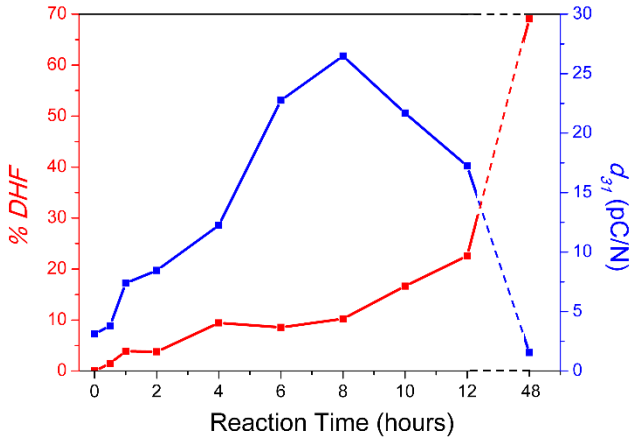

Figure 4.6 Piezoelectric d_{31} coefficient of dehydrofluorinated PVDF with different *%DHF.*

To investigate the possibility of further improved piezoelectricity of the dehydrofluorinated PVDF, the dehydrofluorinated PVDF samples are first drawn and then tested by the DMA method. The mechanical drawing process that is traditionally used for preparing the β-phase PVDF, was applied for the dehydrofluorinated PVDF films. Each film is stretched uniaxially at 100 ˚C to an elongation of 500%. The uniaxial drawing process increases the degree of crystallinity of the dehydrofluorinated PVDF film, thus higher piezoelectric properties are expected. As a result, the drawn dehydrofluorinated PVDF devices generated an open circuit RMS voltage of 15.41 V and a short circuit RMS current of 6.81 μA (Figure 4.7a), higher than that of the undrawn dehydrofluorinated PVDF. A giant d_{31} value of 35.12±0.69 pC/N is obtained after the drawing process due to the increased crystallinity. The obtained d_{31} coefficient is about 40% higher than the undrawn dehydrofluorinated PVDF, and more than 60% higher than that of the commercial drawn PVDF. A comparison of the measured d_{31} coefficients of the dehydrofluorinated PVDF (drawn and undrawn) and previously reported d_{31} coefficients of PVDF and P(VDF-TrFE) copolymers are shown in Figure 4.7b. This significant increase in the d_{31} coefficient of drawn dehydrofluorinated PVDF indicates that the piezoelectric properties of dehydrofluorinated PVDF can be further improved by traditional processing method of mechanical drawing. This study shows that ultrahigh-performance piezoelectric polymers can be developed with a combination of chemical modification such as the dehydrofluorination process and mechanical process such as the uniaxial drawing. Also, the PVDF devices tested with the DMA method are very promising to be

used as stretching mode energy harvesters given their superior electromechanical coupling properties. The energy harvesting performance of the PVDF-based devices will be discussed in the next chapter.

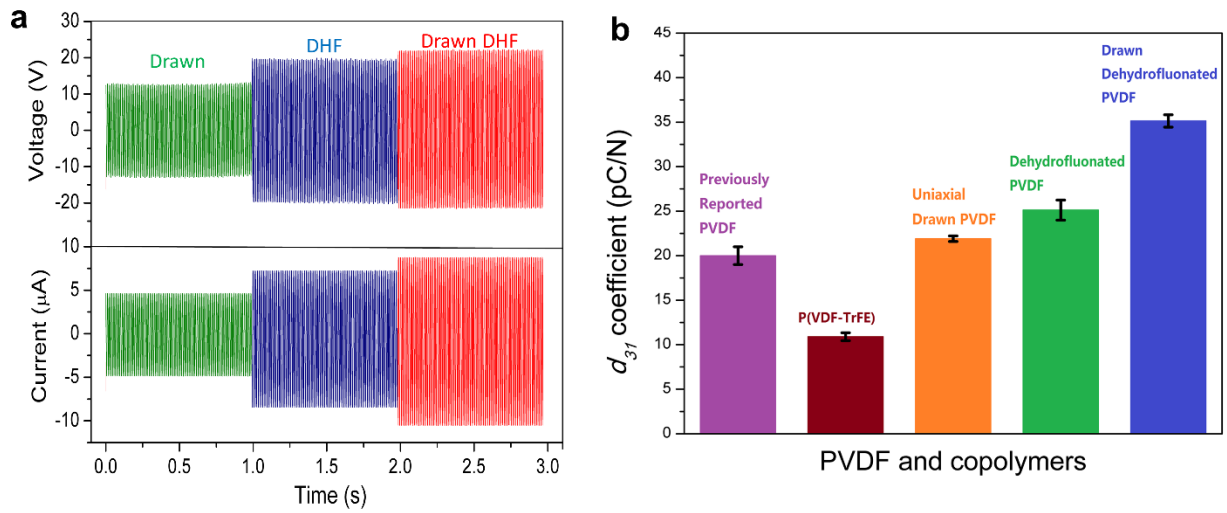

Figure 4.7. DMA measurement on dehydrofluorinated drawn PVDF and d_{31} coefficients. (a) Comparison of open circuit voltage and short circuit current generated by the conventional uniaxial drawn PVDF, the dehydrofluorinated PVDF and the drawn dehydrofluorinated PVDF under 0.5% strain at 100 Hz. (b) Previous reported d_{31} coefficients of the PVDF and its copolymers comparing to that of the dehydrofluorinated PVDF (from the DMA method). (9, 13, 83, 97, 194)

The piezoelectric coefficients measured through direct piezoelectric effect reflect the performance of piezoelectric materials in applications such as sensors and energy harvesters. In this study, the dehydrofluorinated PVDF shows improved piezoelectric properties compared to the conventional PVDF products, with a direct piezoelectric d_{33} coefficient of -39.95±2.42 pC/N and a d_{31} coefficient of 25.12±1.13 pC/N. The fact that the piezoelectricity of the dehydrofluorinated PVDF can be further improved by a conventional mechanical drawing process also provides new approaches in preparing PVDF devices with ultrahigh piezoelectric properties. The performance of the dehydrofluorinated PVDF as an energy harvester will be further investigated in detail in the next chapter.

4.3 Piezoelectric Coefficients Measurement of the Dehydrofluorinated PVDF through Inverse Effect

Inverse piezoelectric effect is the energy conversion effect where a piezoelectric material transfers the electrical energy input to mechanical energy output. This effect is usually exhibited through a generated strain of the piezoelectric material under the stimulus of an external electrical field. To measure the piezoelectric *d* coefficients through inverse effect, a uniaxial external electric field is usually applied onto the sample while the external stress field is usually zero, giving a simplified equation for the d_{ij} coefficient:

$$d_{ij} = \left(\frac{\partial S_i}{\partial E_j} \right)^T$$ with a unit of pm/V, representing displacement per applied voltage.

The measuring techniques of the d_{ij} coefficients mainly work in two ways: measuring the d_{33} coefficient by measuring the strain of the sample in the same direction of the applied electric field; or measuring the d_{31} coefficient by measuring the strain of the sample in the direction perpendicular to the applied electric field. Ideally, the piezoelectric strain coefficients from direct effects and inverse effects should be equal for the same piezoelectric material. However, because of the existence of electrostrictive effects, the apparent inverse piezoelectric coefficients of soft materials are usually different from the direct piezoelectric coefficients. Hence, measurements from both piezoelectric effects are important and necessary to thoroughly understand the electromechanical coupling performance of PVDF.

4.3.1 Refined piezoelectric force microscopy (PFM) method for piezoelectric d_{33} coefficient measurement

To capture the small piezoelectric strain in the thickness direction of the PVDF thin films in the inverse piezoelectric effect, a refined piezoelectric force microscopy (PFM) method is developed.(57, 195) The PFM measurement is conducted on a Park System XE-70 atomic force microscope. To prepare the PFM samples, the dehydrofluorinated PVDF (8 hours treatment by EDA) is spin-coated onto a piece of gold coated silicon wafer to make a thin film. A thin layer of gold is sputter coated on the PVDF films surface, serving as the bottom electrode. A thickness of ~350 nm was measured for the thin film actuator through a non-contact mode topography scan.

The film actuator is then electrically poled by corona at 125˚C at 8 kV prior to testing. A lower voltage is used here to avoid failure of the thin film during poling. As shown in Figure 4.8, the PFM test is performed by attaching a Pt-coated conductive tip with a force constant of 40 N/m on the films surface. The conductive tip is attached to the PVDF film with a normal force of 1200 nN applied, serving as the top PFM electrode. AC voltage signals in a 1 Hz triangle waveform with amplitudes in the range of 0.5 V ~ 1.5 V are first generated by an Agilent 33220A functional generator and then amplified by 200 times and applied across the thin film sample through the top PFM tip electrode and the bottom silicon wafer electrode. An AC signal frequency (17 kHz) on a lock-in amplifier is used to reduce low-frequency noise and drift near the cantilever resonance (325 kHz). The generated displacement in the thickness direction of the dehydrofluorinated PVDF sample under the voltage signal is measured by recoding the tip displacement of the AFM cantilever beam. The electric field across the sample and the generated strain are then calculated accordingly and plotted below, which will be discussed in detail in the following paragraph.

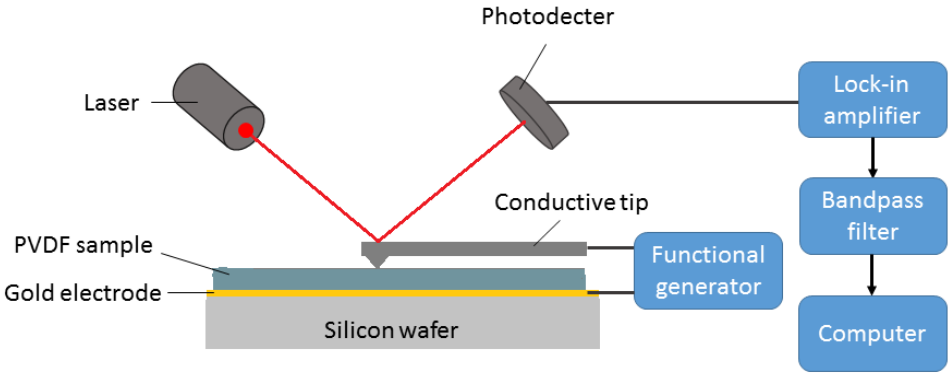

Figure 4.8. PFM setup for piezoelectric strain-electric field loop measurement.

The plots of the piezoelectric strain versus the bipolar electrical field from the dehydrofluorinated PVDF thin film is shown in Figure 4.9a. Switching of the strain direction is observed under the oscillating electric field, and this phenomenon is called a butterfly loop response, which is attributed to the piezoelectric domain motion across the electric coercive field of the PVDF. Similar to the ferroelectric hysteresis, the butterfly response is the evidence of strong piezoelectricity. In Figure 4.9b, a clear 180 ˚ phase change of the dehydrofluorinated PVDF under the bipolar voltage is observed, which shows the repolarization of the piezoelectric domains of the polymer due to the dipole switching. The phase-field loop also indicates the existence of a coercive

field matching with the strain-field loops. A large bipolar piezoelectric strain of up to 3.2% is measured from the dehydrofluorinated PVDF and is comparable to that of the irradiated P(VDF-TrFE) copolymers, which are widely reported as high-performance piezoelectric actuators.(14, 16)

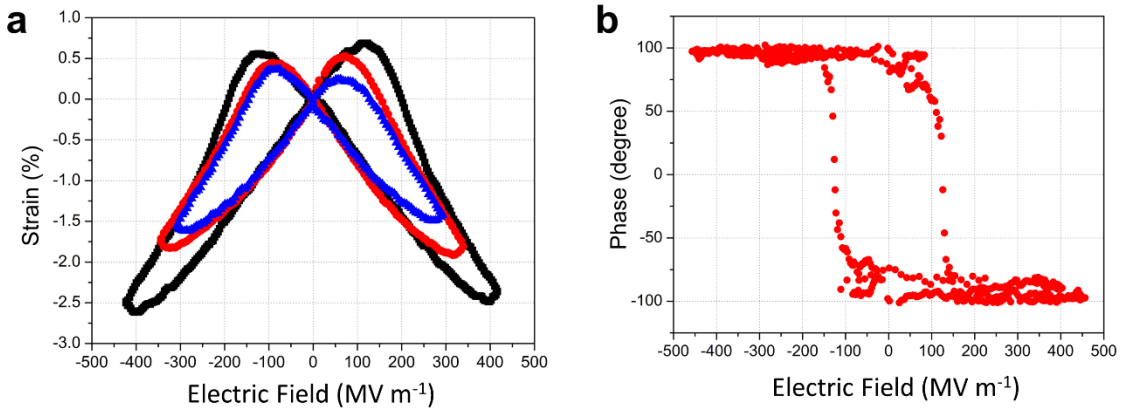

Figure 4.9. PFM measurement of dehydrofluorinated PVDF. (a) Strain versus electrical field plots (the butterfly loop response) measured under AC electric fields with different amplitude and (b) phase response of the dehydrofluorinated PVDF from PFM measurements.

To accurately measure the piezoelectric d_{33} strain coefficient, unipolar voltage signals are applied on the PVDF sample and thus a unipolar strain versus electric field loop is obtained as shown on Figure 4.10a. The results show a maximum unipolar strain of 2.7%, and the d_{33} coefficient is obtained by calculating the slope of the strain versus increasing electric field curve (Figure 4.10b). The slope increases rapidly at low electric fields and reaches a short plateau region when the strain and electric field exhibit a linear relationship. Then the slope starts to decrease at high electric fields because the piezoelectric strain is reaching saturation. The effective d_{33} coefficient is calculated as the slope of the linear region of the strain-electric field curve and a value of -65.59±0.71 pm/V is obtained. This large d_{33} value is a result of the highly aligned dipole domains induced by the large planar conformation amount in dehydrofluorinated PVDF. In previous studies, the high d_{33} values reported for PVDF and its copolymers ranged from -31 pm/V to -35.5 pm/V. (26, 83, 93, 97) The d_{33} value of the dehydrofluorinated PVDF is remarkably larger than that of any reported piezoelectric polymer. Therefore, this method furthermore proves that the newly developed dehydrofluorinated PVDF is an excellent candidate for energy harvesting, sensing and actuating devices because of its superior electromechanical coupling over the existing PVDF based polymers.

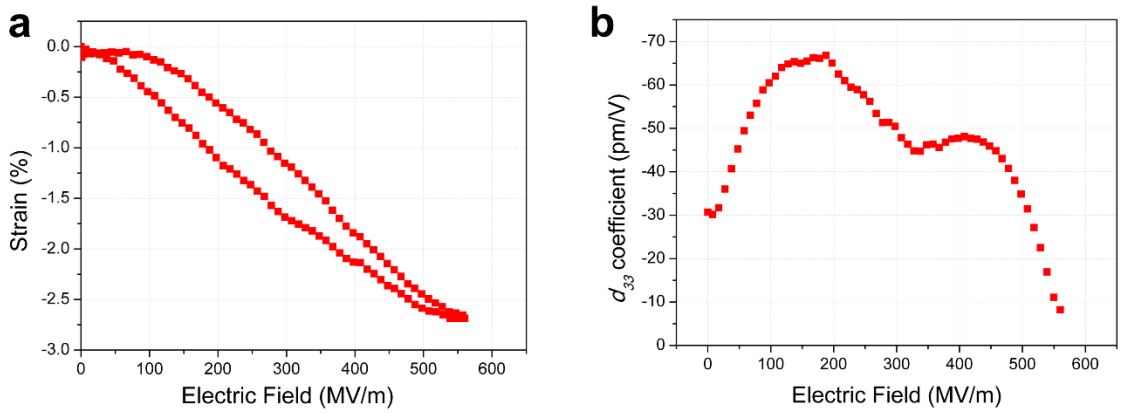

Figure 4.10 PFM measurement of dehydrofluorinated PVDF under unipolar electric fields. (a) Strain versus electric fields loop and (b) calculated d_{33} values along increasing electric fields.

Besides the piezoelectric d_{33} coefficient, the piezoelectric voltage coefficient, or so-called *g* coefficient, is also calculated for evaluating the piezoelectricity of dehydrofluorinated PVDF. The *g* coefficient is calculated by the ratio of the *d* coefficient and the dielectric permittivity. A lower permittivity of PVDF provides greater energy conversation capacity due to lower capacitance which traps a lower portion of the generated charge, compared to a piezoelectric ceramic with high permittivity. A record-breaking high g_{33} value of 0.68±0.021 Vm/N is obtained for the dehydrofluorinated PVDF. As shown in Figure 4.11, the giant g_{33} value of the dehydrofluorinated PVDF is the highest piezoelectric voltage coefficient reported for any piezoelectric material inclusive of single crystal ceramics.(13, 26, 50, 83, 173, 196, 197) This extremely large piezoelectric response reveals the underdeveloped potential of PVDF and greatly improves the prospects of dehydrofluorinated PVDF for energy harvesting and sensing applications.

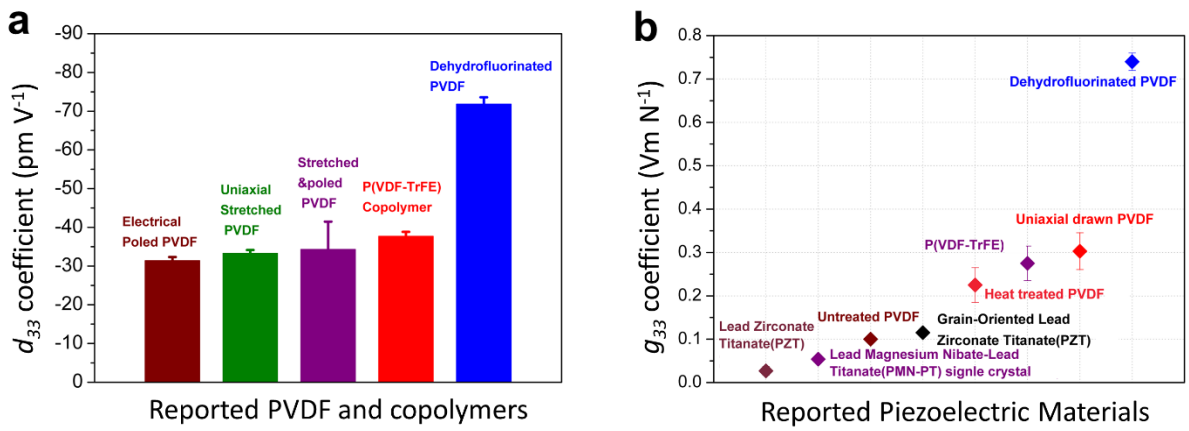

Figure 4.11. Comparison of piezoelectric d_{33} and g_{33} coefficients. (a) Previously reported d_{33} coefficients of PVDF and its copolymers compared to that of dehydrofluorinated PVDF. (26, 83, 93, 97) (b) Previous reported high g_{33} coefficients of piezoelectric materials compared to that of dehydrofluorinated PVDF. (13, 26, 50, 83, 173, 196, 197)

The characterization of the inverse piezoelectric effect shows that the dehydrofluorinated PVDF has large piezoelectric coefficients. Both the measured d_{33} of -65.59±0.71 pm/V and g_{33} of 0.68±0.01 Vm/N are higher than that of any reported PVDF based materials. It's noted that the coefficients obtained through the inverse effect are larger than that obtained from the direct effect discussed earlier in this chapter. This gap is derived from the electrostrictive effect which takes place in the PVDF and contributes to the actuation under an applied electric field. Given the fact that the electrostriction exists in all actuating measurements of soft piezoelectric materials, it should not affect the accuracy for the performance evaluation of the PVDF material as piezoelectric actuators. Besides the high piezoelectricity, the dehydrofluorinated PVDF also exhibits excellent properties such as large actuating strain and high blocking force, which are highly desired in actuator applications such as morphing wings and artificial muscles.

4.4 Investigation of Thermal Stability of β-phase of Dehydrofluorinated PVDF

Besides the superior piezoelectricity, improved thermal stability is also expected in the dehydrofluorination induced β-phase PVDF. Unlike the unstable β-phase PVDF obtained through mechanical processing, the polar phase induced through the dehydrofluorination process will be preserved at high temperatures because of the absence of internal stress which tends to relax at

elevated temperatures. As predicted by the molecular simulation in chapter 2, the β-phase crystallization in the dehydrofluorinated PVDF is energy-preferred, so the dehydrofluorinated PVDF should always crystallize in β-phase after melting or solution casting. A simple demonstration of this thermal stability of β-phase in the dehydrofluorinated PVDF is a phase composition test through melting and recrystallization. In this test, the dehydrofluorinated PVDF and the conventional uniaxial drawn PVDF are heated to 200℃ for 20 minutes, for complete melting, and then slowly cooled down to room temperature. The FTIR spectra of the two PVDF samples are obtained before and after the heat treatment for comparison, as shown in Figure 4.12. The result shows that the phase composition of the dehydrofluorinated PVDF sample remains the same after the heat treatment, while the β-phase of the drawn PVDF sample changes to α-phase after the heat treatment. The thermal stability of the β-phase is very important for the piezoelectric application of PVDF because the improved stability of β-phase will allow the high piezoelectricity of dehydrofluorinated PVDF to survive through many polymer processing techniques, which are not achievable for drawn PVDF. Manufacturing techniques such as extrusion, injection molding, and 3D printing can then be applied in the fabrication process of piezoelectric PVDF devices with complicated structures without compromising the high piezoelectricity of the PVDF materials.

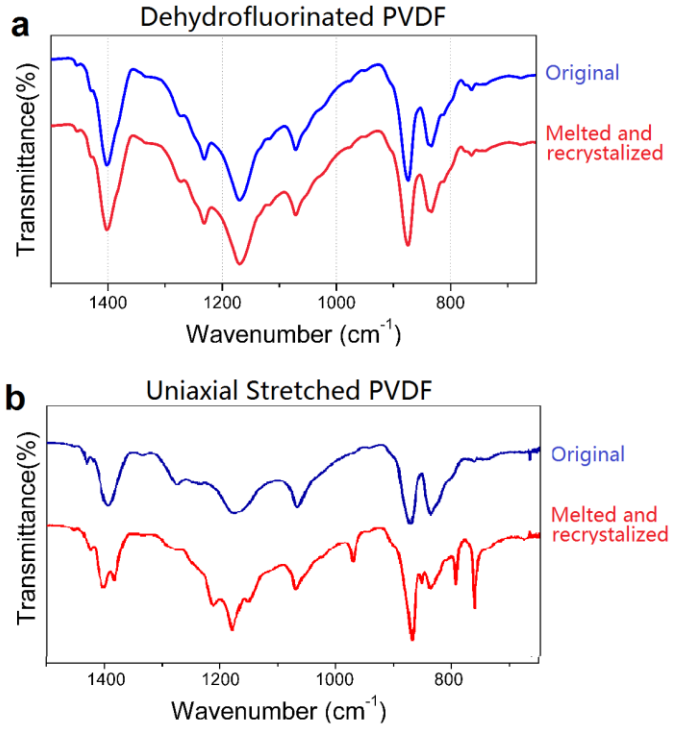

Figure 4.12. FTIR spectra of (a) the dehydrofluorinated PVDF and (b) a conventional uniaxial drawn PVDF, before and after recrystallization from melting.

To further confirm the thermal stability of the β-phase in dehydrofluorinated PVDF and investigate the phase transition of PVDF under elevated temperature, a vary-temperature XRD technique is used to monitor the phase changes within PVDF during thermal treatment. Samples of the dehydrofluorinated PVDF and the conventional drawn PVDF were heated step by step up to 200˚C and then cooled down to room temperature while the XRD patterns are collected at 25℃, 100℃, 150℃ and 200℃, respectively. The XRD patterns are also collected for these samples after they are cooled down to room temperature. As shown in Figure 4.13, the XRD patterns of the dehydrofluorinated PVDF remains the same during the heating process until it entirely turns into an amorphous phase when the material is completely melted at 200℃. This indicates that the dehydrofluorinated PVDF maintains a stable degree of crystallinity throughout the heating process before the temperature increased above its melting point. Upon cooling, the dehydrofluorinated PVDF recrystallizes into a phase composition dominated by β-phase again. However, for the conventional drawn PVDF film subjected to the same heat treatment, the peaks representing the β-phase are clearly broadened and their intensity is reduced with the increased temperature. This

behavior indicates a rapid decrease in the degree of crystallinity due to thermal relaxation of the drawn PVDF. Also, after it is melted to an amorphous phase, the drawn PVDF film eventually crystallizes into the α-phase and loses its piezoelectricity. Unlike the dehydrofluorinated PVDF, the β-phase of the drawn PVDF cannot recover from cooling after the heating process. These results demonstrate that the dehydrofluorinated PVDF possesses the unique property of preserving β-phase at elevated temperatures.

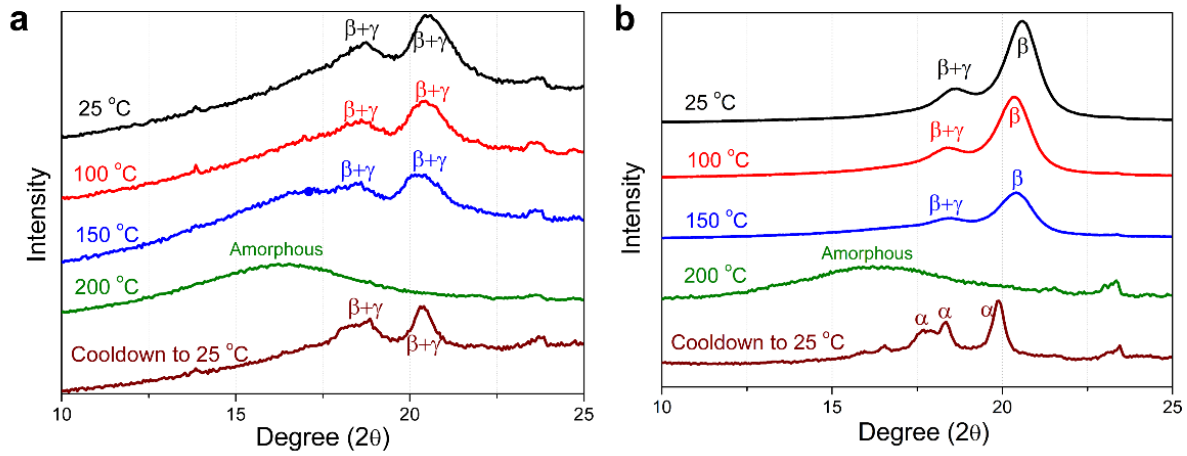

Figure 4.13 High-temperature XRD patterns of (a) the dehydrofluorinated PVDF and (b) the conventional drawn PVDF. The samples are heated up to 200 ˚C and then cool down to room temperature.

The thermal stability of the β-phase in dehydrofluorinated PVDF is further studied by monitoring the phase composition during multiple cycles of the melting-cooling processing. In each cycle, the dehydrofluorinated PVDF is heated up to 200˚C in a convection oven, held at 200˚C for 20 minutes, and then cooled down to room temperature in the oven. The FTIR spectra after each cycle is shown in Figure 4.14, and the β-phase fraction of the sample is calculated by the Beer-Lambert law discussed the chapter before. It is shown that the phase composition of the dehydrofluorinated PVDF is unchanged after up to 5 melting-cooling cycles. The β-phase fraction in the dehydrofluorinated PVDF during the 5 cycles of heat treatments is in the range of 78% to 85%. The preservation of the high β-phase fraction of the dehydrofluorinated PVDF indicates that it is able to survive multiple times of thermal processing. Recycling of the dehydrofluorinated PVDF through melting and remolding while still preserve the β-phase dominated phase composition is then applicable. However, there are still limitations in the thermal stability of the

dehydrofluorination PVDF. It's found that when the dehydrofluorinated PVDF recrystallizes from extremely high temperature, the β-phase fraction of the material may decrease. This decrease of β-phase is first observed when the dehydrofluorinated PVDF is recrystallized after 210℃ (Figure 4.15). Existence of α-phase of the dehydrofluorinated PVDF is found in its FTIR spectrum and the β-phase fraction of the sample decrease to ~65%. The fraction of β-phase is further decreased when the dehydrofluorinated PVDF is heated to higher temperatures. Eventually, after heat treatment over 220℃, the dehydrofluorinated PVDF crystallizes into α-phase instead of β-phase, thus losing most of its piezoelectricity. The loss of β-phase of the dehydrofluorinated PVDF after such high temperature treatment is due to degradation and oxidation. Thus, it should be noted that the processing temperature of the dehydrofluorinated PVDF should not exceed the threshold temperature which is found to be 210℃ in this study to preserve its high β-phase fraction. Nonetheless, this upper limit temperature is already much higher than the processing temperature allowed for the drawn PVDF.

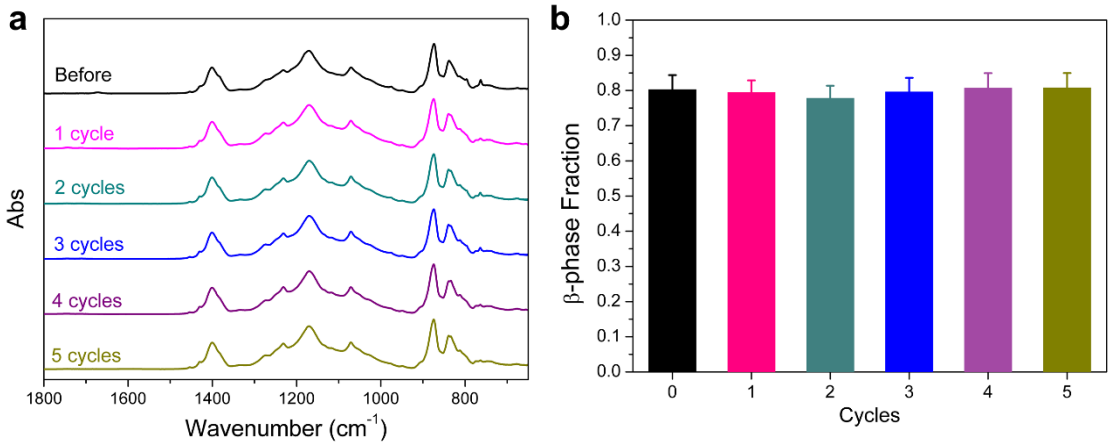

Figure 4.14 Melting-cooling treatment of dehydrofluorinated PVDF. (a) FTIR spectra and (b) β-phase fraction of the dehydrofluorinated PVDF after multiple cycles of melting-cooling treatment.

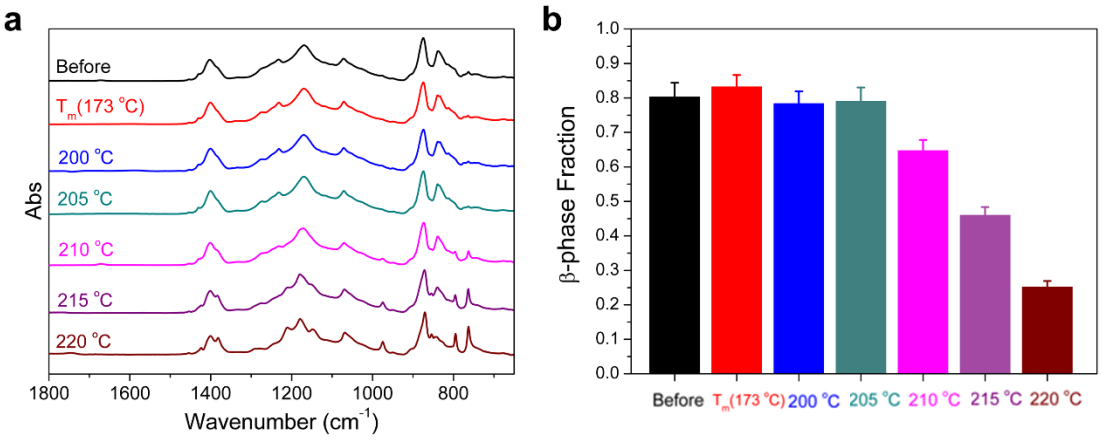

Figure 4.15 High temperature recrystallization of dehydrofluorinated PVDF. (a) FTIR spectra and (b) β-phase fraction of the dehydrofluorinated PVDF recrystallized from different temperature above its melting point.

As the thermal stability and limitation of β-phase in dehydrofluorinated PVDF have been thoroughly demonstrated above, it's not enough to conclude on the wide range of use temperatures for the dehydrofluorinated PVDF. The Curie temperature (T_c) is also very important in evaluating the use temperature of piezoelectrics. T_c is the temperature above which a piezoelectric material loses its piezoelectricity because thermal agitations of dipoles break the polarization. As reported in previous studies, defect-engineered fluoropolymers such as the P(VDF-TrFE) and the PVDF terpolymers have T_c's which are much lower than that of PVDF homopolymers. It's shown that when a high fraction of comonomers are added to the polymer, the T_c of the copolymer can be decreased to room temperature. This low T_c largely limited the application of these polymers in high temperature environments. Thus, an investigation of the T_c of dehydrofluorinated PVDF is necessary. In this study, the melting point and the T_c of the dehydrofluorinated PVDF, the commercial uniaxial stretched PVDF (obtained from TE connectivity, Inc.), and the untreated PVDF (α-phase) are measured by differential scanning calorimetry (DSC). The results show that the two β-phase PVDF samples (the dehydrofluorinated PVDF and the uniaxial stretched PVDF) have similar melting points at ~170 ˚C (Figure 4.16). For the α-phase PVDF, the melting point is found to be lower (164.61 ˚C). The T_c of the conventional drawn PVDF is found to be near its melting point, indicating its T_c of 169.25 ˚C. A large Curie transition peak is observed for the dehydrofluorinated PVDF in the DSC test, indicating the transition of the large piezoelectric domains. The T_c of the dehydrofluorinated PVDF is measured to be 163.34 ˚C, which is slightly

lower than that of the drawn PVDF. These results show that the dehydrofluorination of PVDF will slightly decrease the T_c because of the steric defects introduced into the polymer chains. However, the piezoelectricity can still be preserved up to a temperature near the melting point of PVDF. This wide range of use temperature demonstrates the advantages of the dehydrofluorinated PVDF over the PVDF copolymers in high-temperature applications.

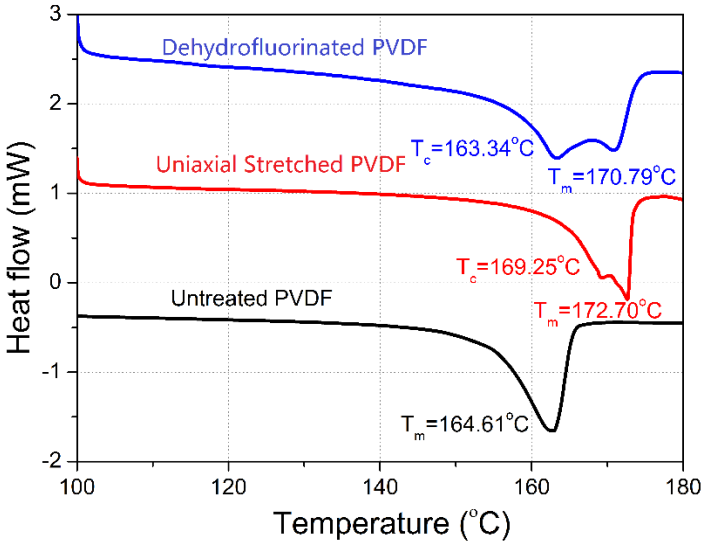

Figure 4.16. DSC measurement of the dehydrofluorinated PVDF, the commercial uniaxial stretched PVDF, and the untreated PVDF. Melting point (T_m) and Curie temperature (T_c) were measured and labeled accordingly.

4.5 Chapter Summary

In this chapter, the extraordinary piezoelectric properties of the dehydrofluorination induced β-phase PVDF are thoroughly demonstrated. The piezoelectricity of the dehydrofluorinated PVDF is investigated by characterization of its direct piezoelectric effect and inverse piezoelectric effect, respectively. In the measurement of each effect, novel characterization techniques are first developed and then validated by commercial standard materials. These measuring methods are shown to provide accurate characterization of piezoelectric coefficients of soft materials. By the Berlincourt method and DMA method, the direct piezoelectric strain coefficients of the dehydrofluorinated PVDF are measured to be a d_{33} of -39.95±2.42 pC/N and a d_{31} of 25.12±1.13 pC/N, which is higher than any previously reported data of PVDF. Additionally, the piezoelectricity of the dehydrofluorinated PVDF is found to be

further improved by the traditional mechanical processing, as the drawn dehydrofluorinated PVDF yields a higher d_{31} coefficient of 35.12±0.69 pC/N**.** By PFM method and blocking force method that measures the inverse effect, the inverse piezoelectric coefficients of the dehydrofluorinated PVDF is measured to be a d_{33} of -65.59±0.71 pm/V. A giant piezoelectric voltage coefficient (g_{33}) of 0.68 Vm/N of the dehydrofluorinated PVDF is also measured as the highest piezoelectric voltage coefficient reported for any piezoelectric material so far. These giant piezoelectric coefficients demonstrate that the developed PVDF is a worthwhile piezoelectric material candidate with great potential for low-cost, high-performance of in commercial applications.

The thermal stability of β-phase in the dehydrofluorinated PVDF is also investigated in this chapter. The Curie temperature of the developed PVDF is found to be slightly decreased by the dehydrofluorination process, but still higher than that of other defect-engineered PVDF copolymers. The varied temperature XRD and heat treatment experiments show that the dehydrofluorinated PVDF can stably recrystallize into high β-phase multiple times after high temperatures below 210 ˚C. Both the improved thermal stability and the eliminated need for mechanical drawing enable a simpler route towards additive manufacturing of PVDF materials with high polar phase content, leading to a wider range of practical applications for piezoelectric polymers.

CHAPTER 5

Development of Additive Manufacturing Method for PVDF and 3D Printed Piezoelectric Devices

5.1 Chapter Introduction

As the large piezoelectricity and high thermal stability of dehydrofluorinated PVDF has been proven, the newly developed material is supposed to gain access to many polymer processing methods which are not possible for conventional drawn PVDF. In this chapter, new possibilities in piezoelectric PVDF device fabrication are investigated by integrating the dehydrofluorinated PVDF with novel additive manufacturing methods. A direct writing method is developed for 3D printing dehydrofluorinated PVDF based on solution dispensing. The direct writing method can print simple 3D structures of PVDF and can also print 2D patterns of PVDF with precisely controlled thicknesses. This method also supports direct printing of electrodes onto printed PVDF structures, enabling one-step fabrication for piezoelectric PVDF devices. The experimental results find that the high β-phase fraction of dehydrofluorinated PVDF can be perfectly preserved. Based on this 3D printing method, PVDF energy harvesters and actuators are designed and fabricated to demonstrate the excellent performance of dehydrofluorinated PVDF originated from their improved piezoelectricity. The design of polymer energy harvesters and their frequency dependency is investigated in order to fully utilize the piezoelectricity of PVDF to increase the energy conversion efficiency in a wider range of stimuli frequencies. As a result, a well-designed dehydrofluorinated PVDF is able to generate a power density of 21.96 mW/cc, which is magnitudes higher than previously reported PVDF devices.

A novel electrospun 3D printing method is also developed and reported in this study. The reported method can achieve micron-level resolution 3D printing of PVDF and provide *in situ* electric poling to the printed material. Network structures and fabrics of PVDF are printed for the first time through this method and the energy harvesting performance of the printed structures are investigated. The results demonstrate that the developed electrospun 3D printing method has great potential for applications in breathable and wearable piezoelectric devices.

5.2 Direct-Writing Method for 3D Printing of Dehydrofluorinated PVDF

Additive manufacturing, or 3D printing, is the new trend in the development of materials processing and manufacturing techniques. The 'additive' feature of these techniques shows the potential of a convenient and economic way to fabricate complex three-dimensional structures. In the fabrication of MEMS and piezoelectric devices, the *in-situ* printing of different materials can lead to a one-step fabrication process, having an advantage over the traditional fabrication processes that requires multiple steps of machining and assembly. However, because of the necessity of mechanical drawing, conventional β-phase PVDF is not suitable for these 3D printing techniques. As discussed in chapter 4, any melting or dissolving of the conventional drawn PVDF will lead to the complete loss of β-phase, as well as its piezoelectricity. However, such limitations do not exist for dehydrofluorinated PVDF. To reveal the full potential of dehydrofluorinated PVDF, it is required to have a versatile fabrication method that alleviates design and fabrication limitations of PVDF based devices. Although most 3D printing techniques for polymeric materials are fused deposition modeling based on filament extrusion, these techniques are not suitable for dehydrofluorinated PVDF because the processing temperature is usually higher than the upper limit found in the last chapter. Simply extruding dehydrofluorinated PVDF through a high temperature extruder may lead to the loss of β-phase.

In this study, an ink-based additive manufacturing technique is developed to demonstrate the compatibility of the dehydrofluorinated PVDF with modern fabrication techniques and visualize its high electromechanical properties. A direct-write (DW) assembly technique is used in this method to print dehydrofluorinated PVDF films and build PVDF based devices. The setup of this direct-writing method is shown in Figure 5.1. In this method, dehydrofluorinated PVDF/DMF solutions, as well as other polymer solutions with controlled rheology, are prepared as printable inks. The inks are dispensed from a syringe which is connected to a liquid dispensing system (Nordson EFD Ultimus™ V High Precision Dispenser) to control the dispensing rate. The syringe is mounted on a digital controlled three-dimensional motion track (Aerotech®) that can achieve precise positioning within 0.2 μm resolution. The ink can be dispensed onto different substrates, including glass, metal and plastic, placed on a heated printing stage. The heated printing stage can control the rate of solvent evaporation in order to avoid the warping problem

that may occur in the solution casting process. Printing of multiple inks is achieved by switching the ink containing syringes. The final thickness of each deposition layer is controlled primarily by a few factors such as PVDF concentration, nuzzle diameter, deposition rate, and speed of printer-head.

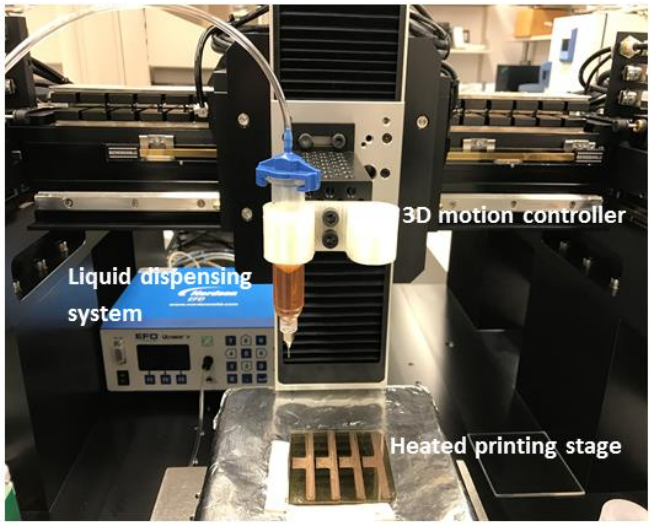

Figure 5.1. Experimental setup of direct-writing method for dehydrofluorinated PVDF.

This direct-writing method is able to conveniently prepare large area PVDF films with precisely controlled thickness in the range of 5 to 200 μm. Meanwhile, the direct-writing method can print well-designed 2-dimensional patterns of PVDF and other polymers to a desired thickness to achieve a 2.5D printing (Figure 5.2). Additionally, this method can print electrode material onto printed PVDF structures in a single printing process. A conductive ink can be prepared by the following process: 1g of poly(lactic acid) (PLA) is dissolved in 10 ml of dichloromethane(DCM), 1g of Silver nanowires (prepared according to the method reported by Sun *et al.*(198)) is added to the PLA/DCM solution. The mixture is then shear mixed followed by sonicating for 30 minutes to achieve a uniform dispersion for the printing. This electrode material can be printed on the PVDF surface with high conductivity and good adhesion. Multiple layers of circuit patterns and interdigitated electrodes can be conveniently printed together with PVDF layers (Figure 5.2b).

Therefore, complex PVDF-based devices composed of multiple materials can be simply manufactured using this direct-writing technique.

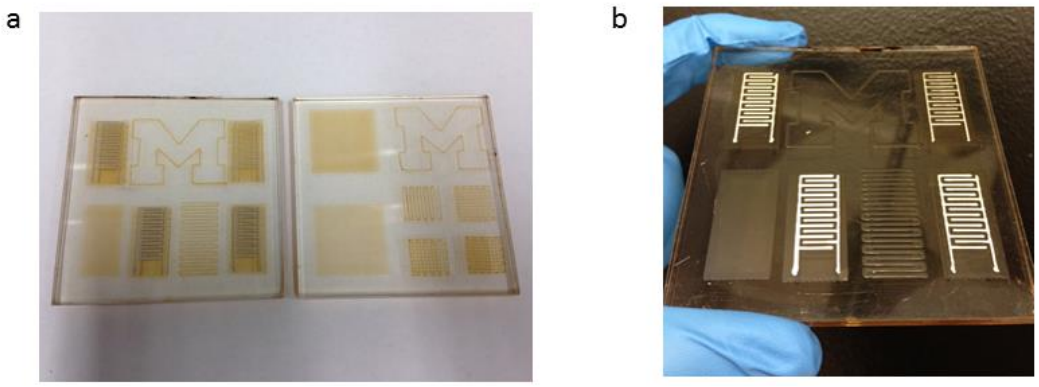

Figure 5.2. Direct-written PVDF samples. (a) Dehydrofluorinated PVDF films with complex geometries and (b) printed interdigitated electrodes with varied line thicknesses.

The phase composition of untreated PVDF and dehydrofluorinated PVDF is confirmed by FTIR and XDR, as shown in Figure 5.3. Since the direct-writing method solidifies PVDF only in the solution casting process, the high β-phase fraction of dehydrofluorinated PVDF can be perfectly preserved. The phase composition of PVDF samples prepared by the direct-writing method are found to have the same phase composition as the samples prepared by conventional doctor-blading methods. In this study, this direct-writing method is frequently used to prepare samples for chemical and electrical measurements and in fabrication of PVDF based energy harvesters and actuators.

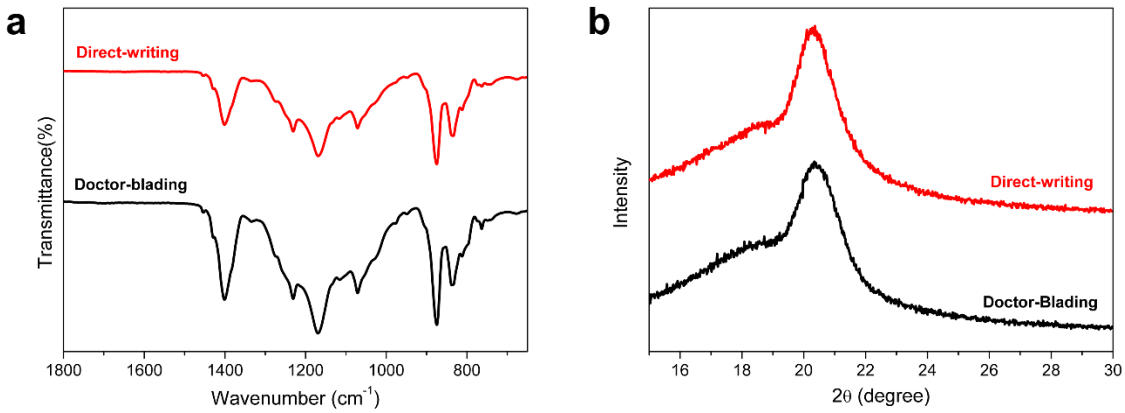

Figure 5.3. Phase composition characterization of dehydrofluorinated PVDF samples prepared by doctor-blading and direct-writing, measured by (a) FTIR and (b) XRD.

5.3 Direct-Written Dehydrofluorinated PVDF Energy Harvesters

Energy harvesting and sensing are among the most popular and promising application of piezoelectric materials. These applications utilize the direct piezoelectric effect to transfer collected mechanical energy to electrical energy. The efficiency of energy conversion is largely dependent on both the piezoelectricity of the used materials and the design of the devices. As the rapid development of small wearable devices, energy harvesters attract huge attention a possible candidate for these devices in order to achieve self-powering devices and avoid the inconvenience from batteries. In order to demonstrate the energy harvesting performance of dehydrofluorinated PVDF, different types of energy harvesters are fabricated and investigated in this study.

5.3.1 Vibrational cantilever beam mode energy harvester

Cantilever beam mode energy harvesters are one of the most reported type of energy harvesters. The most important part of this type of device is a cantilever beam that can vibrate with an external vibrational stimulus and thus generate strains in the piezoelectric part. The cantilever beam obtains the highest energy collecting efficiency when it's stimulated at its own vibrational resonance frequency. Since PVDF is a very soft material, the vibrational resonance frequency of a PVDF film is usually much lower than most ambient vibrations. Thus, PVDF cantilever beam energy harvesters are fabricated by direct-writing a thin layer of PVDF onto a stainless-steel foil. As shown in the schematic of the energy harvesting device (Figure 5.4), the

PVDF coated stainless-steel foil servers as a cantilever, allowing the energy harvesting device to achieve a resonant frequency by capitalizing upon the resonant frequency of the stainless-steel electrode rather than the resonance of the PVDF film. Devices made with β-phase dehydrofluorinated PVDF (treated with EDA for 8 hours) and untreated PVDF are fabricated for comparison purpose. PVDF coated stainless-steel devices are corona poled at elevated temperature (125℃) at 12 kV and then gold is sputtered on the surface as the top electrode before testing. During the vibrational testing, the energy harvesters are attached to a vibration shaker (LDS V408). A shear accelerometer that can give an accurate measurement of the input base acceleration is attached to the shaker and the measured acceleration signal was processed by National Instrument DAQ system (NI USB-4431). The generated voltage was measured by a unity gain voltage follower (LTC6240CS8) with 1TΩ input impedance and capacitance of 3.5 pF and the generated current was measured by a Keithley 6514 electrometer. Measured voltage and current signal were also processed by the National Instrument DAQ system.

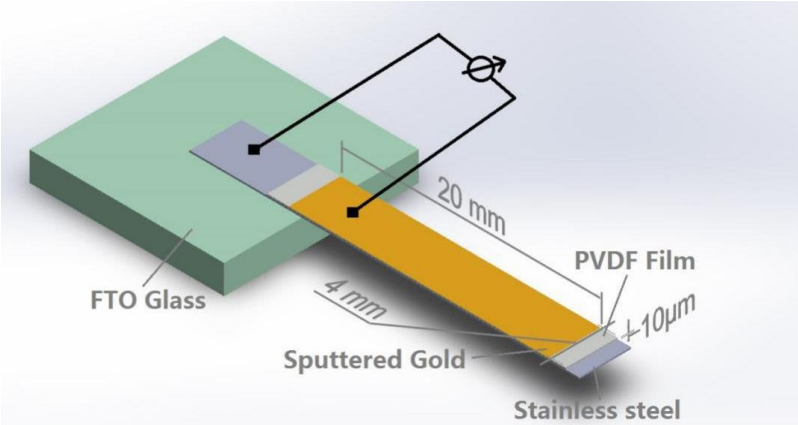

Figure 5.4. Schematic diagram of the PVDF-based cantilever beam energy harvester using stainless-steel as the cantilever.

The resonance frequency of the tested devices is roughly confirmed to be ~40 Hz by inputting a white noise vibration to the devices and measuring the frequency responses. In the vibrational test, a sinusoidal acceleration signal of frequencies close to the device resonance is input to the device to produce the vibration. High open circuit voltage and short circuit current are observed from energy harvesters under an acceleration input at exactly the resonant frequency. A peak to peak (p-p) voltage of ~3.8 V and a p-p current of ~150 nA are generated from EDA treated PVDF by applying 10 g p-p acceleration (Figure 5.5). Additionally, the p-p open circuit voltage

and the p-p short circuit current generated from the untreated PVDF energy harvester with same acceleration input at resonant frequency is measured to be ~0.55 V and ~62 nA respectively, which are much lower than the EDA treated PVDF energy harvester.

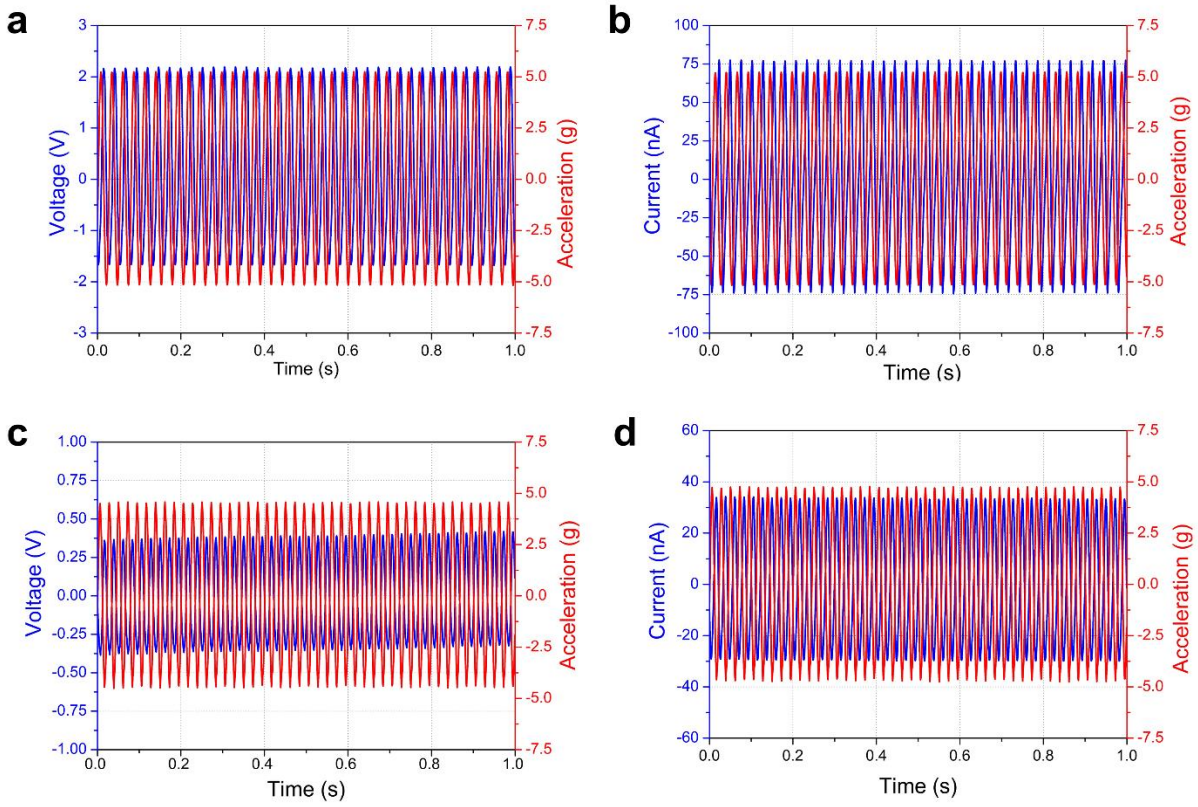

Figure 5.5. Open circuit voltage and short circuit current responses measured from cantilever beam energy harvesters. (a) (b) Dehydrofluorinated PVDF energy harvester and (c) (d) untreated PVDF energy harvester, respectively.

The generated AC power from the energy harvesting devices is calculated by measuring the voltage across several load resistors ranging from 1 MΩ to 20 MΩ. As shown in Figure 5.6, the AC power of EDA treated energy harvesting devices reaches a peak power of 137.1 nW at a load resistor of 10.1 MΩ. Then, the generated power reduces as the load resistance increases because voltage starts saturating towards the open circuit voltage. The peak power density is calculated to be 190.5 μW/cc from 10 g p-p acceleration (Figure.7b). For the untreated PVDF energy harvester, the peak AC power across a 7.7 MΩ load resistor is only 19.5 nW from the same input base

acceleration of 10 g p-p (Figure 7a). The peak power density of the untreated PVDF energy harvester is calculated to be only 24.4 μW/cc (Figure 7b). The power density from an EDA treated PVDF energy harvester is ~8 times higher than the peak power density of the untreated PVDF energy harvester, and the energy harvesting performance is better than most previously reported PVDF energy harvesters.(1, 3, 4, 146) The increased energy harvesting performance of the EDA treated PVDF is due to the higher β-phase content in the material, which will broaden its applications for energy harvesting or sensing.

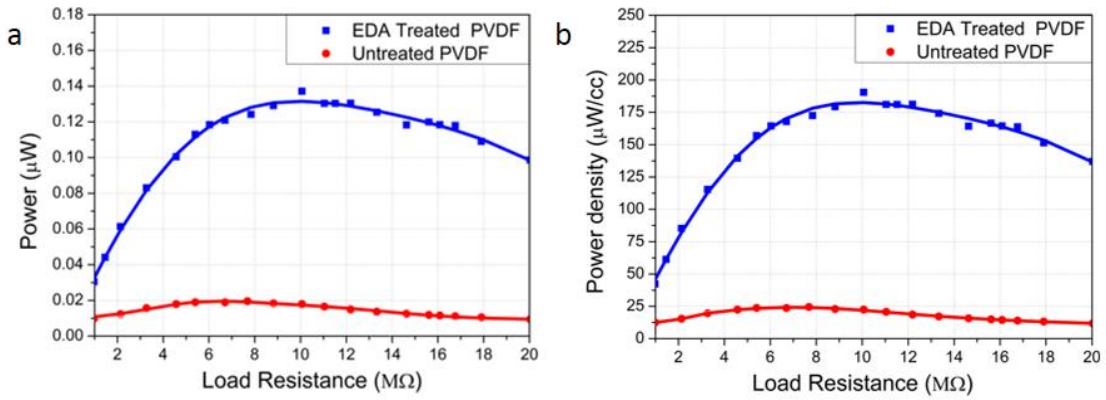

Figure 5.6. Power characterization of PVDF cantilever beam energy harvesters. (a) AC power and (b) power density of the EDA treated PVDF energy harvester across varying load resistance.

5.3.2 Stretching mode PVDF energy harvester

Since PVDF is a soft and flexible material, it's very easy to induce elastic deformation in these materials by external stress. The changes of elastic deformation in PVDF can be utilized as another mode of energy collection. The ambient vibrations can be used to induce periodic strain changes in PVDF thin films from which electric power can be generated, which is how a stretching mode energy harvester works. The stretching mode PVDF energy harvesters are fabricated by a stripe of direct-written PVDF film with fixed dimensions as shown in Figure 5.7. The gold electrodes are applied on both side of the PVDF film though sputter coating. The energy harvesting performance of these stretching mode devices are measured on a DMA instrument which can induce periodic strains with desired amplitude and frequency. The details of this method have been mentioned in chapter 4. To demonstrate the high energy harvesting performance of dehydrofluorinated PVDF, three different kinds of devices were fabricated, conventional drawn

PVDF, dehydrofluorinated PVDF and drawn dehydrofluorinated PVDF. The open circuit voltage and short circuit current measurements are shown in Figure 4.6, which show that the dehydrofluorinated PVDF can generated 55% higher voltage and 65% higher current than the conventional PVDF under a stimulus of 0.5% strain at 100 Hz. The generated voltage and current can be further improved by 10% and 23%, respectively, by applying mechanical drawing to dehydrofluorinated PVDF.

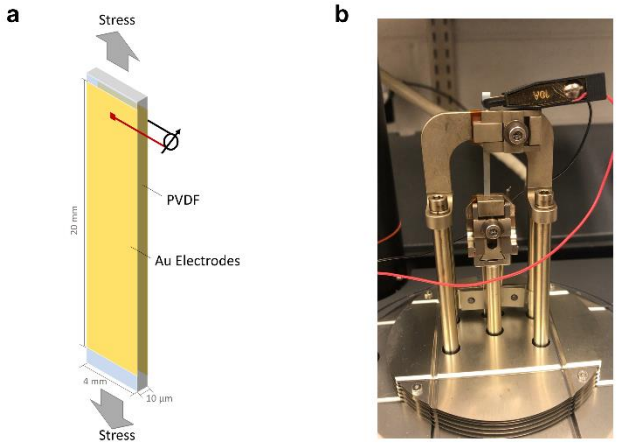

Figure 5.7. (a) Schematic diagram of a PVDF stretching mode energy harvester. (b) Performance measurement on DMA instrument.

The generated power of the energy harvesters is measured by stimulating the devices with the same strain signals across a series of load resistors ranging from 1 MΩ to 10 MΩ. The AC power generated was calculated from the generated RMS voltage value and the electrical resistance. The generated voltage across the resistor increases and saturates along with increasing load resistance, while the calculated power meets a maximum value with an optimum load resistance of 2 MΩ (Figure 5.8). A peak AC power of 36.06 µW is obtained from the dehydrofluorinated PVDF which corresponds to a peak power density of 21.96 mW/cc. The power density from the dehydrofluorinated PVDF stretching mode energy harvester is 115 times higher than the peak power density measured on the cantilever beam mode energy harvester based on the same material and is considerably higher than other previously reported PVDF energy harvesters. (1, 3, 4, 146) This large improvement in power density indicates that the stretching mode energy harvesters have much higher energy conversion efficiency.

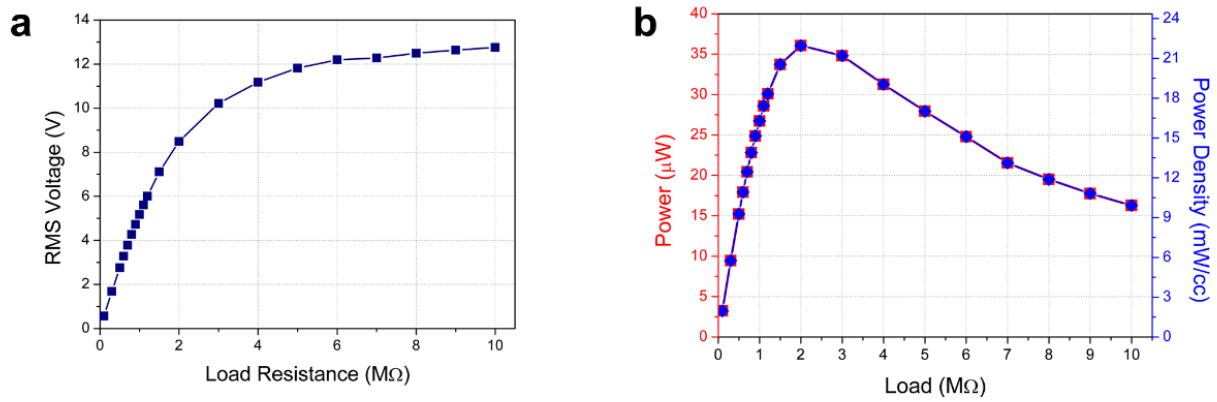

Figure 5.8. Power measurements of a dehydrofluorinated PVDF stretching mode energy harvester. (a) RMS voltage, (b) power output and power density generated by a dehydrofluorinated PVDF stretching mode energy harvester under 0.5% maximum strain at 100 Hz across different load resistances.

For the conventional PVDF energy harvester, the peak AC power across a load resistor of 2 MΩ is only 14.09 μW from the same excitation at 0.5% maximum strain at 100 Hz, leading to a calculated peak power density of only 7.01 mW/cc (Figure 5.9). The power density from the dehydrofluorinated PVDF energy harvester is 3.13 times higher than the peak power density of a conventional PVDF energy harvester. The high output power from the dehydrofluorinated PVDF films further show the giant piezoelectric voltage coefficient and the potential for the dehydrofluorination process to yield piezoelectric polymers without mechanical drawing. However, the power density can be further improved through uniaxial drawing of the dehydrofluorinated PVDF to further increase crystallinity. A maximum power density of 34.80 mW/cc is measured from the drawn dehydrofluorinated PVDF devices across an optimum load resistance of 2 MΩ, with a power output of 50.78 μW (Figure 5.9). This improved performance further confirms that the dehydrofluorination method can be combined with conventional processing methods of PVDF to further extract the potential of these functional polymers for practical applications.

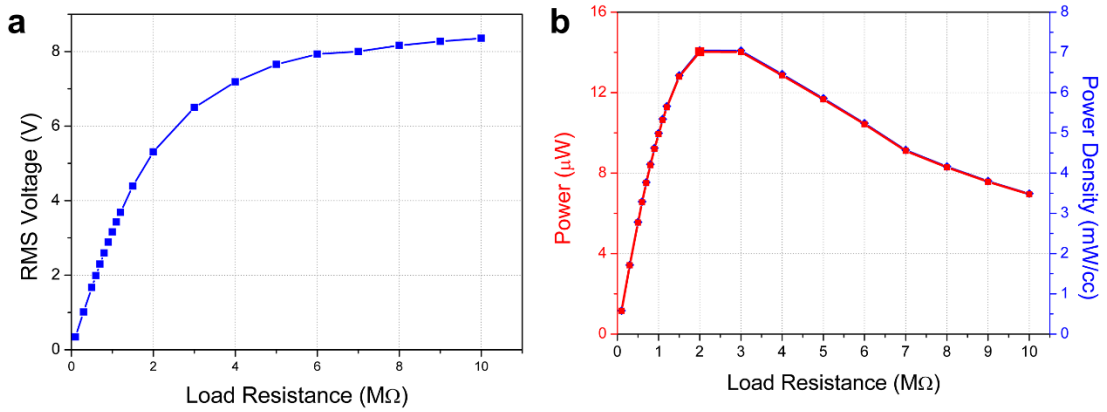

Figure 5.9. Measurement of conventional PVDF stretching mode energy harvester on a tensile frame in the DMA. (a) RMS voltage signal and (b) generated power and power density across different load resistances under 0.5% maximum strain excitation at 100 Hz.

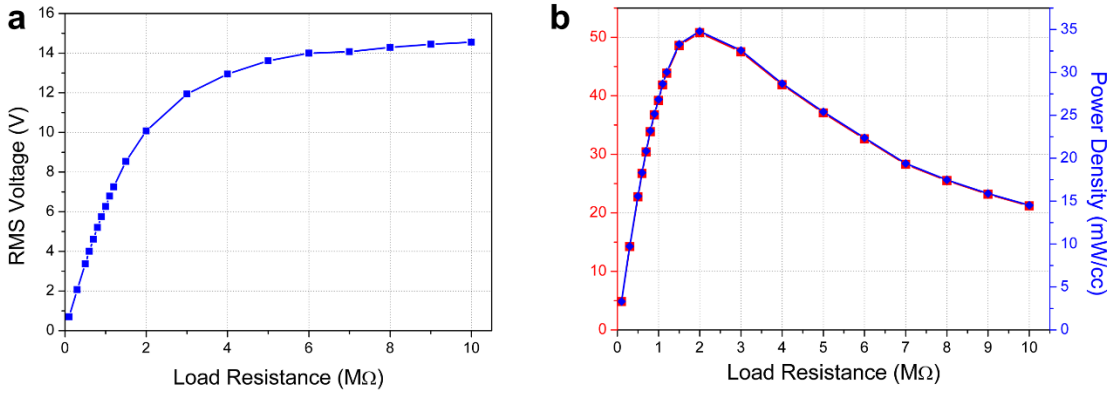

Figure 5.10. Measurement of drawn dehydrofluorinated PVDF stretching mode energy harvester on a tensile frame in the DMA. (a) RMS voltage signal and (b) generated power and power density across different load resistances under 0.5% maximum strain excitation at 100 Hz.

A comparison of the RMS voltage and power density from different stretching mode energy harvesters are shown in Figure 5.11. It shows that the drawn dehydrofluorinated devices can generate voltage about twice that of the voltage generated by conventional PVDF devices, providing a 5 times higher energy density. All PVDF based stretching mode energy harvesters can provide a power density in mW/cc level, which is much higher than the previously discussed cantilever beam energy harvesters. Such large power is sufficient to be used as a power source for small wearable digital devices. The stretching mode energy harvesters also benefit from there simple design by reducing more than 80% of the devices weight compared to the cantilever beam

devices. Since there is no need for a cantilever and supporting material in the stretching mode energy harvesters, the device completely consists of PVDF serving as both the functional component and the structural component. This design of energy harvester provides an approach to fully utilize the giant piezoelectricity in PVDF.

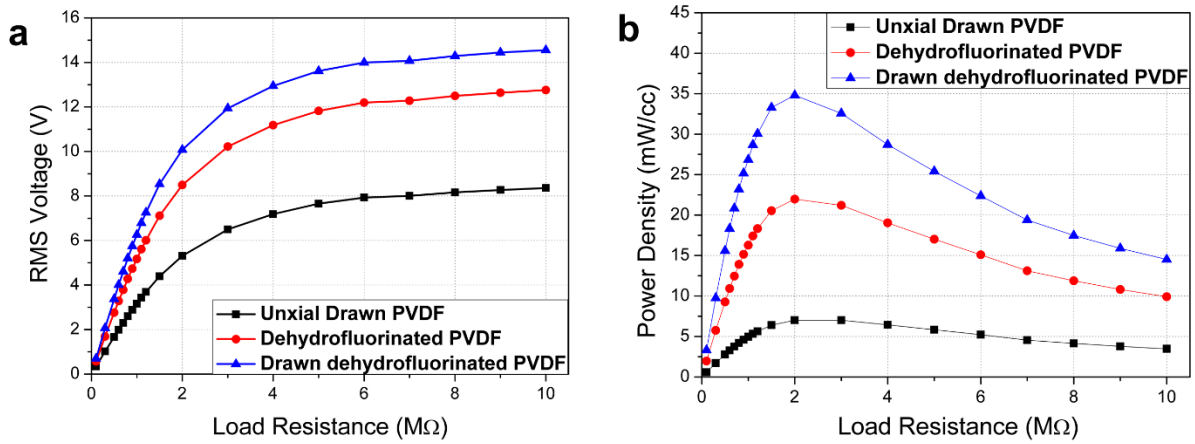

Figure 5.11. Comparison of energy harvesting performance of PVDF based stretching mode energy harvesters. (a) RMS voltage signal and (c) power density across different load resistances under 0.5% maximum strain excitation, measured from conventional uniaxial drawn PVDF, dehydrofluorinated PVDF and drawn dehydrofluorinated PVDF.

To demonstrate the feasibility of the DHF-PVDF energy harvesters as a power supply for wearable electric devices, an array of green light-emitting diodes (LEDs) are connected to the energy harvester with a LED bridge rectifying circuit. The DHF-PVDF energy harvester is able to turn on a LED array containing 6 green LEDs when it is excited at frequencies ranging from 5 Hz to 100 Hz with a maximum strain of 0.5% (Figure 5.12). This indicates a high energy-conversion efficiency of DHF-PVDF under excitation of a wide range of frequencies, including the low frequency range of human motions. The large energy harvesting capacity of DHF-PVDF is demonstrated by using it as the power supply for a larger LED array. When excited at 100Hz under a maximum strain of 0.5%, the DHF-PVDF energy harvester is able to light up a maximum number of 42 green LEDs, as shown in Figure 5.12b. The high output power from the dehydrofluorinated PVDF films further show the huge piezoelectric voltage coefficient and the potential for the dehydrofluorination process to yield piezoelectric polymers that do not require drawing to induce the formation of β-phase, making them suitable for integration into additive manufacturing processes as functional materials.

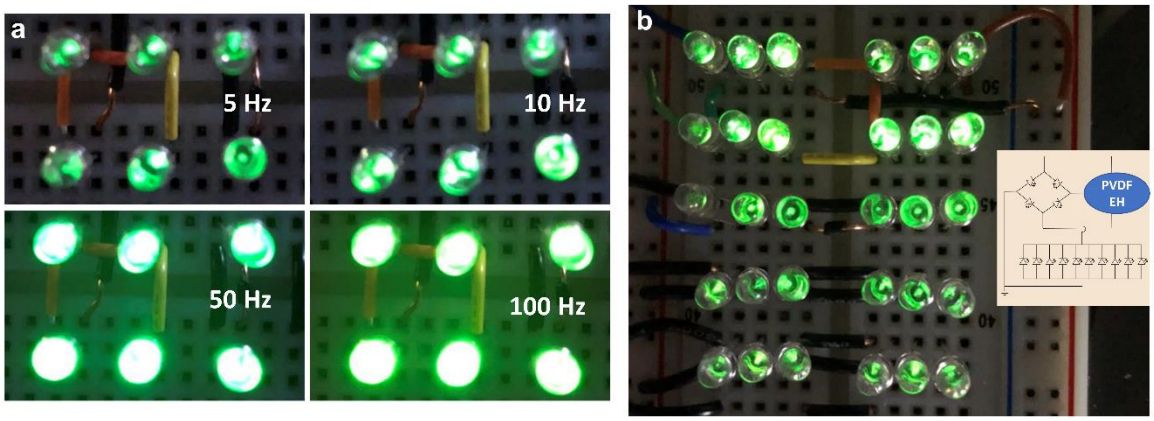

Figure 5.12. PVDF energy harvester powered LED arrays. (a) LED array containing 6 green LED bulbs lit up by a dehydrofluorinated PVDF energy harvester excited at different frequency. (b) LED array containing 42 green bulbs lit up by the same device excited at 100Hz under 0.5% maximum strain excitation. The inset shows the circuit diagram of the LEDs array.

5.3.3 Frequency dependency of PVDF energy harvesters

Frequency dependency is another major concern on the performance of energy harvesters. As discussed previously, the cantilever beam harvesters can only achieve high power output when the external stimulus is near to the resonance frequency of the cantilever. The resonance frequency is only determined by the dimension and stiffness of the cantilever material. At other frequencies away from the resonance, the cantilever cannot generate a large deformation during the vibration, leading to a low energy conversion efficiency. This results in a situation that, although satisfactory energy density is achieved at specific frequency, the actual performance of the energy harvester is very poor when it's subjected to ambient vibrations with a wide range of frequencies. This frequency dependency can be found in many reports of energy harvesters, and largely limits their application. In this study, the frequency dependency of the stretching mode energy harvesters is investigated. Since the excitation of PVDF in stretching mode energy harvester doesn't rely on the vibration of cantilevers, it's expected that the energy conversion efficiency is less influenced from the stimuli frequency.

The investigation of frequency dependency is performed by applying strains to the stretching mode energy harvesters with the same amplitude but different frequency. Figure 5.12 shows the energy generating performance of a dehydrofluorinated PVDF energy harvester across

different load resistors measured at 10 Hz, 50 Hz and 100 Hz, respectively. At all frequency the RMS voltage is saturating towards the same open circuit voltage with increasing load resistance. The optimum resistance for the maximum generated power increases as the frequency decreases and found to be in a reciprocal relationship with the frequency. Eventually, a peak power density of 2.17 mW/cc is observed across an optimum load resistor of 23 MΩ under a stimulus of 0.5% strain at 10 Hz. At 50 Hz, the dehydrofluorinated PVDF generated a peak power density of 10.53 mW/cc observed across an optimum load resistor of 5 MΩ. Compared to the peak power density of 21.96 mW/cc obtained at 100 Hz, it seems that the power generating performance is largely decreased with the frequency. However, it should be noted that the input stimuli possess different energies because of the different frequencies. As the input power from a sinusoidal force wave is proportional to the frequency, the ratio between the strains stimuli at 10 Hz, 50 Hz and 100 Hz equals 1:5:10. The ratio of peak power density measured from the stretching mode energy harvester at 10 Hz, 50 Hz and 100 Hz is 2.17 mW/cc: 10.53 mW/cc: 21.96 mW/cc respectively, which is very close to the ratio of the input power. This result indicates that frequency will not affect the energy conversion efficiency of the stretching mode energy harvesters.

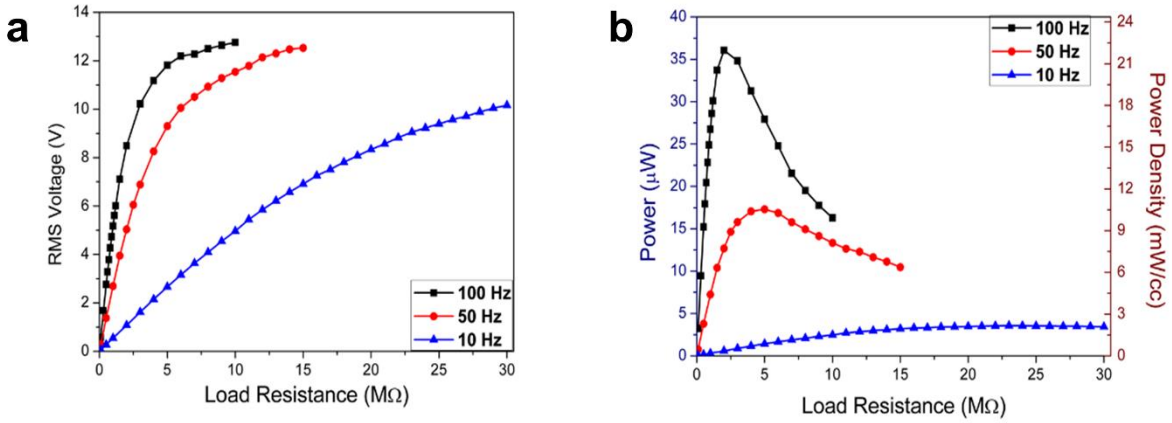

Figure 5.13. (a) RMS voltage, (b) power and power density across different load resistances measured at 10 Hz, 50 Hz and 100 Hz.

The same frequency dependence study was performed on the conventional PVDF energy harvesters and drawn dehydrofluorinated PVDF energy harvesters as a comparison (Figure 5.13 and Figure 5.14). The conventional PVDF device gives a peak power density value of 0.72 mW/cc at an optimum load resistance of 26 MΩ at 10 Hz, and 3.49 mW/cc at an optimum load resistance

of 5 MΩ at 50 Hz (Figure 5.13). For the drawn dehydrofluorinated PVDF energy harvesters, a peak power density of 3.16 mW/cc is obtained at an optimum load resistance of 21 MΩ at 10 Hz, while a peak power density of 15.79 mW/cc is observed at an optimum load resistance of 4 MΩ at 50 Hz (Figure 5.14). The power density is found to be proportional to the frequency, indicating a constant energy conversion efficiency. The power density of dehydrofluorinated PVDF and drawn dehydrofluorinated PVDF are approximately 3 times higher and 5 times higher than the conventional drawn PVDF, respectively. These results further demonstrate the excellent capacity of dehydrofluorinated PVDF for energy conversion, which has been indicated by the giant piezoelectric coupling coefficients. Such high energy harvesting performance indicates the potential of dehydrofluorinated PVDF as a valuable candidate material for wide-frequency energy harvesting and sensing applications.

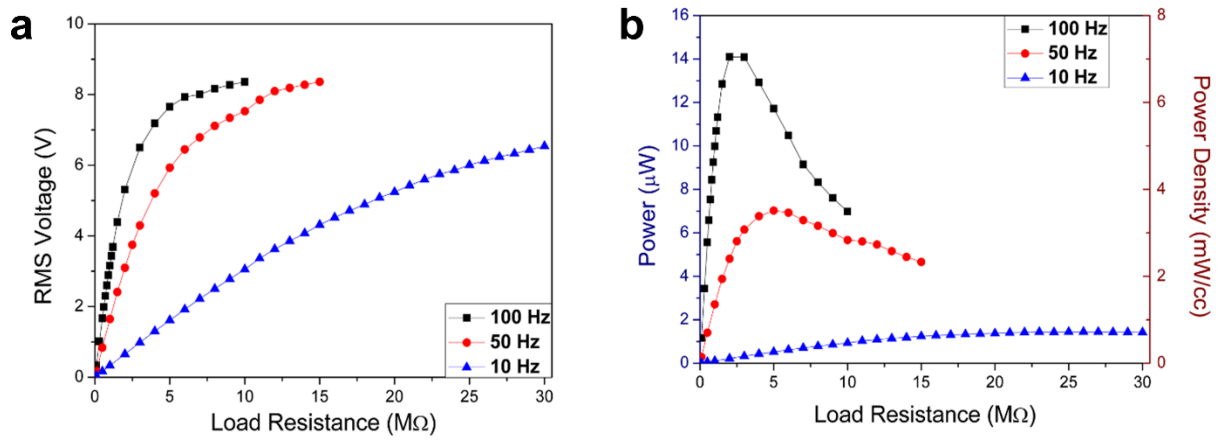

Figure 5.14. (a) RMS voltage, (b) power and power density of conventional drawn PVDF energy harvester across different load resistances measured at 10 Hz, 50 Hz and 100 Hz.

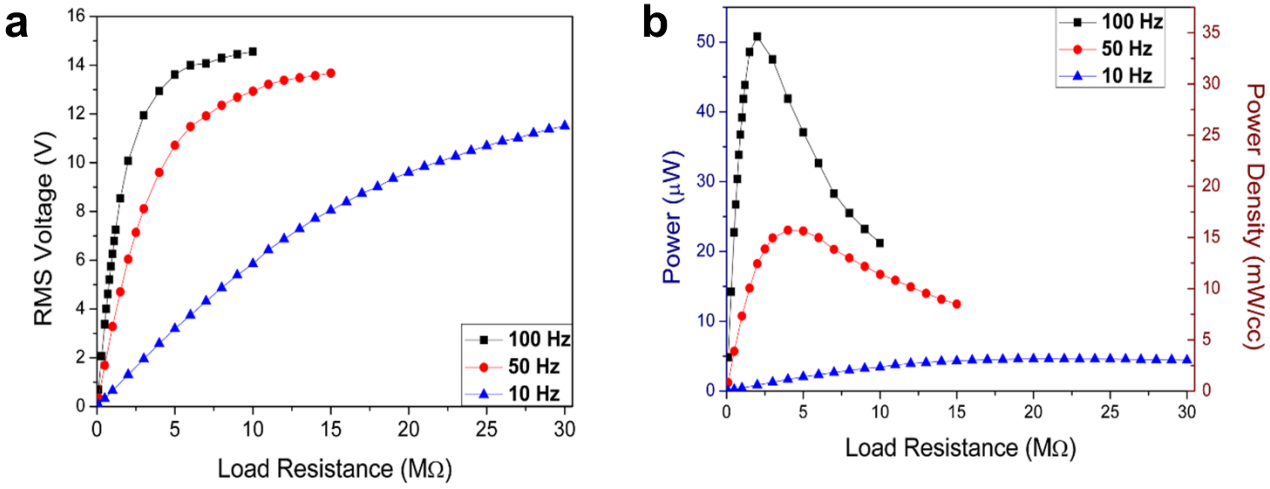

Figure 5.15. (a) RMS voltage, (b) power and power density of drawn dehydrofluorinated PVDF energy harvester across different load resistances measured at 10 Hz, 50 Hz and 100 Hz.

5.4 Direct-Written Dehydrofluorinated PVDF Actuators

Actuators are another popular and promising application of piezoelectric materials. These applications utilize the inverse piezoelectric effect to transfer electrical energy to mechanical stress or deformation. Piezoelectric ceramic actuators have been widely used in nano-positioning and high strain rate applications because of their fast and precise responses to electric fields. However, the use of these materials as actuators are limited because the properties of ceramic materials restrict piezoelectric ceramics from generating large strains. Thus, piezoelectric polymers that can generate large strains in a fast and precise manor have attracted lots of interests and will find their use in applications such as artificial muscles, robotics and morphing wing aircrafts. In this study, in order to demonstrate the actuating performance of dehydrofluorinated PVDF, bilayer actuators of dehydrofluorinated PVDF are fabricated and investigated.

Utilizing the optimized processing parameters, a bilayer piezoelectric actuator consisting of dehydrofluorinated PVDF and polylactic acid (PLA) is fabricated by the direct-writing (DW) method (Figure 5.15). A clear and smooth thin film of dehydrofluorinated PVDF with a thickness of 15 microns is prepared using the DW method. After depositing gold nanoparticles as the electrode, a thin layer of PLA is deposited on the PVDF film to create an asymmetric beam structure. Once an electric field is applied on the PVDF layer, deformations will be induced in the

longitude and thickness direction of the PVDF film, while the PLA film is not affected by the electric field. An asymmetric strain distribution will be induced in the PVDF/PLA bilayer which leads to a large bending deformation of the actuator.

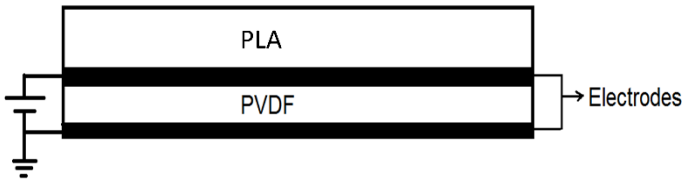

Figure 5.16. A schematic diagram of the PVDF/PLA bilayer actuator.

The actuating experiment is performed by applying a bipolar electric field up to ±125 MV/m to the actuator. The bilayer is originally curved because of the different shrinkage ratio of the two layers during the drying process. Large deformation is observed as the curvature of the bilayer decreases and eventually the bilayer is straightened when the applied field reaches the maximum value. Similar deformation is observed when an electric field is applied regardless of its direction across the film thickness. Under high electric field, a negative strain along the field direction is generated in the dehydrofluorinated PVDF layer as well as an expansive strain perpendicular to the field direction, which cause a difference in length between the active and inactive layers. This mismatch in length in an addition to the high electromechanical coupling of dehydrofluorinated PVDF which leads to such a large deformation observed here. As a result, the maximum piezoelectric strain of 3.2% measured from dehydrofluorinated PVDF by PFM method is translated to a visible large deformation of a PVDF based actuator.

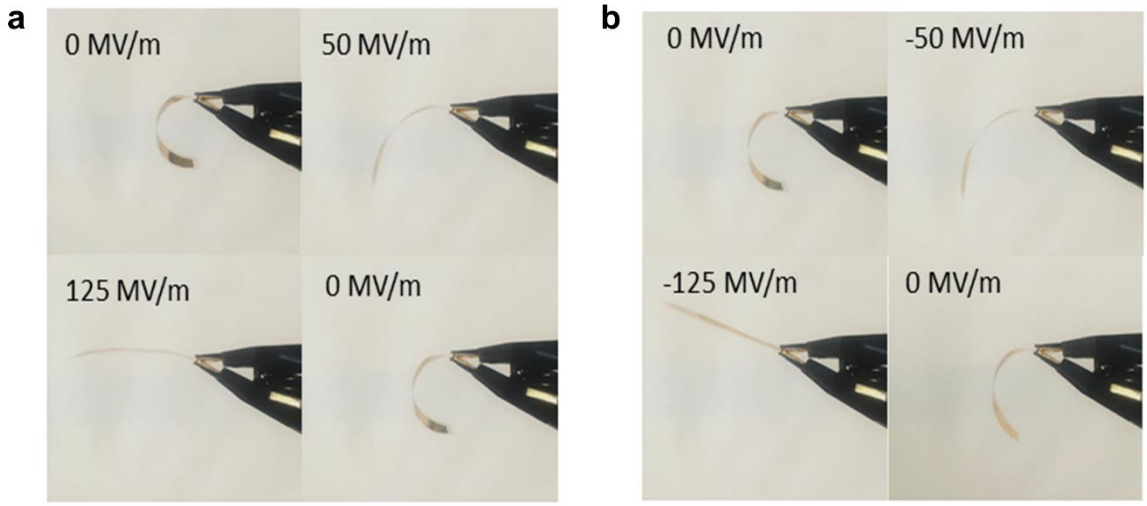

Figure 5.17. (a) and (b) Dehydrofluorinated PVDF/PLA bilayer actuator under electric field up to ±125 MV/m.

5.5 Electrospun-Assisted 3D Printing Method for PVDF

Another 3D printing method for PVDF developed in this study is based on a different mechanism. As discussed above, the reported direct-writing method can print complex 2D patterns of PVDF with precisely controlled thickness to achieve a semi-3D printing of PVDF. However, the resolution of the printed 2D patterns are largely limited by the size of nozzles used in the printing. Although the piezoelectric devices can be printed in one step by the direct-writing method, electric poling of the devices is still required to maximize the piezoelectric performance. In order to further improve the printing resolution and overcome such inconveniences, a novel electrospun-assisted 3D printing method is developed. The new method is based on the near-field electrospinning method which has been reported for preparing continuous and oriented polymer nanofibers. The experimental setup used for the electrospun-assisted 3D printing of PVDF is shown in Figure 5.17. This method utilizes a setup combining electrospinning and 3D printing, where polymers are first electrospun from solution into nanofibers and then accurately deposited on to a grounded substrate using an automated stage. High concentration PVDF/DMF solutions (up to 30 wt.%) are used as inks for the printing of PVDF. The printing resolution is controlled by the voltage and distance between the nozzle and grounded substrate, the viscosity of the polymer solution and the speed of the nozzle motion.

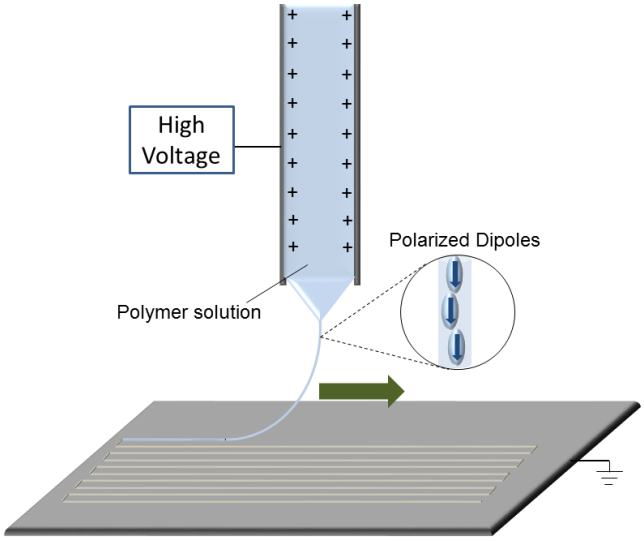

Figure 5.18. Experimental setup for electrospun-assisted 3D printing of PVDF.

During the electrospinning process, mechanical stretching and electrical poling take place simultaneously on the spun PVDF nanofibers through the electric field applied between the printing head and substrate. Such stretching and poling effect can further improve the piezoelectricity of the dehydrofluorinated PVDF and maximize their performance in the printed device. Through this method, thin single PVDF fibers can be printed and used as the basic building block for 3D structures of PVDF (Figure 5.18). The diameter of a single printed fiber is measured to be 1 to 3 μm, which is much smaller than the diameter of the nozzle (200 μm). Chemical characterization results show that the printed dehydrofluorinated PVDF contains a high fraction of β-phase. The PFM measurement of the printed sample yields a high piezoelectric d_{33} coefficient of -85.93 m/V, which is higher than the result obtained from dehydrofluorinated films. This high d_{33} value indicates that the piezoelectricity of dehydrofluorinated PVDF is further improved by the stretching and poling effect during the electrospinning.

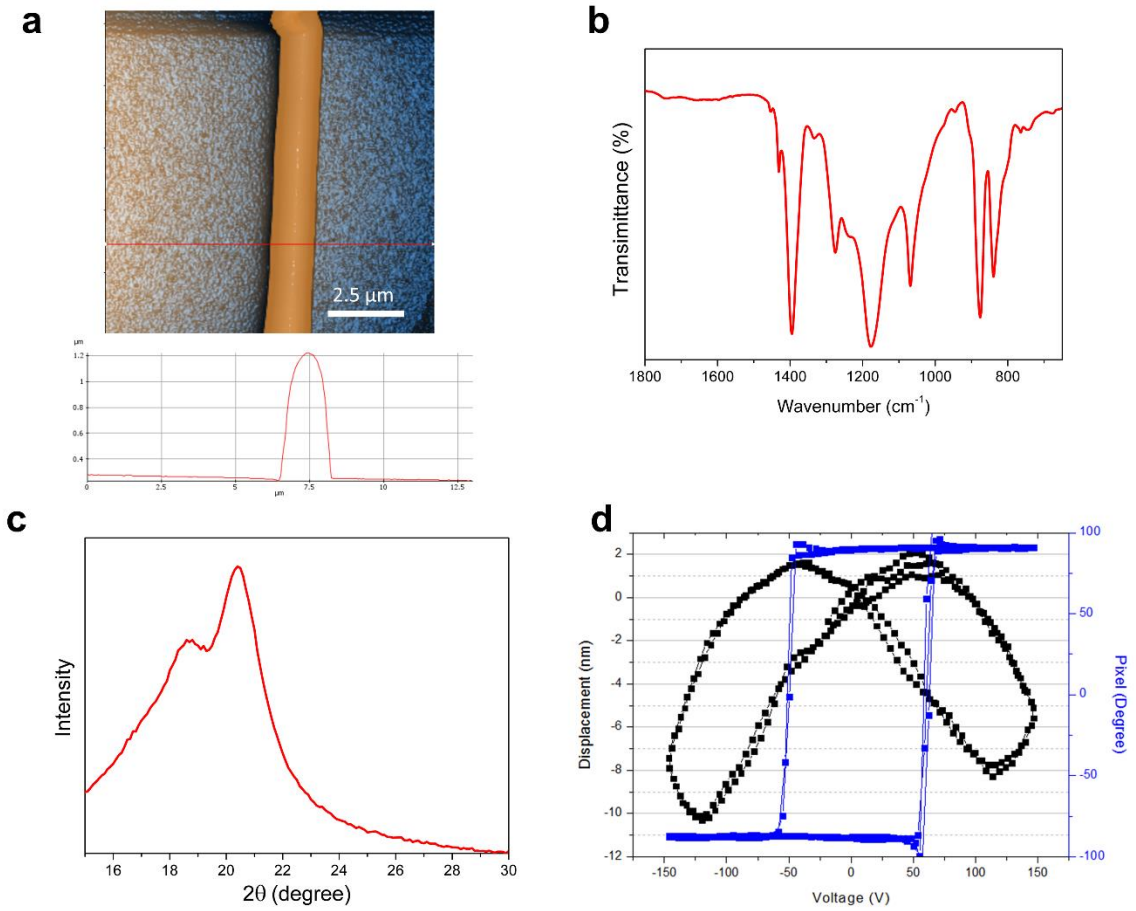

Figure 5.19. Microscale PVDF fiber printed by electrospun-assisted 3D printing method. (a) AFM scanning, (b) FTIR spectra, (c) XRD pattern and (d) PFM measurement of a single PVDF fiber printed by electrospun-assisted 3D printing method.

PVDF grids are printed by the electrospun-assisted 3D printed method to demonstrate its 3D printing capability. This method is able to build a PVDF structure over 80 layers to form a thin wall structure of ~3 mm height. The printed PVDF grids are highly flexible and breathable. The morphology of the printed PVDF grids are observed through SEM imaging (Figure 5.19). These images show that the electrospun PVDF fibers are perfectly placed on top of previously printed layers as the designed printing pattern. The layer thickness of the printed PVDF structure is measured to be 3 to 4 µm, while the wall thickness is about 10 µm. The difference between the dimensions of a single printed fiber and the actual printed layer is because the solvent-containing fiber flows on the printed surface once deposited and then dries into a belt shape layer. It should

be noted that when printing PVDF structures consisting of a large number of layers, mismatching of two neighboring layers will occur at higher layer numbers. The mismatching is caused by the electrostatic repulsion from the top of the printed structure where charge is accumulated. Such a problem can be partially released by using an AC electric field as the driven field for electrospinning.

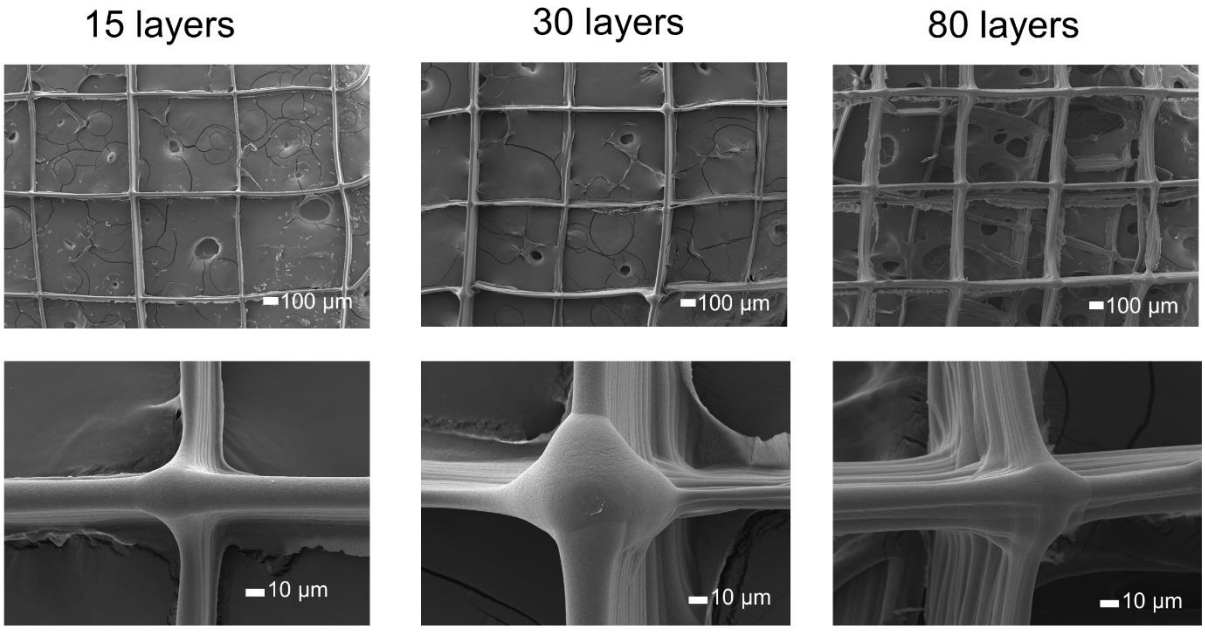

Figure 5.20. SEM images of electrospun-assisted 3D printed PVDF grids.

The electrospun-assisted 3D printing method can print PVDF structures on any grounded surfaces without direct contact, which may provide a new approach to the fabrication of wearable piezoelectric devices. To demonstrate the capacity of this novel 3D printing method in PVDF device fabrication, a wearable energy harvester is prepared by printing PVDF grids on a latex glove. As shown in Figure 5.20, the printing area of the latex glove is an electrode by sputtered gold prior to printing. A PVDF grid containing 80 layers is printed on the latex glove. The printed PVDF grid shows great adhesion and flexibility on the glove. The voltage generating performance of the wearable energy harvester is tested by applying a periodic strain signal with amplitude of 0.5% and frequency of 5 Hz. An open circuit voltage signal with a p-p value of 200mV is collected from the device.

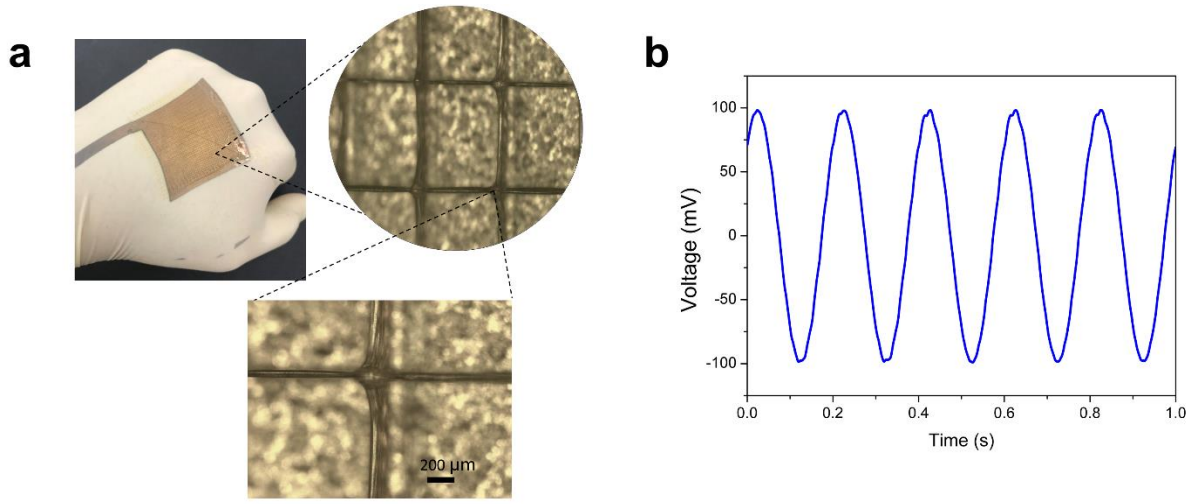

Figure 5.21. (a) Wearable PVDF energy harvester on a glove and (b) generated open circuit voltage signal.

As a newly developed 3D printing method for PVDF, the electrospun-assisted 3D printing method still suffers from several problems such as low printing speeds and decreased accuracy in printing tall structures. Although further optimization and improvement is required, the method provides a novel approach for high resolution PVDF printing and applicable research directions for the fabrication of micro- and nano-scale piezoelectric devices.

5.6 Chapter Summary

This chapter focuses on the additive manufacturing method and application of the newly developed dehydrofluorination induced β-phase PVDF. A direct-writing method is developed as a novel 3D printing method for dehydrofluorinated PVDF. The direct-writing method can print 2D patterns of PVDF with precisely controlled thickness while preserving the β-phase fraction of dehydrofluorinated PVDF. Cantilever beam mode energy harvesters and newly developed stretching mode energy harvesters are fabricated by the direct-writing method. The stretching mode energy harvester based on dehydrofluorinated PVDF shows a high-power density of 21.96 mW/cc, over 3 times higher than conventional drawn PVDF based devices. The energy harvesting performance is further improved by applying drawing to the dehydrofluorinated PVDF. A giant

power density of 34.80 mW/cc is obtained from drawn dehydrofluorinated PVDF based devices, demonstrating the high energy conversion efficiency. Such high-power output from these dehydrofluorinated PVDF is sufficient to serve as the power source for small wearable digital devices like pacemakers. Further investigation in the frequency dependency shows that the stretching mode energy harvesters exhibit a high energy conversion efficiency irrelevant to the frequency. The great potential of dehydrofluorinated PVDF as well as the design of stretching mode energy harvesters in wide-frequency energy harvesting and sensing applications are well demonstrated. Dehydrofluorinated PVDF/PLA bilayer actuators are also fabricated through the direct-writing method. The fabricated actuator is able to translate the 3.2% piezoelectric strain from dehydrofluorinated PVDF to a large deformation.

A newly developed electrospun-assisted 3D printing method is also introduced for high resolution 3D printing of PVDF. This method can provide *in situ* stretching and electric poling while print PVDF 3D structure with micron-level high resolution. It's shown that the piezoelectricity of the printed dehydrofluorinated PVDF can be further improved, yielding a piezoelectric d_{33} coefficient of -85.93 pm/V. A wearable and breathable PVDF energy harvester is fabricated by printing PVDF grids on a glove through the electrospun-assisted 3D printing method. The device is able to generate a voltage signal of 200 mV p-p value under a 0.5% strain. The techniques and results presented in this chapter demonstrate that by integrating dehydrofluorinated PVDF with additive manufacturing methods, piezoelectric energy harvesters and actuators with greater performance can be fabricated in a more convenient process, compared to the manufacturing techniques used for conventional drawn PVDF. The new materials and new 3D printing methods provide novel approaches to the development of future piezoelectric devices.

CHAPTER 6

Conclusions

The piezoelectric polymer PVDF has attracted great attention because of its piezoelectric properties and unique features as a soft material. Compared to traditional piezoelectric ceramics, PVDF can generate many times larger piezoelectric strain and has broader access to fabrication techniques. With these advantages, PVDF and its copolymers are found to have great potential in frontier research fields such as self-powered wearable devices, artificial muscles and soft robotics. The piezoelectric property of PVDF is related to the composition of crystalline phases. To guarantee high performance in piezoelectric applications, PVDF with a high fraction of β-phase is required. However, conventional techniques for preparation of β-phase PVDF mostly use a mechanical drawing method which lead to low thermal stability and limited product form (only applicable to films and fibers). Some non-mechanical methods such as low temperature evaporation and annealing have been developed, but still cannot solve the problems found from the mechanical methods. The difficulty of preparing β-phase PVDF is due to the large differences between the conformational energy of the phases in PVDF. A defect-engineering strategy is developed to change the original conformational energy of PVDF by introducing other comonomers. Based on this strategy, PVDF copolymers such as P(VDF-TrFE) that can stably crystalize β-phase have been successfully developed. However, the copolymerization method also leads to many undesired changes to the bulk properties of PVDF. Although the β-phase formation is promoted, the copolymers exhibit a low Curie temperature and low breakdown strength comparing to PVDF homopolymer, restricting their application in high temperature and high voltage conditions. Nonetheless, the defect-engineering strategy indicates a new approach to non-mechanical β-phase preparation.

This dissertation explored the relationship between molecular structure and the crystallization behavior of PVDF based fluoropolymers. A chemical modification method was designed and developed to prepare a defect-engineered PVDF which promoted β-phase fraction. The new developed method utilized a dehydrofluorination reaction to introduce carbon-carbon

double bonds to the backbones of the PVDF molecules. Molecular simulations showed that the conformational potential energy of α-phase and β-phase were effectively changed by dehydrofluorination and the β-phase formation became the state of lowest energy in PVDF after 15% of carbon-carbon double bonds were introduced. The results demonstrated that the introduced carbon-carbon double bonds induced steric hindrance in the α-phase formation while reduced the potential energy level of the β-phase formation in terms of steric and electrostatic interactions. The experimental dehydrofluorination of PVDF was performed in the form of a simple room temperature solution reaction process. In order to control the extent of dehydrofluorination, the experimental process was optimized in term of dehydrofluorination agents, concentration and reaction time. The results showed that β-phase formation was effectively promoted in dehydrofluorinated PVDF. With a dehydrofluorination extent of *%DHF* = ~20%, the dehydrofluorinated PVDF contained a β-phase fraction of over 80%. Thus, the efficiency of dehydrofluorination method to promote β-phase formation was thoroughly proven through both theoretical and experimental approaches.

The piezoelectricity of dehydrofluorinated PVDF was investigated by both conventional and newly developed characterization techniques, through both direct and inverse piezoelectric effects. Berlincourt method and a newly developed DMA method were used to evaluate the piezoelectric property of dehydrofluorinated PVDF through direct piezoelectric effect. The direct piezoelectric strain coefficients were measured to be d_{33} = -39.95±2.42 pC/N and d_{31} = 25.12±1.13 pC/N, which are higher than any previously reported data for PVDF. By using the PFM method, giant inverse piezoelectric strain coefficients were reached, d_{33} = -65.59±0.71 pm/V. A huge piezoelectric voltage coefficient (g_{33}) of 0.68±0.01 Vm/N for dehydrofluorinated PVDF was also obtained as the highest piezoelectric voltage coefficient reported for any piezoelectric material so far. The characterization results also showed that dehydrofluorinated PVDF can generate a large 3.2% piezoelectric strain and a blocking force of up to 14,000 times its own weight. These record-breaking piezoelectric coefficients and excellent piezoelectric performances demonstrate that the dehydrofluorination method can further exploit the potentials of PVDF as a high-performance piezoelectric material. The thermal stability of β-phase in dehydrofluorinated PVDF was also investigated, showing that dehydrofluorinated PVDF could stably recrystallize into high β-phase multiple times from any high temperature below 210 ˚C. This high thermal stability of dehydrofluorinated PVDF broadens its application under harsh conditions.

Two additive manufacturing methods were developed in this dissertation and using these methods high-performance energy harvesters and actuators were fabricated by processing dehydrofluorinated PVDF. The direct-writing method was developed to utilize the promoted β-phase formation of dehydrofluorinated PVDF. This ink-based printing method can print 2D patterns of PVDF with precisely controlled thickness while perfectly preserving the β-phase fraction in dehydrofluorinated PVDF. On the other hand, the electrospun-assisted 3D printing method was a versatile additive manufacturing method designed for PVDF and other piezoelectric polymers. This method can achieve micron-level high resolution meanwhile provide *in situ* stretching and electric poling to the printed material. Cantilever beam energy harvesters and stretching mode energy harvesters based on dehydrofluorinated PVDF were fabricated by the direct-writing method. The cantilever beam energy harvester based on dehydrofluorinated PVDF yielded a power density of 190 μW/cc, which is higher than any reported PVDF based energy harvesters with similar designs. The dehydrofluorinated PVDF stretching mode energy harvester yielded a giant power density of 21.96 mW/cc which is 3 times higher than similar devices based on conventional drawn PVDF. The energy harvesting performance was further improved by applying mechanical drawing to dehydrofluorinated PVDF. A massive power density of 34.80 mW/cc was obtained from drawn dehydrofluorinated PVDF base devices, demonstrating the high energy conversion efficiency. Such high-power output from these dehydrofluorinated PVDF devices is sufficient to serve as a power source for small wearable digital devices such as heart pacemakers. Dehydrofluorinated PVDF/PLA bilayer actuators were also fabricated through the direct-writing method. The fabricated actuator was able to translate the 3.2% piezoelectric strain from dehydrofluorinated PVDF to a large deformation. A wearable and breathable PVDF energy harvester was fabricated by printing dehydrofluorinated PVDF grids on a glove through the electrospun-assisted 3D printing method. The device was able to generate a voltage signal of 200 mV p-p value under a 0.5% strain. These results demonstrated that the high piezoelectricity observed from dehydrofluorinated PVDF could lead to excellent performances in applications such as energy harvesters and actuator. Furthermore, by integrating dehydrofluorinated PVDF with novel additive manufacturing methods, this dissertation provided new approaches to the development of future piezoelectric devices.

6.1 Contributions

This dissertation investigated the structure-property relationship in piezoelectric fluoropolymers and developed a novel dehydrofluorination method to prepare β-phase PVDF with high piezoelectric properties and improved thermal stability. This work provided a solution for the decades-long problem in the PVDF community and has made numerous contributions detailed in the following section.

The relationship between molecular structure and crystallization behavior of PVDF based fluoropolymer was investigated in a molecular simulation method for the first time. The conformational potential energy calculations on molecular models of P(VDF-TrFE) and dehydrofluorinated PVDF successfully predicted the preferred phase formation during the crystallization of these fluoropolymers. This method, for the first time, provided a quantitative explanation of the different crystallization behaviors of PVDF and P(VDF-TrFE). The molecular simulation strategy provided a new approach for future development of piezoelectric polymers though molecular designing.

This dissertation developed a novel dehydrofluorination method to intrinsically promote the β-phase formation in PVDF. The effectiveness of this method was thoroughly proven by both theoretical and experimental approaches. The optimized experimental parameters allowed the production of dehydrofluorinated PVDF with an optimum dehydrofluorination extent (*%DHF= 10%*), which lead to a high β-phase fraction over 80%. The simplified PVDF dehydrofluorination process was expected to be applicable for large-scale manufacturing. The developed method avoided the necessity of mechanical drawing in β-phase PVDF preparation, providing a solution for the decades-long problem in the PVDF community.

Based on the developed dehydrofluorination method, high β-phase fraction PVDF was prepared and their piezoelectric properties were investigated. This dissertation performed a thorough evaluation on the piezoelectricity of dehydrofluorinated PVDF through newly developed characterization methods. The DMA method and blocking force method were designed in this work and used to conveniently measure the piezoelectric strain coefficient d_{31} through direct and inverse piezoelectric effects, respectively. Record-breaking high piezoelectric strain coefficients were observed from dehydrofluorinated PVDF through both direct and inverse effects, showing a maximum 117% increased d_{33} and 40% increased d_{31} coefficients comparing to conventional

drawn PVDF. A giant piezoelectric voltage coefficient (g_{33}) of 0.41 Vm/N for dehydrofluorinated PVDF was also obtained to be the highest among all reported piezoelectric materials. These results demonstrated that the newly developed dehydrofluorinated PVDF was a worthwhile material candidate for high performance piezoelectric applications. Improved thermal stability was also observed in dehydrofluorinated PVDF, as it can recrystallize to β-phase from any temperature below 210 ˚C. This unique feature removed the restriction in high temperature applications and opened access to various polymer processing method.

This dissertation developed two novel additive manufacturing methods to fabricate high performance energy harvesters and actuators with dehydrofluorinated PVDF. The power density of dehydrofluorinated PVDF based stretching mode energy harvester reached up to 34.80 mW/cc, almost 5 times higher than similar devices based on conventional drawn PVDF. The newly developed electrospun-assisted 3D printing method demonstrated its potential in fabricating breathable piezoelectric fabrics. By integrating dehydrofluorinated PVDF with novel additive manufacturing methods, this dissertation provided new approaches to the development of future piezoelectric devices.

6.2 Recommendations for Future Work

This dissertation performed fundamental research on the dehydrofluorination of PVDF. The results showed that promoted β-phase formation occurs in properly dehydrofluorinated PVDF treated by any organic dehydrofluorination agents. Although in this dissertation only the experimental process of EDA induced dehydrofluorination in a DMF solution was optimized, it was expected that there are other reaction systems based on other bases that are suitable for the dehydrofluorination of PVDF. By further investigating the possibility of other dehydrofluorination agents and solvents, more efficient methods for preparation of dehydrofluorinated PVDF may be developed for large-scale manufacturing of high β-phase PVDF.

In the case of developing a 3D printing method, this dissertation provided two additive manufacturing methods designed for dehydrofluorinated PVDF. However, the fabrication of large and complex 3D structure of PVDF is still not feasible. The electrospun-assisted 3D printing method is very promising in the fabrication of piezoelectric devices because of the high printing

accuracy and the *in situ* electric poling feature. However, it still suffers from problems such as low printing speed and difficulty in printing tall structure. Further research in development of PVDF 3D printing techniques can be of great importance to fully utilize the high piezoelectricity of dehydrofluorinated PVDF.

REFERENCES

1. Chang C, Tran VH, Wang J, Fuh Y, Lin L. Direct-write piezoelectric polymeric nanogenerator with high energy conversion efficiency. Nano letters. 2010;10(2):726-31.

2. Lang C, Fang J, Shao H, Ding X, Lin T. High-sensitivity acoustic sensors from nanofibre webs. Nature communications. 2016;7:11108.

3. Sun C, Shi J, Bayerl DJ, Wang X. PVDF microbelts for harvesting energy from respiration. Energy & Environmental Science. 2011;4(11):4508-12.

4. Cha S, Kim SM, Kim H, Ku J, Sohn JI, Park YJ, et al. Porous PVDF as effective sonic wave driven nanogenerators. Nano letters. 2011;11(12):5142-7.

5. Persano L, Dagdeviren C, Su Y, Zhang Y, Girardo S, Pisignano D, et al. High performance piezoelectric devices based on aligned arrays of nanofibers of poly (vinylidenefluoride-co-trifluoroethylene). Nature communications. 2013;4:1633.

6. Trung TQ, Lee N. Flexible and Stretchable Physical Sensor Integrated Platforms for Wearable Human‐Activity Monitoringand Personal Healthcare. Adv Mater. 2016;28(22):4338-72.

7. Dario P, Carrozza MC, Benvenuto A, Menciassi A. Micro-systems in biomedical applications. J Micromech Microengineering. 2000;10(2):235.

8. Mirfakhrai T, Madden JD, Baughman RH. Polymer artificial muscles. Materials today. 2007;10(4):30-8.

9. Herr HM, Kornbluh RD. New horizons for orthotic and prosthetic technology: artificial muscle for ambulation. Smart Structures and Materials 2004: Electroactive Polymer Actuators and Devices (EAPAD); International Society for Optics and Photonics; 2004.

10. Kornbluh RD, Pelrine R, Prahlad H, Heydt R. Electroactive polymers: An emerging technology for MEMS. MEMS/MOEMS components and their applications; International Society for Optics and Photonics; 2004.

11. Lee M, Chen C, Wang S, Cha SN, Park YJ, Kim JM, et al. A hybrid piezoelectric structure for wearable nanogenerators. Adv Mater. 2012;24(13):1759-64.

12. Lee J, Lee KY, Gupta MK, Kim TY, Lee D, Oh J, et al. Highly stretchable piezoelectric‐pyroelectric hybrid nanogenerator. Adv Mater. 2014;26(5):765-9.

13. Wang H, Zhang QM, Cross LE, Sykes AO. Piezoelectric, dielectric, and elastic properties of poly (vinylidene fluoride/trifluoroethylene). J Appl Phys. 1993;74(5):3394-8.

14. Zhang QM, Bharti V, Zhao X. Giant electrostriction and relaxor ferroelectric behavior in electron-irradiated poly (vinylidene fluoride-trifluoroethylene) copolymer. Science. 1998;280(5372):2101-4.

15. Cross LE. Ferroelectric materials for electromechanical transducer applications. Mater Chem Phys. 1996;43(2):108-15.

16. Bharti V, Cheng Z, Gross S, Xu T, Zhang QM. High electrostrictive strain under high mechanical stress in electron-irradiated poly (vinylidene fluoride-trifluoroethylene) copolymer. Appl Phys Lett. 1999;75(17):2653-5.

17. Lovinger AJ, Cais RE. Structure and morphology of poly (trifluoroethylene). Macromolecules. 1984;17(10):1939-45.

18. Broadhurst MG, Davis GT, McKinney JE, Collins RE. Piezoelectricity and pyroelectricity in polyvinylidene fluoride—A model. J Appl Phys. 1978;49(10):4992-7.

19. Giannetti E. Semi‐crystalline fluorinated polymers. Polym Int. 2001;50(1):10-26.

20. Nalwa HS. Ferroelectric polymers: chemistry: physics, and applications. CRC Press; 1995.

21. Nagai M, Nakamura K, Uehara H, Kanamoto T, Takahashi Y, Furukawa T. Enhanced electrical properties of highly oriented poly (vinylidene fluoride) films prepared by solid‐state coextrusion. Journal of Polymer Science Part B: Polymer Physics. 1999;37(18):2549-56.

22. Du C, Zhu B, Xu Y. Effects of stretching on crystalline phase structure and morphology of hard elastic PVDF fibers. J Appl Polym Sci. 2007;104(4):2254-9.

23. Wegener M, Küunstler W, Gerhard-Multhaupt R. Poling behavior and optical absorption of partially dehydrofluorinated and uniaxially stretched polyvinylidene fluoride. Ferroelectrics. 2006;336(1):3-8.

24. Li L, Zhang M, Rong M, Ruan W. Studies on the transformation process of PVDF from α to β phase by stretching. RSC Advances. 2014;4(8):3938-43.

25. Sencadas V, Gregorio Jr R, Lanceros-Méndez S. α to β phase transformation and microestructural changes of PVDF films induced by uniaxial stretch. Journal of Macromolecular Science®. 2009;48(3):514-25.

26. Newman BA, Yoon CH, Pae KD, Scheinbeim JI. Piezoelectric activity and field‐induced crystal structure transitions in poled poly (vinylidene fluoride) films. J Appl Phys. 1979;50(10):6095-100.

27. Furukawa T. Ferroelectric properties of vinylidene fluoride copolymers. Phase Transitions: A Multinational Journal. 1989;18(3-4):143-211.

28. Tashiro K, Tadokoro H, Kobayashi M. Structure and piezoelectricity of poly (vinylidene fluoride). Ferroelectrics. 1981;32(1):167-75.

29. Su R, Tseng J, Lu M, Lin M, Fu Q, Zhu L. Ferroelectric behavior in the high temperature paraelectric phase in a poly (vinylidene fluoride-co-trifluoroethylene) random copolymer. Polymer. 2012;53(3):728-39.

30. Yang L, Li X, Allahyarov E, Taylor PL, Zhang QM, Zhu L. Novel polymer ferroelectric behavior via crystal isomorphism and the nanoconfinement effect. Polymer. 2013;54(7):1709-28.

31. Wang H, Zhang QM, Cross LE, Sykes AO. Piezoelectric, dielectric, and elastic properties of poly (vinylidene fluoride/trifluoroethylene). J Appl Phys. 1993;74(5):3394-8.

32. Curie J. Développement par compression de l'électricité polaire dans les cristaux hémièdres à faces inclinées. Bull.Soc.Fr.Mineral. 1880;3:90.

33. Curie J, Curie P. Contractions et dilatations produites par des tensions électriques dans les cristaux hémièdres à faces inclinées. Compt.Rend. 1881;93:1137-40.

34. Birkholz M. Crystal-field induced dipoles in heteropolar crystals II: Physical significance. Zeitschrift für Physik B Condensed Matter. 1995;96(3):333-40.

35. Jaffe B. Piezoelectric ceramics. Elsevier; 2012.

36. Cady WG. Piezoelectricity: Volume Two. Courier Dover Publications; 2018.

37. Arnau A, Soares D. Fundamentals of piezoelectricity. In: Piezoelectric transducers and applications. Springer; 2009. p. 1-38.

38. Safari A, Akdogan EK. Piezoelectric and acoustic materials for transducer applications. Springer Science & Business Media; 2008.

39. Kochervinskii VV. Piezoelectricity in crystallizing ferroelectric polymers: Poly (vinylidene fluoride) and its copolymers (A review). Crystallography Reports. 2003;48(4):649-75.

40. Damjanovic D. Ferroelectric, dielectric and piezoelectric properties of ferroelectric thin films and ceramics. Reports on Progress in Physics. 1998;61(9):1267.

41. Li L, Chew ZJ. Microactuators: Design and technology. In: Smart Sensors and MEMs (Second Edition). Elsevier; 2018. p. 313-54.

42. Becker RO, Marino AA. Chapter 4: Electrical Properties of Biological Tissue (Piezoelectricity). Electromagnetism & Life. 1982.

43. Minary-Jolandan M, Yu M. Nanoscale characterization of isolated individual type I collagen fibrils: polarization and piezoelectricity. Nanotechnology. 2009;20(8):085706.

44. Sharma SK, Chauhan VS, Yadav CS. A theoretical model for the electromagnetic radiation emission from ferroelectric ceramics. Materials Today Communications. 2018;14:180-7.

45. Jaffe B. Piezoelectric ceramics. Elsevier; 2012.

46. Yamashita YJ, Hosono Y. High Curie temperature piezoelectric single crystals of the Pb (In1/2Nb1/2) O3-Pb (Mg1/3Nb2/3) O3-PbTiO3 ternary materials system. Handbook of Advanced Dielectric, Piezoelectric and Ferroelectric Materials. 2008:205-31.

47. Kimura M, Ando A, Maurya D, Priya S. Lead Zirconate Titanate-Based Piezoceramics. In: Advanced Piezoelectric Materials (Second Edition). Elsevier; 2017. p. 95-126.

48. Shrout TR, Zhang SJ. Lead-free piezoelectric ceramics: Alternatives for PZT? Journal of Electroceramics. 2007;19(1):113-26.

49. Yin Z, Luo H, Wang P, Xu G. Growth, characterization and properties of relaxor ferroelectric PMN-PT single crystals. Ferroelectrics. 1999;229(1):207-16.

50. Hwang G, Park H, Lee J, Oh S, Park K, Byun M, et al. Self‐powered cardiac pacemaker enabled by flexible single crystalline PMN‐PT piezoelectric energy harvester. Adv Mater. 2014;26(28):4880-7.

51. Saito Y, Takao H, Tani T, Nonoyama T, Takatori K, Homma T, et al. Lead-free piezoceramics. Nature. 2004;432(7013):84.

52. Zhang Y, Sun H, Chen W. A brief review of Ba (Ti 0.8 Zr 0.2) O 3-(Ba 0.7 Ca 0.3) TiO 3 based lead-free piezoelectric ceramics: past, present and future perspectives. Journal of Physics and Chemistry of Solids. 2017.

53. Wang XX, Tang XG, Chan H. Electromechanical and ferroelectric properties of (Bi 1⁄2 Na 1⁄2) TiO 3–(Bi 1⁄2 K 1⁄2) TiO 3–BaTiO 3 lead-free piezoelectric ceramics. Appl Phys Lett. 2004;85(1):91-3.

54. Xu S, Hansen BJ, Wang ZL. Piezoelectric-nanowire-enabled power source for driving wireless microelectronics. Nature communications. 2010;1:93.

55. Bowland CC, Malakooti MH, Zhou Z, Sodano HA. Highly aligned arrays of high aspect ratio barium titanate nanowires via hydrothermal synthesis. Appl Phys Lett. 2015;106(22):222903.

56. Lin Y, Liu Y, Sodano HA. Hydrothermal synthesis of vertically aligned lead zirconate titanate nanowire arrays. Appl Phys Lett. 2009;95(12):122901.

57. Zhou Z, Tang H, Sodano HA. Scalable synthesis of morphotropic phase boundary lead zirconium titanate nanowires for energy harvesting. Adv Mater. 2014;26(45):7547-54.

58. Zhou Z, Tang H, Sodano HA. Vertically aligned arrays of BaTiO3 nanowires. ACS applied materials & interfaces. 2013;5(22):11894-9.

59. Koka A, Zhou Z, Sodano HA. Vertically aligned BaTiO 3 nanowire arrays for energy harvesting. Energy & Environmental Science. 2014;7(1):288-96.

60. Cung K, Han BJ, Nguyen TD, Mao S, Yeh Y, Xu S, et al. Biotemplated synthesis of PZT nanowires. Nano letters. 2013;13(12):6197-202.

61. Kong YC, Yu DP, Zhang B, Fang W, Feng SQ. Ultraviolet-emitting ZnO nanowires synthesized by a physical vapor deposition approach. Appl Phys Lett. 2001;78(4):407-9.

62. Malakooti MH, Patterson BA, Hwang H, Sodano HA. ZnO nanowire interfaces for high strength multifunctional composites with embedded energy harvesting. Energy & Environmental Science. 2016;9(2):634-43.

63. Lin Y, Ehlert G, Sodano HA. Increased interface strength in carbon fiber composites through a ZnO nanowire interphase. Advanced functional materials. 2009;19(16):2654-60.

64. Ehlert GJ, Sodano HA. Zinc oxide nanowire interphase for enhanced interfacial strength in lightweight polymer fiber composites. ACS applied materials & interfaces. 2009;1(8):1827-33.

65. Fukada E. History and recent progress in piezoelectric polymers. IEEE Trans Ultrason Ferroelectr Freq Control. 2000;47(6):1277-90.

66. Tajitsu Y, Kawai S, Kanesaki M, Date M, Fukada E. Microactuators with piezoelectric polylactic acid fibers—toward the realization of tweezers for biological cells. Ferroelectrics. 2004;304(1):195-200.

67. Mathur SC, Scheinbeim JI, Newman BA. Piezoelectric properties and ferroelectric hysteresis effects in uniaxially stretched nylon‐11 films. J Appl Phys. 1984;56(9):2419-25.

68. Newman BA, Chen P, Pae KD, Scheinbeim JI. Piezoelectricity in nylon 11. J Appl Phys. 1980;51(10):5161-4.

69. Lovinger AJ. Ferroelectric polymers. Science. 1983;220(4602):1115-21.

70. Kawai H. The piezoelectricity of poly (vinylidene fluoride). Japanese Journal of Applied Physics. 1969;8(7):975.

71. Tamura M, Ogasawara K, Ono N, Hagiwara S. Piezoelectricity in uniaxially stretched poly (vinylidene fluoride). J Appl Phys. 1974;45(9):3768-71.

72. Higashihata Y, Sako J, Yagi T. Piezoelectricity of vinylidene fluoride-trifluoroethylene copolymers. Ferroelectrics. 1981;32(1):85-92.

73. Ohigashi H, Koga K. Ferroelectric copolymers of vinylidenefluoride and trifluoroethylene with a large electromechanical coupling factor. Japanese Journal of Applied Physics. 1982;21(8A):L455.

74. Park S, Shrout TR. Ultrahigh strain and piezoelectric behavior in relaxor based ferroelectric single crystals. J Appl Phys. 1997;82(4):1804-11.

75. Simpson JO, Welch SS, Clair TLS. Novel Piezoelectric Polyimides. MRS Online Proceedings Library Archive. 1995;413.

76. Zhang R, Jiang B, Cao W. Elastic, piezoelectric, and dielectric properties of multidomain 0.67 Pb (Mg 1/3 Nb 2/3) O 3–0.33 PbTiO 3 single crystals. J Appl Phys. 2001;90(7):3471-5.

77. Cheng Z, Zhang Q. Field-activated electroactive polymers. MRS Bull. 2008;33(3):183-7.

78. Bae S, Kahya O, Sharma BK, Kwon J, Cho HJ, Ozyilmaz B, et al. Graphene-P (VDF-TrFE) multilayer film for flexible applications. ACS nano. 2013;7(4):3130-8.

79. Lovinger AJ. Annealing of poly (vinylidene fluoride) and formation of a fifth phase. Macromolecules. 1982;15(1):40-4.

80. Prest Jr WM, Luca DJ. The formation of the γ phase from the α and β polymorphs of polyvinylidene fluoride. J Appl Phys. 1978;49(10):5042-7.

81. El Mohajir B, Heymans N. Changes in structural and mechanical behaviour of PVDF with processing and thermomechanical treatments. 1. Change in structure. Polymer. 2001;42(13):5661-7.

82. Ruan L, Yao X, Chang Y, Zhou L, Qin G, Zhang X. Properties and Applications of the β Phase Poly (vinylidene fluoride). Polymers. 2018;10(3):228.

83. Katsouras I, Asadi K, Li M, Van Driel TB, Kjaer KS, Zhao D, et al. The negative piezoelectric effect of the ferroelectric polymer poly (vinylidene fluoride). Nature materials. 2016;15(1):78.

84. Li M, Wondergem HJ, Spijkman M, Asadi K, Katsouras I, Blom PW, et al. Revisiting the δ-phase of poly (vinylidene fluoride) for solution-processed ferroelectric thin films. Nature materials. 2013;12(5):433.

85. Tang C, Li B, Sun L, Lively B, Zhong W. The effects of nanofillers, stretching and recrystallization on microstructure, phase transformation and dielectric properties in PVDF nanocomposites. European Polymer Journal. 2012;48(6):1062-72.

86. Mohammadi B, Yousefi AA, Bellah SM. Effect of tensile strain rate and elongation on crystalline structure and piezoelectric properties of PVDF thin films. Polym Test. 2007;26(1):42-50.

87. Salimi A, Yousefi AA. Analysis method: FTIR studies of β-phase crystal formation in stretched PVDF films. Polym Test. 2003;22(6):699-704.

88. Lanceros-Mendez S, Mano JF, Costa AM, Schmidt VH. FTIR and DSC studies of mechanically deformed β-PVDF films. Journal of Macromolecular Science, Part B. 2001;40(3-4):517-27.

89. Kaura T, Nath R, Perlman MM. Simultaneous stretching and corona poling of PVDF films. J Phys D. 1991;24(10):1848.

90. Chang W, Fang T, Liu S, Lin Y. Phase transformation and thermomechanical characteristics of stretched polyvinylidene fluoride. Materials Science and Engineering: A. 2008;480(1-2):477-82.

91. Chang W, Fang T, Lin Y. Thermomechanical and optical characteristics of stretched polyvinylidene fluoride. Journal of Polymer Science Part B: Polymer Physics. 2008;46(10):949-58.

92. Newman BA, Yoon CH, Pae KD, Scheinbeim JI. Piezoelectric activity and field‐induced crystal structure transitions in poled poly (vinylidene fluoride) films. J Appl Phys. 1979;50(10):6095-100.

93. Mahadeva SK, Berring J, Walus K, Stoeber B. Effect of poling time and grid voltage on phase transition and piezoelectricity of poly (vinyledene fluoride) thin films using corona poling. J Phys D. 2013;46(28):285305.

94. Salimi A, Yousefi AA. Conformational changes and phase transformation mechanisms in PVDF solution‐cast films. Journal of Polymer Science Part B: Polymer Physics. 2004;42(18):3487-95.

95. Liu F, Hashim NA, Liu Y, Abed MM, Li K. Progress in the production and modification of PVDF membranes. J Membr Sci. 2011;375(1-2):1-27.

96. Gregorio J, Rinaldo, Cestari M. Effect of crystallization temperature on the crystalline phase content and morphology of poly (vinylidene fluoride). Journal of Polymer Science Part B: Polymer Physics. 1994;32(5):859-70.

97. Gregorio Jr R, Borges DS. Effect of crystallization rate on the formation of the polymorphs of solution cast poly (vinylidene fluoride). Polymer. 2008;49(18):4009-16.

98. GALPERIN EL, Kosmynin BP, Bychkov RA. ABOUT THIRD FORM OF POLYVINYLIDENEFLUORIDE CRYSTALLS. VYSOKOMOLEKULYARNYE SOEDINENIYA SECTION B. 1970;12(7).

99. Benz M, Euler WB, Gregory OJ. The role of solution phase water on the deposition of thin films of poly (vinylidene fluoride). Macromolecules. 2002;35(7):2682-8.

100. Lovinger AJ. Crystalline transformations in spherulites of poly (vinylidene fluoride). Polymer. 1980;21(11):1317-22.

101. Lovinger AJ. Crystallization and morphology of melt‐solidified poly (vinylidene fluoride). Journal of Polymer Science: Polymer Physics Edition. 1980;18(4):793-809.

102. Osaki S, Ishida Y. Effects of annealing and isothermal crystallization upon crystalline forms of poly (vinylidene fluoride). Journal of Polymer Science: Polymer Physics Edition. 1975;13(6):1071-83.

103. Satapathy S, Pawar S, Gupta PK, Varma K. Effect of annealing on phase transition in poly (vinylidene fluoride) films prepared using polar solvent. Bull Mater Sci. 2011;34(4):727.

104. Grubb DT, Choi KW. The annealing of solution grown crystals of alpha and gamma poly (vinylidene fluoride). J Appl Phys. 1981;52(10):5908-15.

105. Yang D, Chen Y. β-phase formation of poly (vinylidene fluoride) from the melt induced by quenching. J Mater Sci Lett. 1987;6(5):599-603.

106. Kang SJ, Park YJ, Sung J, Jo PS, Park C, Kim KJ, et al. Spin cast ferroelectric beta poly (vinylidene fluoride) thin films via rapid thermal annealing. Appl Phys Lett. 2008;92(1):012921.

107. Doll WW, Lando JB. The polymorphism of poly (vinylidene fluoride) IV. The structure of high-pressure-crystallized poly (vinylidene fluoride). Journal of Macromolecular Science, Part B. 1970;4(4):889-96.

108. Hattori T, Kanaoka M, Ohigashi H. Improved piezoelectricity in thick lamellar β‐form crystals of poly (vinylidene fluoride) crystallized under high pressure. J Appl Phys. 1996;79(4):2016-22.

109. Lovinger AJ. Crystallization of the β phase of poly (vinylidene fluoride) from the melt. Polymer. 1981;22(3):412-3.

110. Satyanarayana KC, Bolton K. Molecular dynamics simulations of α-to β-poly (vinylidene fluoride) phase change by stretching and poling. Polymer. 2012;53(14):2927-34.

111. Li M, Wondergem HJ, Spijkman M, Asadi K, Katsouras I, Blom PW, et al. Revisiting the δ-phase of poly (vinylidene fluoride) for solution-processed ferroelectric thin films. Nature materials. 2013;12(5):433.

112. Martín J, Zhao D, Lenz T, Katsouras I, de Leeuw DM, Stingelin N. Solid-state-processing of δ-PVDF. Materials Horizons. 2017;4(3):408-14.

113. Lin D, Chang C, Huang F, Cheng L. Effect of salt additive on the formation of microporous poly (vinylidene fluoride) membranes by phase inversion from LiClO4/water/DMF/PVDF system. Polymer. 2003;44(2):413-22.

114. Chen S, Yao K, Tay FEH, Liow CL. Ferroelectric poly (vinylidene fluoride) thin films on Si substrate with the β phase promoted by hydrated magnesium nitrate. J Appl Phys. 2007;102(10):104108.

115. Dhakras D, Borkar V, Ogale S, Jog J. Enhanced piezoresponse of electrospun PVDF mats with a touch of nickel chloride hexahydrate salt. Nanoscale. 2012;4(3):752-6.

116. Yoon S, Prabu AA, Kim KJ, Park C. Metal Salt‐Induced Ferroelectric Crystalline Phase in Poly (vinylidene fluoride) Films. Macromolecular Rapid Communications. 2008;29(15):1316-21.

117. Thakur P, Kool A, Bagchi B, Hoque NA, Das S, Nandy P. The role of cerium (iii)/yttrium (iii) nitrate hexahydrate salts on electroactive β phase nucleation and dielectric properties of poly (vinylidene fluoride) thin films. RSC Advances. 2015;5(36):28487-96.

118. Jana S, Garain S, Sen S, Mandal D. The influence of hydrogen bonding on the dielectric constant and the piezoelectric energy harvesting performance of hydrated metal salt mediated PVDF films. Physical Chemistry Chemical Physics. 2015;17(26):17429-36.

119. Martins P, Costa CM, Lanceros-Mendez S. Nucleation of electroactive β-phase poly (vinilidene fluoride) with CoFe2O4 and NiFe2O4 nanofillers: a new method for the preparation of multiferroic nanocomposites. Applied Physics A. 2011;103(1):233-7.

120. Martins P, Caparros C, Gonçalves R, Martins PM, Benelmekki M, Botelho G, et al. Role of nanoparticle surface charge on the nucleation of the electroactive β-poly (vinylidene fluoride) nanocomposites for sensor and actuator applications. The Journal of Physical Chemistry C. 2012;116(29):15790-4.

121. Ye H, Shao W, Zhen L. Crystallization kinetics and phase transformation of poly (vinylidene fluoride) films incorporated with functionalized baTiO3 nanoparticles. J Appl Polym Sci. 2013;129(5):2940-9.

122. Wang W, Zhang S, Srisombat L, Lee TR, Advincula RC. Gold‐Nanoparticle‐and Gold‐Nanoshell‐Induced Polymorphism in Poly (vinylidene fluoride). Macromolecular Materials and Engineering. 2011;296(2):178-84.

123. You Y, Liao W, Zhao D, Ye H, Zhang Y, Zhou Q, et al. An organic-inorganic perovskite ferroelectric with large piezoelectric response. Science. 2017;357(6348):306-9.

124. Hao YN, Wang XH, O'Brien S, Lombardi J, Li LT. Flexible BaTiO3/PVDF gradated multilayer nanocomposite film with enhanced dielectric strength and high energy density. Journal of Materials Chemistry C. 2015;3(37):9740-7.

125. Martins P, Costa CM, Botelho G, Lanceros-Mendez S, Barandiaran JM, Gutierrez J. Dielectric and magnetic properties of ferrite/poly (vinylidene fluoride) nanocomposites. Mater Chem Phys. 2012;131(3):698-705.

126. Lund A, Gustafsson C, Bertilsson H, Rychwalski RW. Enhancement of β phase crystals formation with the use of nanofillers in PVDF films and fibres. Composites Sci Technol. 2011;71(2):222-9.

127. El Achaby M, Arrakhiz FZ, Vaudreuil S, Essassi EM, Qaiss A. Piezoelectric β-polymorph formation and properties enhancement in graphene oxide–PVDF nanocomposite films. Appl Surf Sci. 2012;258(19):7668-77.

128. Ramasundaram S, Yoon S, Kim KJ, Park C. Preferential formation of electroactive crystalline phases in poly (vinylidene fluoride)/organically modified silicate nanocomposites. Journal of Polymer Science Part B: Polymer Physics. 2008;46(20):2173-87.

129. Ke K, Pötschke P, Jehnichen D, Fischer D, Voit B. Achieving β-phase poly (vinylidene fluoride) from melt cooling: Effect of surface functionalized carbon nanotubes. Polymer. 2014;55(2):611-9.

130. Yu S, Zheng W, Yu W, Zhang Y, Jiang Q, Zhao Z. Formation mechanism of β-phase in PVDF/CNT composite prepared by the sonication method. Macromolecules. 2009;42(22):8870-4.

131. Chakradhar R, Prasad G, Bera P, Anandan C. Stable superhydrophobic coatings using PVDF–MWCNT nanocomposite. Appl Surf Sci. 2014;301:208-15.

132. Kim KJ, Cho YJ, Kim YH. Factors determining the formation of the β crystalline phase of poly (vinylidene fluoride) in poly (vinylidene fluoride)-poly (methyl methacrylate) blends. Vibrational Spectroscopy. 1995;9(2):147-59.

133. Leonard C, Halary JL, Monnerie L, Broussoux D, Servet B, Micheron F. FTIR EVIDENCE OF BETA-CRYSTAL PHASE FORMATION IN PVDF PMMA BLENDS. POLYMER COMMUNICATIONS. 1983;24(4):110-4.

134. Gregorio Jr R, de Souza Nociti, N Chaves Pereira. Effect of PMMA addition on the solution crystallization of the alpha and beta phases of poly (vinylidene fluoride)(PVDF). J Phys D. 1995;28(2):432.

135. Li M, Stingelin N, Michels JJ, Spijkman M, Asadi K, Feldman K, et al. Ferroelectric phase diagram of PVDF: PMMA. Macromolecules. 2012;45(18):7477-85.

136. Hahn BR, Herrmann-Schönherr O, Wendorff JH. Evidence for a crystal-amorphous interphase in PVDF and PVDF/PMMA blends. Polymer. 1987;28(2):201-8.

137. Huang Y, Bu N, Duan Y, Pan Y, Liu H, Yin Z, et al. Electrohydrodynamic direct-writing. Nanoscale. 2013;5(24):12007-17.

138. Duan Y, Huang Y, Yin Z, Bu N, Dong W. Non-wrinkled, highly stretchable piezoelectric devices by electrohydrodynamic direct-writing. Nanoscale. 2014;6(6):3289-95.

139. Liu ZH, Pan CT, Lin LW, Lai HW. Piezoelectric properties of PVDF/MWCNT nanofiber using near-field electrospinning. Sensors and Actuators A: Physical. 2013;193:13-24.

140. Wang YR, Zheng JM, Ren GY, Zhang PH, Xu C. A flexible piezoelectric force sensor based on PVDF fabrics. Smart Mater Struct. 2011;20(4):045009.

141. Andrew JS, Clarke DR. Effect of electrospinning on the ferroelectric phase content of polyvinylidene difluoride fibers. Langmuir. 2008;24(3):670-2.

142. Mandal D, Yoon S, Kim KJ. Origin of piezoelectricity in an electrospun poly (vinylidene fluoride‐trifluoroethylene) nanofiber web‐based nanogenerator and nano‐pressure sensor. Macromolecular rapid communications. 2011;32(11):831-7.

143. Costa LMM, Bretas RES, Gregorio R. Effect of solution concentration on the electrospray/electrospinning transition and on the crystalline phase of PVDF. Materials Sciences and Applications. 2010;1(04):247.

144. Pu J, Yan X, Jiang Y, Chang C, Lin L. Piezoelectric actuation of direct-write electrospun fibers. Sensors and Actuators A: Physical. 2010;164(1-2):131-6.

145. Chang C, Tran VH, Wang J, Fuh Y, Lin L. Direct-write piezoelectric polymeric nanogenerator with high energy conversion efficiency. Nano letters. 2010;10(2):726-31.

146. Soin N, Shah TH, Anand SC, Geng J, Pornwannachai W, Mandal P, et al. Novel "3-D spacer" all fibre piezoelectric textiles for energy harvesting applications. Energy & Environmental Science. 2014;7(5):1670-9.

147. Klinge U, Klosterhalfen B, Öttinger AP, Junge K, Schumpelick V. PVDF as a new polymer for the construction of surgical meshes. Biomaterials. 2002;23(16):3487-93.

148. Choi SW, Kim JR, Ahn YR, Jo SM, Cairns EJ. Characterization of electrospun PVDF fiber-based polymer electrolytes. Chemistry of materials. 2007;19(1):104-15.

149. Damaraju SM, Wu S, Jaffe M, Arinzeh TL. Structural changes in PVDF fibers due to electrospinning and its effect on biological function. Biomedical Materials. 2013;8(4):045007.

150. Chen S, Li X, Yao K, Tay FEH, Kumar A, Zeng K. Self-polarized ferroelectric PVDF homopolymer ultra-thin films derived from Langmuir–Blodgett deposition. Polymer. 2012;53(6):1404-8.

151. Jiang Y, Ye Y, Yu J, Yang Y, Xu J, Wu Z. A study on ferroelectric PVDF ultrathin films prepared by LB technique. Integrated Ferroelectr. 2007;88(1):21-6.

152. Kliem H, Tadros-Morgane R. Extrinsic versus intrinsic ferroelectric switching: experimental investigations using ultra-thin PVDF Langmuir–Blodgett films. J Phys D. 2005;38(12):1860.

153. Zhu H, Mitsuishi M, Miyashita T. Facile Preparation of Highly Oriented Poly (vinylidene fluoride) Langmuir–Blodgett Nanofilms Assisted by Amphiphilic Polymer Nanosheets. Macromolecules. 2012;45(22):9076-84.

154. Lovinger AJ, Davis DD, Cais RE, Kometani JM. The role of molecular defects on the structure and phase transitions of poly (vinylidene fluoride). Polymer. 1987;28(4):617-26.

155. Farmer BL, Hopfinger AJ, Lando JB. Polymorphism of poly (vinylidene fluoride): potential energy calculations of the effects of head‐to‐head units on the chain conformation and packing of poly (vinylidene fluoride). J Appl Phys. 1972;43(11):4293-303.

156. Soulestin T, Ladmiral V, Dos Santos FD, Améduri B. Vinylidene fluoride-and trifluoroethylene-containing fluorinated electroactive copolymers. How does chemistry impact properties? Progress in Polymer Science. 2017;72:16-60.

157. Yagi T, Tatemoto M, Sako J. Transition behavior and dielectric properties in trifluoroethylene and vinylidene fluoride copolymers. Polym J. 1980;12(4):209.

158. Samara GA, Bauer F. The effects of pressure on the β molecular relaxation and phase transitions of the ferroelectric copolymer P (VDF0. 7TrFe0. 3). Ferroelectrics. 1992;135(1):385-99.

159. Zhang QM, Bharti V, Kavarnos G. Poly (vinylidene fluoride)(PVDF) and its copolymers. Encyclopedia of Smart Materials. 2002.

160. Soulestin T, Marcelino Dos Santos Filho, Pedro, Ladmiral V, Totée C, Silly G, Lannuzel T, et al. Influence of trans-1, 3, 3, 3-Tetrafluoropropene on the Structure–Properties Relationship of VDF-and TrFE-Based Terpolymers. Macromolecules. 2017;50(2):503-14.

161. Bruno A. Controlled radical (co) polymerization of fluoromonomers. Macromolecules. 2010;43(24):10163-84.

162. Boyer C, Valade D, Sauguet L, Ameduri B, Boutevin B. Iodine transfer polymerization (ITP) of vinylidene fluoride (VDF). Influence of the defect of VDF chaining on the control of ITP. Macromolecules. 2005;38(25):10353-62.

163. David G, Boyer C, Tonnar J, Ameduri B, Lacroix-Desmazes P, Boutevin B. Use of iodocompounds in radical polymerization. Chem Rev. 2006;106(9):3936-62.

164. Koga K, Ohigashi H. Piezoelectricity and related properties of vinylidene fluoride and trifluoroethylene copolymers. J Appl Phys. 1986;59(6):2142-50.

165. Barique MA, Ohigashi H. Annealing effects on the Curie transition temperature and melting temperature of poly (vinylidene fluoride/trifluoroethylene) single crystalline films. Polymer. 2001;42(11):4981-7.

166. Kunstler W. Piezo-and pyroelectric properties of dehydrofluorinated PVDF films. Electrets, 1994.(ISE 8), 8th International Symposium on; IEEE; 1994.

167. Beach JV, Shea KJ. Designed catalysts. A synthetic network polymer that catalyzes the dehydrofluorination of 4-fluoro-4-(p-nitrophenyl) butan-2-one. J Am Chem Soc. 1994;116(1):379-80.

168. Zhu L, Wang Q. Novel ferroelectric polymers for high energy density and low loss dielectrics. Macromolecules. 2012;45(7):2937-54.

169. Chung T_C, Petchsuk A, Taylor GW. Ferroelectric polymers with large electrostriction; based on semicrystalline VDF/TrFE/CTFE terpolymers. Ferroelectrics Letters Section. 2001;28(5-6):135-43.

170. Yang L, Tyburski BA, Dos Santos FD, Endoh MK, Koga T, Huang D, et al. Relaxor ferroelectric behavior from strong physical pinning in a poly (vinylidene fluoride-co-trifluoroethylene-co-chlorotrifluoroethylene) random terpolymer. Macromolecules. 2014;47(22):8119-25.

171. Wang Z, Zhang Z, Chung TM. High dielectric VDF/TrFE/CTFE terpolymers prepared by hydrogenation of VDF/CTFE copolymers: synthesis and characterization. Macromolecules. 2006;39(13):4268-71.

172. Bauer F, Fousson E, Zhang QM. Recent advances in highly electrostrictive P (VDF-TrFE-CFE) terpolymers. IEEE Trans Dielectr Electr Insul. 2006;13(5):1149-54.

173. Kepler RG, Anderson RA. Ferroelectric polymers. Adv Phys. 1992;41(1):1-57.

174. Haque RI, Vié R, Germainy M, Valbin L, Benaben P, Boddaert X. Inkjet printing of high molecular weight PVDF-TrFE for flexible electronics. Flexible and Printed Electronics. 2015;1(1):015001.

175. Kolda RR, Lando JB. The effect of hydrogen-fluorine defects on the conformational energy of polytrifluoroethylene chains. Journal of Macromolecular Science, Part B: Physics. 1975;11(1):21-39.

176. Lando JB, Doll WW. The polymorphism of poly (vinylidene fluoride). I. The effect of head-to-head structure. Journal of Macromolecular Science, Part B: Physics. 1968;2(2):205-18.

177. Tashiro K, Takano K, Kobayashi M, Chatani Y, Tadokoro H. Structure and ferroelectric phase transition of vinylidene fluoride-trifluoroethylene copolymers: 2. VDF 55% copolymer. Polymer. 1984;25(2):195-208.

178. Xu H, Cheng Z, Olson D, Mai T, Zhang QM, Kavarnos G. Ferroelectric and electromechanical properties of poly (vinylidene-fluoride–trifluoroethylene–chlorotrifluoroethylene) terpolymer. Appl Phys Lett. 2001;78(16):2360-2.

179. Legrand JF. Structure and ferroelectric properties of P (VDF-TrFE) copolymers. Ferroelectrics. 1989;91(1):303-17.

180. Sun F, Dongare AM, Asandei AD, Alpay SP, Nakhmanson S. Temperature dependent structural, elastic, and polar properties of ferroelectric polyvinylidene fluoride (PVDF) and trifluoroethylene (TrFE) copolymers. Journal of Materials Chemistry C. 2015;3(32):8389-96.

181. Lu Y, Claude J, Zhang Q, Wang Q. Microstructures and Dielectric Properties of the Ferroelectric Fluoropolymers Synthesized via Reductive Dechlorination of Poly (vinylidene fluoride-co-chlorotrifluoroethylene) s. Macromolecules. 2006;39(20):6962-8.

182. Li H, Tan K, Hao Z, He G. Preparation and crystallization behavior of poly (vinylidene fluoride‐ter‐chlorotrifluoroethylene‐ter‐trifluoroethylene). J Appl Polym Sci. 2011;122(5):3007-15.

183. Casar G, Li X, Malič B, Zhang QM, Bobnar V. Impact of structural changes on dielectric and thermal properties of vinylidene fluoride–trifluoroethylene-based terpolymer/copolymer blends. Physica B: Condensed Matter. 2015;461:5-9.

184. Lando JB, Olf HG, Peterlin A. Nuclear magnetic resonance and x‐ray determination of the structure of poly (vinylidene fluoride). Journal of Polymer Science Part A‐1: Polymer Chemistry. 1966;4(4):941-51.

185. Doll WW, Lando JB. Polymorphism of poly (vinylidene fluoride). III. The crystal structure of phase II. Journal of Macromolecular Science, Part B: Physics. 1970;4(2):309-29.

186. Sun H. COMPASS: an ab initio force-field optimized for condensed-phase applications overview with details on alkane and benzene compounds. The Journal of Physical Chemistry B. 1998;102(38):7338-64.

187. Sun H, Ren P, Fried JR. The COMPASS force field: parameterization and validation for phosphazenes. Computational and Theoretical Polymer Science. 1998;8(1-2):229-46.

188. Kise H, Ogata H. Phase transfer catalysis in dehydrofluorination of poly (vinylidene fluoride) by aqueous sodium hydroxide solutions. Journal of Polymer Science: Polymer Chemistry Edition. 1983;21(12):3443-51.

189. Wegener M, Küunstler W, Gerhard-Multhaupt R. Poling behavior and optical absorption of partially dehydrofluorinated and uniaxially stretched polyvinylidene fluoride. Ferroelectrics. 2006;336(1):3-8.

190. Qu P, Liu X, Wang S, Xiao C, Liu S. Moderate dehydrofluorinated PVDF with high energy density. Mater Lett. 2018;221:275-8.

191. Berlincourt D, Jaffe H, Shiozawa LR. Electroelastic properties of the sulfides, selenides, and tellurides of zinc and cadmium. Physical Review. 1963;129(3):1009.

192. Berlincourt DA, Curran DR, Jaffe H. Piezoelectric and piezomagnetic materials and their function in transducers. Physical Acoustics: Principles and Methods. 1964;1(Part A):247.

193. Huang Z, Zhang Q, Corkovic S, Dorey R, Whatmore RW. Comparative measurements of piezoelectric coefficient of PZT films by berlincourt, interferometer, and vibrometer methods. IEEE Trans Ultrason Ferroelectr Freq Control. 2006;53(12).

194. Kepler RG, Anderson RA. Piezoelectricity and pyroelectricity in polyvinylidene fluoride. J Appl Phys. 1978;49(8):4490-4.

195. Xu S, Poirier G, Yao N. PMN-PT nanowires with a very high piezoelectric constant. Nano letters. 2012;12(5):2238-42.

196. Kang SJ, Park YJ, Sung J, Jo PS, Park C, Kim KJ, et al. Spin cast ferroelectric beta poly (vinylidene fluoride) thin films via rapid thermal annealing. Appl Phys Lett. 2008;92(1):012921.

197. Yan Y, Zhou JE, Maurya D, Wang YU, Priya S. Giant piezoelectric voltage coefficient in grain-oriented modified PbTiO 3 material. Nature communications. 2016;7:13089.

198. Sun Y, Yin Y, Mayers BT, Herricks T, Xia Y. Uniform silver nanowires synthesis by reducing AgNO3 with ethylene glycol in the presence of seeds and poly (vinyl pyrrolidone). Chemistry of Materials. 2002;14(11):4736-45.